NAVAL POSTGRADUATE SCHOOL
Monterey, California

DTIC
S ELECTE D
JAN 1 8 1996
G

THESIS

MECHANICAL AND MICROSTRUCTURAL PROPERTIES OF ULTRA-LOW CARBON BAINITIC STEEL WELD METAL

by

Victor Reck Jr.

June 1995

Thesis Advisor: Alan G. Fox

Approved for public release; distribution is unlimited.

DTIC QUALITY INSPECTED 1

19960116 036

REPORT DOCUMENTATION PAGE

Form Approved OMB No. 0704

Public reporting burden for this collection of information is estimated to average 1 hour per response, including the time for reviewing instruction, searching existing data sources, gathering and maintaining the data needed, and completing and reviewing the collection of information. Send comments regarding this burden estimate or any other aspect of this collection of information, including suggestions for reducing this burden, to Washington headquarters Services, Directorate for Information Operations and Reports, 1215 Jefferson Davis Highway, Suite 1204, Arlington, VA 22202-4302, and to the Office of Management and Budget, Paperwork Reduction Project (0704-0188) Washington DC 20503.

1. AGENCY USE ONLY *(Leave blank)*	2. REPORT DATE June 1995	3. REPORT TYPE AND DATES COVERED Master's Thesis

4. TITLE AND SUBTITLE **MECHANICAL AND MICROSTRUCTURAL PROPERTIES OF ULTRA-LOW CARBON BAINITIC STEEL WELD METAL**	5. FUNDING NUMBERS
6. AUTHOR(S) Reck, Victor Jr.	
7. PERFORMING ORGANIZATION NAME(S) AND ADDRESS(ES) Naval Postgraduate School Monterey CA 93943-5000	8. PERFORMING ORGANIZATION REPORT NUMBER
9. SPONSORING/MONITORING AGENCY NAME(S) AND ADDRESS(ES) Naval Surface Warfare Center Carderock Division, Annapolis Detachment Annapolis, MD 21402	10. SPONSORING/MONITORING AGENCY REPORT NUMBER

11. SUPPLEMENTARY NOTES The views expressed in this thesis are those of the author and do not reflect the official policy or position of the Department of Defense or the U.S. Government.

12a. DISTRIBUTION/AVAILABILITY STATEMENT Approved for public release; distribution unlimited	12b. DISTRIBUTION CODE

13. ABSTRACT *(maximum 200 words)* Because of its reduced susceptibility to cracking, Ultra-Low Carbon Bainitic (ULCB) steel weld wire is being investigated as a consumable for Gas Tungsten Arc (GTA) and Gas Metal Arc (GMA) welding of Navy high strength (100 ksi) steels. In the present work, a candidate ULCB weld wire was investigated for GTA and GMA welding processes as a function of both welding power and cover gas. The strength and Charpy V-notch toughness of the resulting welds was investigated. It was found that the GTA weld using 100% argon cover gas had excellent toughness (well above Navy requirements), but the strength was at the minimum specification. The GMA welds using a cover gas of 95% argon - 5% CO2 (C5) showed the opposite trend in that they were well within the range of strength specifications, but their toughness was unsatisfactory. Chemical, mechanical and microstructural studies of these welds were performed. GMA welds using C5 cover gas had a higher weld metal carbon and oxygen, columnar grains, a lath bainite or martensite microstructure, and a high non-metallic inclusion volume fraction. All of these factors contributed to the poor toughness of the GMA welds. The GTA welds using argon cover gas had a low weld metal carbon and oxygen content, an equiaxed microstructure of ferrite, and a low volume fraction of inclusions, which led to a lower strength and higher toughness. Further work aimed at understanding these differences between the ULCB steel weld metals produced by the GMA and GTA processes is currently underway.

14. SUBJECT TERMS Ultra-Low Carbon Bainitic (ULCB), Non-metallic inclusions, Gas Metal Arc Welding, Gas Tungsten Arc Welding	15. NUMBER OF PAGES 126
	16. PRICE CODE

17. SECURITY CLASSIFICATION OF REPORT Unclassified	18. SECURITY CLASSIFICATION OF THIS PAGE Unclassified	19. SECURITY CLASSIFICATION OF ABSTRACT Unclassified	20. LIMITATION OF ABSTRACT UL

NSN 7540-01-280-5500

Standard Form 298 (Rev. 2-89)
Prescribed by ANSI Std. 239-18

Approved for public release: distribution is unlimited.

MECHANICAL AND MICROSTRUCTURAL PROPERTIES OF ULTRA-LOW CARBON BAINITIC STEEL WELD METAL

Victor Reck Jr.
Lieutenant, United States Navy
B.S., United States Merchant Marine Academy, 1988

Submitted in partial fulfillment
of the requirements for the degree of

MASTER OF SCIENCE IN MECHANICAL ENGINEERING

from the

NAVAL POSTGRADUATE SCHOOL
June 1995

Author: ______________________________
Victor Reck Jr.

Approved by: A. G. Fox
Alan G. Fox, Thesis Advisor

Matthew Kelleher
Matthew D. Kelleher, Chairman
Department of Mechanical Engineering

ABSTRACT

Because of its reduced susceptibility to cracking, Ultra-Low Carbon Bainitic (ULCB) steel weld wire is being investigated as a consumable for Gas Tungsten Arc (GTA) and Gas Metal Arc (GMA) welding of Navy high strength (100 ksi) steels. In the present work, a candidate ULCB weld wire was investigated for GTA and GMA welding processes as a function of both welding power and cover gas. The strength and Charpy V-notch toughness of the resulting welds was investigated. It was found that the GTA welds using 100% argon cover gas had excellent toughness (well above Navy requirements), but the strength was at the minimum specification. The GMA welds using a cover gas of 95% argon - 5% CO_2 (C5) showed the opposite trend in that they were well within the range of strength specifications, but their toughness was unsatisfactory. Chemical, mechanical and microstructural studies of these welds were performed. GMA welds using C5 cover gas had higher weld metal carbon and oxygen, columnar grains, a lath bainite or martensite microstructure, and had a high non-metallic inclusion volume fraction. All of these factors contributed to the poor toughness of these GMA welds. The GTA welds using argon cover gas had low weld metal carbon and oxygen content, an equiaxed microstructure of ferrite, and a low volume fraction of inclusions, which led to a lower strength and higher toughness. Further work aimed at understanding these differences between the ULCB steel weld metals produced by the GMA and GTA processes is currently underway.

Accesion For
NTIS CRA&I ☒
DTIC TAB ☐
Unannounced ☐
Justification ....
By ....
Distribution /
Availability Codes
Dist | Avail and / or Special
A-1

TABLE OF CONTENTS

I. INTRODUCTION 1

II. BACKGROUND 3
  A. HIGH STRENGTH LOW ALLOY STEEL IN CONSTRUCTION 3
  B. CHARACTERISTICS OF ULTRA-LOW CARBON BAINITIC STEELS 4
    1. Bainitic Microstructures 4
    2. Alloying Effects 5
    3. Strength 5
    4. Toughness 6
    5. Cooling Rate Considerations 6
  C. WELDING PROCESSES 7
    1. Gas Metal Arc Welding 7
    2. Gas Tungsten Arc Welding 8
  D. DEOXIDATION AND NON-METALLIC INCLUSIONS 8
    1. Sources 9
    2. Composition 9
    3. Deoxidizers 9
      a. Aluminum 10
      b. Titanium 10
      c. Silicon 10
      d. Manganese 11

4. Acicular Ferrite 11

E. SCOPE OF THE PRESENT WORK 12

III. EXPERIMENTAL PROCEDURE 21

A. WELD SAMPLES 21

B. SAMPLE PREPARATION 21

C. MECHANICAL TESTING 22

1. Microhardness Testing 22

2. Tensile Testing 22

3. Fracture Toughness Testing 22

D. SCANNING ELECTRON MICROSCOPY 23

E. TRANSMISSION ELECTRON MICROSCOPY 23

F. OPTICAL MICROSCOPY 24

IV. RESULTS AND DISCUSSION 31

A. WELD METAL COMPOSITION 31

B. NON-METALLIC INCLUSIONS 32

1. Composition 32

2. Size and Volume Fraction 33

C. MECHANICAL PROPERTIES 34

1. Tensile Testing 34

2. Microhardness 35

3. Impact Testing 35

        a. CVN Impact Curves 36
        b. FATT Comparisons 37
    D. FRACTOGRAPHY 38
    E. MICROSTRUCTURAL ANALYSIS 41
        1. Macroscopic 41
        2. Microscopic 42

V. SUMMARY 89
    A. CONCLUSIONS 89
    B. RECOMMENDATIONS 90

APPENDIX A. CVN FRACTURE SURFACES 93

APPENDIX B. OPTICAL MACROSCOPIC PHOTOGRAPHS 97

LIST OF REFERENCES 101

INITIAL DISTRIBUTION LIST 105

LIST OF FIGURES

2.1 Weldability Diagram 15

2.2 Relationship Between 50% Transformation Temperature and Tensile Strength for Bainitic Steels 16

2.3 ULCB Strength as Related to B_s Temperature 16

2.4 Comparison of Measured and Calculated Strength Versus B_s Temperature for Various Bainitic Steels 17

2.5 Effect of Manganese Content on CVN Performance on Submerged Arc Welds of HY-100 Steels 18

2.6 CCT Diagram for HSLA-100 19

2.7 CCT Diagram for Low-Carbon, Low-Alloy Steel Weld Metal 19

2.8 Sketch of GMA Welding Process 20

2.9 Sketch of GTA Welding Process 20

4.1 Weld Metal Aluminum vs. Oxygen 50

4.2 Weld Metal Silicon vs. Oxygen 51

4.3 Weld Metal Manganese vs. Oxygen 52

4.4 Weld Metal Carbon vs. Oxygen 53

4.5 Inclusion Aluminum vs. Weld Metal Oxygen 54

4.6 Inclusion Titanium vs. Weld Metal Oxygen 55

4.7 Inclusion Manganese vs. Weld Metal Oxygen 56

4.8 Inclusion Silicon vs. Weld Metal Oxygen 57

4.9 Inclusion Size and Volume Fraction (V_f) vs. Weld Metal Oxygen 58

4.10 Inclusion Size and Volume Fraction (V_f) vs. Weld Metal Oxygen (Less than 200 ppm) (M-GMA) 59

4.11 Inclusion Size and Volume Fraction (Vf) vs. Weld Metal Oxygen (Greater than 200 ppm) (T - GTA) 60

4.12 Ultimate Tensile Strength (UTS) and Yield Strength (YS) vs. Weld Metal Oxygen (T - GTA) 61

4.13 Yield Strength (YS) vs. Weld Power 62

4.14 Yield Strength (YS) vs. Weld Metal Carbon 63

4.15 Vicker's Hardness (HV) vs. Ultimate Tensile Strength (UTS) 64

4.16 CVN Toughness Curves for All Weld Samples 65

4.17 CVN Toughness Compraing GMA and GTA Welds Using Argon Cover Gas at 60 KJ/in. Power 66

4.18 CVN Toughness Comparing GMA and GTA Welds Using C5 Cover Gas at 81 and 97 KJ/in. Power 67

4.19 CVN Toughness Comparing Argon and C5 Cover Gas GMA Welds at 60 KJ/in. Power 68

4.20 CVN Toughness Comparing GTA Argon - 60 KJ/in. Power and C5 - 81 KJ/in. Power Welds 69

4.21 CVN Toughness Comparing GMA - C5 Cover Gas Welds at Various Power Levels 70

4.22 CVN Toughness Comparing Weld Samples MV6 (GMA/Argon/60) to MV20 (GTA/C5/81) 71

4.23 CVN Toughness Showing the Improvement of Toughness Achieved by Using Argon Cover Gas and GTA Welds 72

4.24 Fracture Appearance Transition Temperature (FATT) vs. Weld Metal Oxygen 73

4.25 Fracture Appearance Transition Temperature (FATT) vs. Inclusion Volume Fraction (V_f) 74

4.26 Fracture Appearance Transition Temperature (FATT) vs. Average Inclusion Size 75

4.27 Fracture Appearance Transition Temperature (FATT) vs. Weld Metal Carbon 76

4.28 Fracture Appearance Transition Temperature (FATT) vs. Ultimate Tensile Strength (UTS) 77

4.29 MV5 - Showing the Fracture Surface of a Typical Ductile Sample 78

4.30 MV4 - Showing Void Formation by Inclusions in Ductile Samples 78

4.31 MV2 - GTA Weld Using Argon Cover Gas 79

4.32 MV6 - GMA Weld Using Argon Cover Gas 79

4.33 MV4 - GMA Weld Using C5 Cover Gas 80

4.34 MV20 - GTA Weld Using C5 Cover Gas Showing Extensive Areas of Ductility and Crack Formation by Large Inclusions 80

4.35 MV20 - Showing Void Formation by Inclusions in Ductile Regions of Lower Shelf Samples 81

4.36 MV4 - GMA Weld Using C5 Cover Gas Showing Extensive Intergranular Cracking 81

4.37 MV5 - GMA Weld Using C5 Cover Gas Showing Intergranular Cracking and Ductile Areas 82

4.38 MV1 - GMA Weld Using C5 Cover Gas Showing Intergranular Cracking 82

4.39 MV1 - GMA Weld Using C5 Cover Gas Showing Intergranular Cracking and Uneven Cleavage 83

4.40 MV6 - GMA Weld Using Argon Cover Gas Showing Uneven Cleavage Connected by Ductile Ridges 83

4.41 MV2 - GTA Weld Using Argon Cover Gas 84

4.42 MV20 - GTA Weld Using C5 Cover Gas Showing Cleavage and Ductile Areas Nucleated by Inclusions 84

4.43 MV5 - Showing Lathlike Microstructure Typical to Columnar Grains of GMA Welds Using C5 Cover Gas (400 x) 85

4.44 MV5 - Showing the Extension and Continuity of Laths in Columnar Grains (400 x) 85

4.45 MV1 - Showing Lathlike Packets of Bainite/Martensite in Grain Refined Regions of Typical GMA Welds Using C5 Cover Gas (200 x) 86

4.46 MV6 - Showing Lathlike Microstructures in the Columnar Region of a GMA Weld Sample Using Argon Cover Gas (400 x) 86

4.47 MV6 - Showing Lathlike and Equiaxed Microstructures in Grain Refined Regions of a GMA Weld Using Argon Cover Gas (400 x) 87

4.48 MV20 - Showing Lathlike Bainite/Martensite in Grain Refined Regions of a GTA Weld Using C5 Cover Gas (400 x) 87

4.49 MV2 - Showing Equiaxed Ferrite Microstructure in a GTA Weld Using Argon Cover Gas (400 x) 88

A.1 MV1 Ductile and Brittle Fracture Surfaces (6.4 x) 93

A.2 MV2 Ductile and Brittle Fracture Surfaces (6.4 x) 93

A.3 MV4 Ductile and Brittle Fracture Surfaces (6.4 x) 94

A.4 MV5 Ductile and Brittle Fracture Surfaces (6.4 x) 94

A.5 MV6 Ductile and Brittle Fracture Surfaces (6.4 x) 95
A.6 MV20 Ductile and Brittle Fracture Surfaces (6.4 x) 95
B.1 MV1 (GMA/C5/60 KJ/in.) 97
B.2 MV2 (GTA/Argon/60 KJ/in.) 97
B.3 MV4 (GMA/C5/97 KJ/in.) 98
B.4 MV5 (GMA/C5/30 KJ/in.) 98
B.5 MV6 (GMA/Argon/60 KJ/in.) 99
B.6 MV20 (GTA/Argon & C5/81 KJ/in.) 99

LIST OF TABLES

2.1 Nominal Composition of HY-100, HSLA-100 and ULCB (CS1B) Consumable 14

3.1 Welding Parameters 25

3.2 Weld Metal Compositions (wt%) 26

3.3 Chemical Analysis Methods 27

3.4 Weld Sample Ultimate Tensile Strength and Yield Strength (ksi.) 28

3.5 Weld Sample CVN Energy (J) and (Total % Ductility) 29

4.1 MV20 Inclusion Chemical Composition (at%) 44

4.2 MV20 Inclusion Oxides (wt%) 45

4.3 Inclusion Element and Oxide Compositions (wt%) 46

4.4 Inclusion Statistics 47

4.5 Inclusion Size Distribution Data 48

4.6 Weld Sample Vicker's Hardness Data 49

ACKNOWLEDGMENTS

I would like to thank my advisor, Dr. Alan Fox for his advice and encouragement during the course of this thesis work. His knowledge of the subject was invaluable and his enthusiasm made this difficult project truly enjoyable. I would like to thank Richard Hashimoto for his many hours of assistance and training. Additionally, thanks are due to Douglas Shelton for his valuable assistance and suggestions.

I. INTRODUCTION

In recent years, the U.S. Navy has begun to replace the High Yield steels, HY-80 and HY-100 with High Strength Low Alloy (HSLA) steels such as HSLA-100. The reasoning behind this change in construction steels was that the high carbon content of HY steels has rendered it susceptible to hydrogen cracking within the Heat Affected Zone (HAZ) of welded sections due to the presence of hard untempered martensite. To eliminate such cracking, complex preheat controls and limits on weld power are necessary during welding. On the other hand, the HSLA series of steels derives its strength from a copper precipitated second phase and requires no preheat due to the absence of high carbon martensite in the HAZ. Without preheat, the welding process is both simplified and a substantial cost reduction may be realized.

Unfortunately, no weld consumable has been approved specifically for the use in HSLA joining. In fact, the Navy currently uses weld consumables developed for HY-100 welding. Since these consumables were developed for the higher carbon HY-100 steel, preheat and occasionally postheating are required (DeLoach, 1993). Therefore, until an effective consumable is designed specifically for HSLA-100 joining, the potential of this steel will not be fully realized.

Currently, the Naval Surface Warfare Center (NSWC), Annapolis in conjunction with the Naval Postgraduate School (NPS) are actively developing an Ultra-Low Carbon Bainitic (ULCB) consumable for use in Gas Metal Arc (GMA) welding. Consideration has been given to the ULCB consumable based on a demonstrated high strength (100 ksi.) and toughness (comparable to HSLA-100) derived from its bainitic structure, despite its extremely low carbon content (0.02 wt. %). As an added advantage, use of the ULCB weld consumable should eliminate preheat and postheat requirements.

It is generally understood that grain refinement in multipass Gas Tungsten Arc (GTA) welding processes produces improved weld toughness over the columnar grain structure produced by the GMA process. However, the low deposition rate of GTA welding has driven researchers to concentrate on developing a tough weld consumable for the higher deposition GMA welding processes. The specific focus of this study is to investigate the microstructure and mechanical properties of one ULCB weld consumable formulation, developed by NSWC. To that end, both the effect of cover gas and power input, with relationship to strength and toughness of GTA and GMA welding processes, will be investigated.

II. BACKGROUND

A. HIGH STRENGTH LOW ALLOY STEEL IN CONSTRUCTION

For a number of years HY-100 steels have been used in the construction of new ships and submarines as a replacement for the heavier and lower strength HY-80 steel. However, fabrication costs and lengthy production schedules led the Navy to develop a substitute steel with similar strength and toughness characteristics of HY-100 steel. The end result of this development program was the certification of the High Strength Low Alloy (HSLA) steel HSLA-100 (Czyryca, 1990). The fundamental differences between HY-100 and HSLA-100 steel concerns how each steel derives its strength. Where the strength and toughness of the higher carbon HY-100 steel depends primarily upon tempered martensite, low carbon HSLA steels derives its strength from a copper precipitate phase distributed in a bainitic or low-carbon martensite matrix (Green, 1993). Nominal compositions for HY-100 and HSLA-100 are shown in Table 2.1. Additional discussions regarding further comparison between theses two steels can be found elsewhere (Beno, 1994).

One major benefit resulting from the use of HSLA-100 steel is that it is easy to weld. Figure 2.1 is a diagram of the weldability of high strength Navy steels as it relates to carbon content and equivalent carbon content. As shown in Figure 2.1, the Carbon Equivalent (CE) value is a measure of the hardenability of a high strength steel when alloying elements are added to the steel as an addition to and substitute for carbon. It is referred to as an equivalent, since fractions of various alloys will produce a hardenability through solid solution alloying that is equivalent to that of carbon. Hence, the low-carbon content HSLA steels, having a CE similar to that of higher carbon HY steels, are equally high in strength without the existence of a hard, martensitic heat affected zone (HAZ) and thus there is no longer a need for preheat to prevent hydrogen underbead cracking (Czyryca, 1990). Unfortunately, weld consumable development and certification has yet to produce an adequate consumable that is tailored specifically to HSLA steels. Current construction practice requires the use of consumables that were developed for HY-100 steels, making preheat a necessary requirement (DeLoach, 1990). Thus, the full benefit of using HSLA-100 steels cannot be realized until an adequate weld consumable is developed and certified.

B. CHARACTERISTICS OF ULTRA-LOW CARBON BAINITIC STEELS

1. Bainitic Microstructures

Bainite is a product of an austenitic transformation and forms as needles or plates consisting of ferrite and cementite phase (Callister, 1991). Bainite forms in a range of temperatures between the low strength ferrite+pearlite reaction and the high strength martensite reaction. Because of this temperature to strength relationship, the maximum tensile strength that can be realized in a bainitic structure will generally be less than that of martensite. However, as carbon content approached zero, such as in ULCB steels, it was shown that the difference in strengths between bainite and martensite approached zero (Pickering, 1978). Figure 2.2 shows the relationship between transformation temperatures and strength.

Bainite forms intragranularly from austenite as an aggregate of ferrite and cementite (granular bainite), and can be further classified into categories of upper bainite and lower bainite (Bhadeshia, 1990). Upper bainite forms at relatively high temperatures and consists of sheaves of ferritic plates with cementite trapped between them. (Bhadeshia, 1990). Sometimes this microstructure is more explicitly referred to as ferrite with an aligned second phase (Liu, 1992). At these higher temperatures, carbon is mobile and diffuses in front of the growing bainite where it is trapped in the form of cementite between the laths (Pickering, 1978). Lower bainite forms at lower temperatures, with finer cementite particles trapped within the plates (Bhadeshia, 1990). Since lower bainite forms at lower temperatures, carbon cannot diffuse as readily, and is precipitated within the laths (Pickering, 1978).Again, a more explicit classification of this microstructure is that of ferrite with a non-aligned second phase (Liu, 1992).

2. Alloying Effects

The key philosophy in the use of ULCB weld consumables is to minimize carbon to the lowest amount possible (generally around 0.02%). While carbon is the best strengthening agent available, expensive preheating and careful heat input controls must be employed to resolve problems involving hydrogen cracking, and its detrimental effect on toughness (Cullison, 1994). Hence, major alloying elements such as manganese, molybdenum, nickel, titanium and niobium must be added to maintain strength and toughness. However, studies conducted by the NSWC on ULCB weld consumables concluded that the exact combination of alloying elements necessary to achieve optimum strength and toughness cannot be predicted due to the probable interaction between these (DeLoach, 1993).

There exists a complicated interrelation between alloying elements in ULCB weld metal as it relates to strength and toughness. Directly, solid solution alloying maintains an equivalent carbon amount which determines hardenability (Czyryca, 1990). Indirectly, alloying elements affect the strength and toughness of the weld through cooling rate sensitivity, inclusion formation, and microstructural variations. Additional alloying effects related to strength, toughness and cooling rate will be discussed in the following sections.

3. Strength

The key to maximizing the strength potential of bainite is to depress the temperature at which bainite begins to form, commonly referred to as the Bainite Start (B_s) temperature. Figure 2.3 and Figure 2.4 clearly demonstrate how both ultimate tensile strength and yield strength increase as B_s decreases. Control of B_s is particularly important in the ULCB series of steel, since the carbon content is so low (<0.022) that the formation of martensite is difficult, and the transformation to ferrite is inevitable. Garcia, Lis and DeArdo also concluded that strength varied linearly with B_s, and additions of molybdenum, a known CE contributor (Figure 2.1), and boron improved the yield strength (Garcia, 1990). A more recent study by Wang and Kao showed that dissolved niobium in austenite and free boron resulted in granular bainite microstructure containing bainitic-ferrite as well as martensite/austenite constituent, leading to high strength. Additionally, nickel, molybdenum and manganese were shown to be necessary for the production of granular bainite through the delay of polygonal ferrite formation by B_s depression. Molybdenum was found to be the most effective of the three (Wang, 1993).

In addition to solid solution strengthening (Blicharski, 1988), and B_s depression (Wang, 1993) by nickel, molybdenum and manganese, ULCB steels also derive their strength from dislocation substructures. Bainite forms from a diffusional shear transformation mechanism (Pickering, 1978). Thus, it is often suggested that the large amount of dislocations associated with bainite are a direct results of this shear transformation, a widely held theory that may not necessarily be correct (Bhadeshia, 1990). Nevertheless, qualitative examination of bainite suggests that the dislocation density of bainitic ferrite appears to increase as B_s is reduced.

4. Toughness

Toughness of ULCB steels is also affected by alloying elements. Pickering initially identified that nickel improved toughness (Pickering, 1978). Wang and Kao arrived at the same conclusion regarding nickel and also determined that manganese had no observable effect on toughness, while molybdenum actually reduced toughness (Wang, 1993). McDonald reported that the addition of molybdenum, in excess of 2%, markedly reduced toughness (McDonald, 1992), while research by NSWC (DeLoach, 1993) concluded that toughness peaked in the neighborhood of 1.30-1.35 wt% nickel as shown in Figure 2.5. In the case of plate steels of various gauge sizes, it has also been determined that the bainite transformation Continuous Cooling Transformation (CCT) should be as flat as possible (Pickering, 1978). This would allow the bainite structure to form over a wide range of cooling rates.

5. Cooling Rate Considerations

In addition to depressing the B_s as possible, it is also very important to have the bainite portion of the Continuous Cooling Transformation (CCT) diagram as flat as possible. This allows for the widest range of cooling rates with a minimum variation of properties (Pickering, 1978). Hence, the formation of the optimum microstructure with regards to strength and toughness can be achieved over a wide variation of welding heat inputs and section sizes.

Figure 2.6 is the CCT diagram for a nominal composition HSLA-100 steel showing regions of Austenite (A), Martensite (M), Granular Bainite (GB), and Proeutectoid Ferrite (PF). As can be seen, there exists an extensive martensitic region at high cooling rates while granular bainite and proeutectoid ferrite form at lower cooling rates (Wilson, 1988). The ULCB weld consumable attempts to depress and extend the GB region so that desired microstructures of predominantly granular bainite with small amounts of acicular ferrite can form at higher heat inputs. Figure 2.7 is a generalization of the effects of alloying and heat input (cooling rate) effects upon low-carbon, low-alloy steels. Research has shown that alloying with molybdenum and nickel was the least sensitive to cooling rate, while manganese, niobium and carbon increased cooling rate sensitivity (DeLoach, 1993).

C. WELDING PROCESSES

As stated previously the main objective of this study is to develop a suitable weld consumable for use with Gas Metal Arc (GMA) welding. Nevertheless, it is very important to understand how this consumable performs with respect to the Gas Tungsten Arc (GTA) welding process. With this knowledge, specific microstructural information that can only be obtained from GTA welding allows for investigation of specific variables such as cover gas and heat input without the effects of weld microstructure. The following sections briefly outline the GMA and GTA welding processes.

1. Gas Metal Arc Welding

GMA welding is an electric arc welding process where an arc is formed between a consumable electrode and the metal being welded. Figure 2.8 is a sketch of the GMA welding process. Typically, the arc and weld pool are shielded by argon, helium, or a combination of carbon dioxide and another gas. A mixture of carbon dioxide and an inert gas is generally preferred due to arc instabilities experienced when pure, inert gas is used exclusively. For this study, either pure argon or a combination of 5% CO_2 and 95% argon (C5) was used as a shield gas.

The weld bead produced by GMA welding can be characterized as papillary in nature, and extends deeply into the base metal or previous weld passes. Since most of the heat input is absorbed by the consumable electrode, these welds have a high per pass deposition rates. The size of the weld HAZ with respect the fusion zone is relatively small. Thus, the columnar grain structure of the fusion zone is generally maintained throughout, even when multiple passes are employed.

2. Gas Tungsten Arc Welding

GTA welding is also an electric arc welding process where the arc is formed between an non-consumable tungsten electrode and the workpiece. Joining can then be accomplished with a consumable filler wire or without a filler (autogenous). Figure 2.9 is a sketch of the GTA welding process. Typically, inert shield gases such as argon or helium are used to shield the arc and weld zone. All welds in the study were conducted using a consumable filler rod and either argon or C5 cover gas.

GTA welds are semi-circular in shape with approximately one-third the deposition per pass as compared to GMA welds with a much slower deposition rate. Since GTA welds are relative small in size, the HAZ of any given weld almost entirely encompasses the previous weld passes. Hence, extensive grain refinement occurs throughout the weld fusion zone, with the exception of the final pass which remains columnar.

D. DEOXIDATION AND NON-METALLIC INCLUSIONS

The size, composition, number and morphology of non-metallic inclusions are extremely important to the strength and toughness of high grade HSLA and ULCB steels. While inclusions that are larger than 1-2 microns (large inclusions) in size have been shown to be initiation sites for both ductile and brittle fracture in steels, inclusions that are less than 1-2 microns in size (small inclusions) can have a beneficial microstructural effect in that they restrict austenite grain growth and can provide nucleation sites for acicular ferrite (Kiessling, 1989). Precise control in current steel manufacturing techniques allows for a reduction oxygen and sulfur contents high grade engineering steels to as little as 10 ppm, resulting in minute quantities of inclusions in these steels. While these remaining inclusions are large enough to have a detrimental effect on toughness, their minute quantity renders them insignificant (Kiessling, 1989). However, oxygen activity can be high, as in the case of welding with an oxygen containing cover gas (such as C5), that the formation of numerous small inclusions occur.

1. Sources

The two main sources of inclusions are referred to as indigenous and exogenous. Exogenous inclusions are the result of steel making, slag and reoxidation. Since the steel considered here is of high quality, and the welding processes are clean, the formation of a critical amount of exogenous inclusions is unlikely. Indigenous inclusions are the result of deoxidization and desulfidization of the weld pool. Oxide inclusions result from the deoxidization of the weld pool by alloying components, where the oxygen supply is provided by additions of carbon dioxide to the cover gas. Similarly, sulfide inclusions are formed intentionally through the addition of sulfide formation alloys, primarily manganese.

2. Composition

The typical inclusion composition of the weld metal of this study is expected to include the following oxides: Al_2O_3, Ti_xO_y (the oxidation state of titanium oxide is unclear), SiO_2, MnO and occasionally Cr_2O_3. Additionally, manganese combines with any additional sulfur in the weld pool to form MnS.

3. Deoxidizers

As previously noted, the GMA welding process relies on a mildly oxidizing gas (5% CO_2), primarily for arc stabilization. As the consumable proceeds into the weld pool in a melted state, it picks up oxygen from the cover gas. Reaction between free carbon in the weld pool and this dissolved oxygen results in the formation of carbon monoxide which can give rise to weld porosity during solidification. Therefore, it is necessary to reduce the oxygen in the weld pool through the addition of deoxidizes (Widgery, 1975). Many of the alloying elements used in the welding of high strength steels are highly reactive with oxygen and must be supplemented by a fluxing agent or from the weld consumable. Several of the alloys which act as deoxidizing agents are discussed below.

a. Aluminum

Aluminum is a strong deoxidizer and the most reactive of the weld metal elements. The result of aluminum addition to the weld pool is the oxide Al_2O_3 (Kiessling, 1979). Several researchers have reported that inclusions with large amounts of aluminum have improved toughness as a result of acicular ferrite formation (Bhatti, 1984 and Abson, 1986); but others found no such correlation between composition and the formation of acicular ferrite (Dowling, 1986). Additionally, Komizo reported that high oxygen contents in the weld metal rendered aluminum less effective with regards to microstructure and toughness (Komizo, 1989).

b. Titanium

Titanium is also a strong deoxidizer, and is reported to form as either TiO (Abson, 1986, Grong, 1986 and Bhatti, 1984) as Ti_2O_3 (Ohkita, 1988), or as TiO_2 (Kiessling, 1978 and Edwards, 1990). Nevertheless, most agree that titanium is often beneficial regarding the improvement of toughness due to its ability to promote acicular ferrite formation (Grong, 1986 and Ohkita, 1988).

c. Silicon

While silicon does provide some amount of deoxidizing effect through the formation of SiO_2. Silicon is referred to as an "necessary evil" that is optimized between 0.3-0.5%. Lower levels of silicon have the effect of reducing Charpy toughness, and being detrimental to weld electrode characteristics. Likewise, above this range, weld metal toughness is also seen to suffer (Abson, 1986 and Grong, 1986). Silicon has not been shown to contribute significantly to the formation of acicular ferrite (Komizo, 1989).

d. Manganese

Manganese is a relatively weak oxidizer which generally appears in the form of MnO, although it also tends to form complex oxides with other elements such as silicon (Kiessling, 1978). As an alloying element, manganese is probably the most important with respect to increasing strength and toughness (Abson, 1986 and Grong, 1986). However, the ability of manganese to provide improved toughness has been challenged in recent years (Wang, 1993). Another key reason that manganese is added in relatively high quantities is to ensure that MnS and not FeS forms. While the low melting temperature and surface tension of FeS can result in solidification cracking, the higher melting temperature and more globular morphology of MnS does not (Kou, 1987).

4. Acicular Ferrite

Acicular ferrite is probably one of the most important structures in weld steels as is directly responsible for high toughness. It is formed intragranularly in a basket-weave pattern that provides the maximum resistance to crack propagation (Kou, 1987). While its formation in large quantities is generally not expected in GTA and GTA welds of ULCB steels, its relationship to bainitic ferrite, in that if forms needles of intragranular ferrite, is worth mentioning (Bhadeshia, 1990). While it is generally understood that inclusions are the nucleation sites for acicular ferrite, the relationship between inclusion composition and acicular ferrite formation is unclear. Bhatti et al. reported that chemical composition was responsible for the formation of acicular ferrite formation, and that acicular ferrite favored aluminum rather than manganese inclusions as a formation site. (Bhatti, 1984). In another study, Ohkita et al. reported that acicular ferrite was nucleated by titanium oxides (Ohkita, 1988). Neither Bhatti et al. or Abson et al. were able to correlate oxygen composition and acicular ferrite nucleation (Bhatti, 1984 and Abson, 1986), but Francis et al reported that acicular ferrite volume fractions were influenced by oxygen (Francis, 1990). Dowling et al. rejected all previous reports, concluding that inclusion composition was not at all related to the volume fraction of acicular ferrite. Rather, they found that inclusions were inert substrates from which inclusions nucleated in accordance with classical heterogeneous nucleation theory (Dowling, 1986). With this amount of contradictory information available, Edwards and Liu concluded that the association between particular compositions and microstructures may not be valid. Rather, it was felt that the data suggested that minute quantities of specific elements, especially aluminum and titanium, vice the bulk composition of the inclusion, influence the resulting microstructure the most (Edwards, 1990).

E. SCOPE OF THE PRESENT WORK

The Naval Surface Warfare Center (NSWC) and Naval Postgraduate School (NPS) are active investigating the properties of a ULCB weld consumables developed by NSWC. The ultimate goal of the research will be to develop a suitable weld consumable for use in HSLA-100 weld construction that meets the strength requirements of HSLA-100 steel, while eliminating heat input limitations as well as any preheat and postheat requirements. The ULCB weld consumable formulation (designated CS1B by NSWC), used to conduct the MV series of welds, was found to have strength and toughness properties that meet the mechanical property requirements of MIL-120S consumables developed for HY-100 steels, currently used to weld HSLA-100 steels. The strength and toughness requirements are as follows: 1) The yield strength must be 102-122 ksi, and 2) The minimum Charpy V-Notch (CVN) impact energy must be 45 ft-lb at -60°F and 60 ft-lb at 0°F (DeLoach, 1993).

NSWC has reported that while GTA weldments conducted with this consumable have a higher toughness than GMA welds made under the same condition, while the GMA welds display a higher tensile strength. Work by Butler concluded that type, size, number and distribution of nonmetallic inclusions in GTA weldments did not affect toughness (Butler, 1993). Beno concurred with this conclusion and further suggested that suggested that the columnar grain structure of GMA welds actually attributed to reduced toughness (Beno, 1994). Finally, Brothers felt that the formation of acicular ferrite, a key microstructure responsible for high toughness in steels, depended on the non-metallic inclusion composition (especially those high in aluminum and titanium) and not the inclusion volume fraction (Brothers, 1994).

With these conclusions in mind, this study will focus on weld microstructure and mechanical properties of several ULCB weldments in an attempt to provide a clearer indication of why the upper shelf CVN impact toughness is unsatisfactory in GMA welds. To this end , microstructural and mechanical studies will be conducted on multi pass GMA and GTA welds of various power levels (30-97 KJ/in.) and cover gases (argon or C5).

Table 2.1 Nominal Compositions of HY-100, HSLA-100 and ULCB (CS1B Consumable)

(HY/HSLA- Czyryca, 1990), (ULCB, NSWC)

	HY-100	HSLA-100	ULCB (CS1B consumable)
C	0.17	0.04	0.025
Mn	0.25	0.90	2.27
P	0.01	0.01	0.006
S	0.005	0.005	0.005
Si	0.25	0.25	0.21
Cr	1.40	0.60	0.24
Ni	2.90	3.50	1.99
Mo	0.40	0.60	0.97
Cu	0.05	1.60	-----
Nb	-----	0.03	0.053
V	0.01	-----	-----
C.E.	0.81	0.81	0.813

C.E.= Carbon Equivalent

$C.E.=C+(Mn+Si)/6+(Ni+Cu)/15+(Cr+Mo+V)/5$

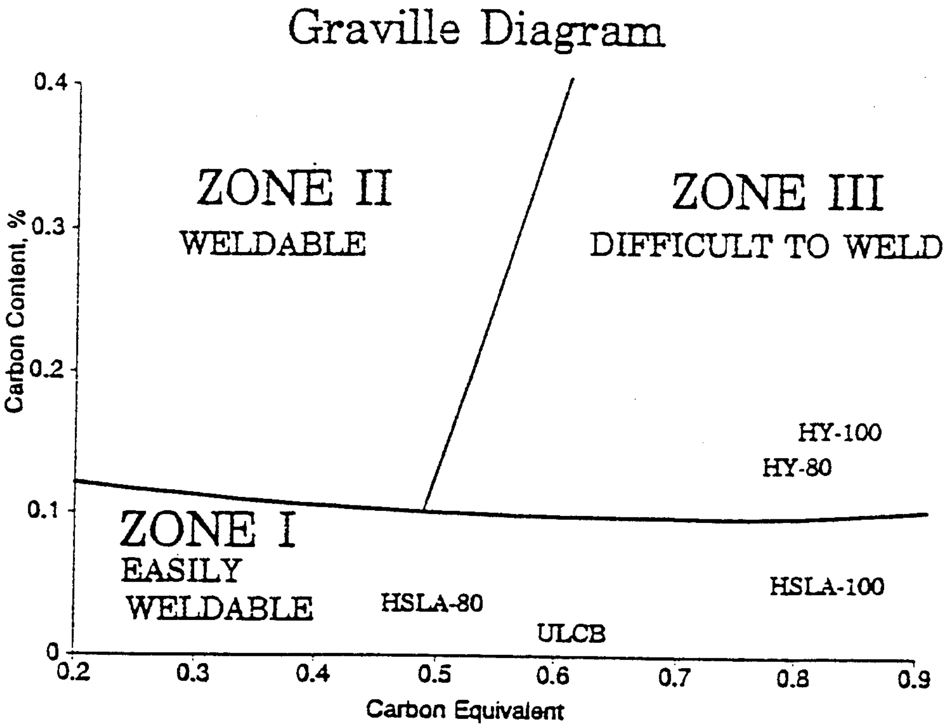

$$C.E. = C + \frac{Mn + Si}{6} + \frac{Ni + Cu}{15} + \frac{Cr + Mo + V}{5}$$

Figure 2.1 Weldability Diagram

(Graville, 1978)

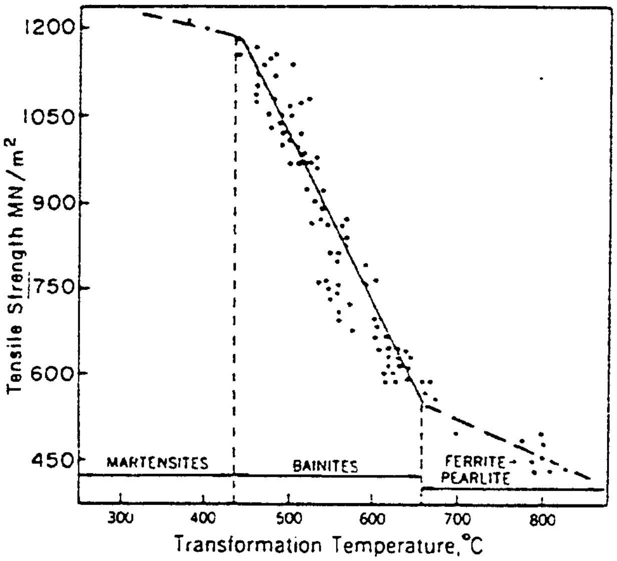

Figure 2.2 Relationship Between 50% Transformation Temperature and Tensile Strength for Bainitic Steels

(Pickering, 1978)

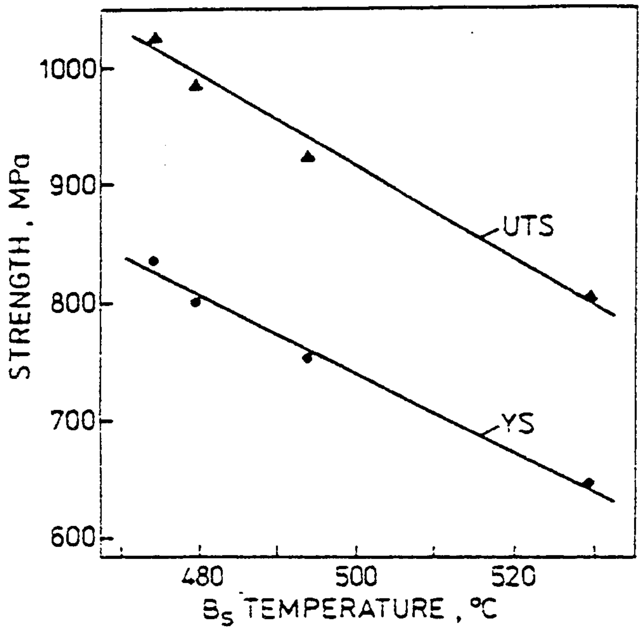

Figure 2.3 ULCB Strength as Related to B_s Temperature

(Blicharski, 1988)

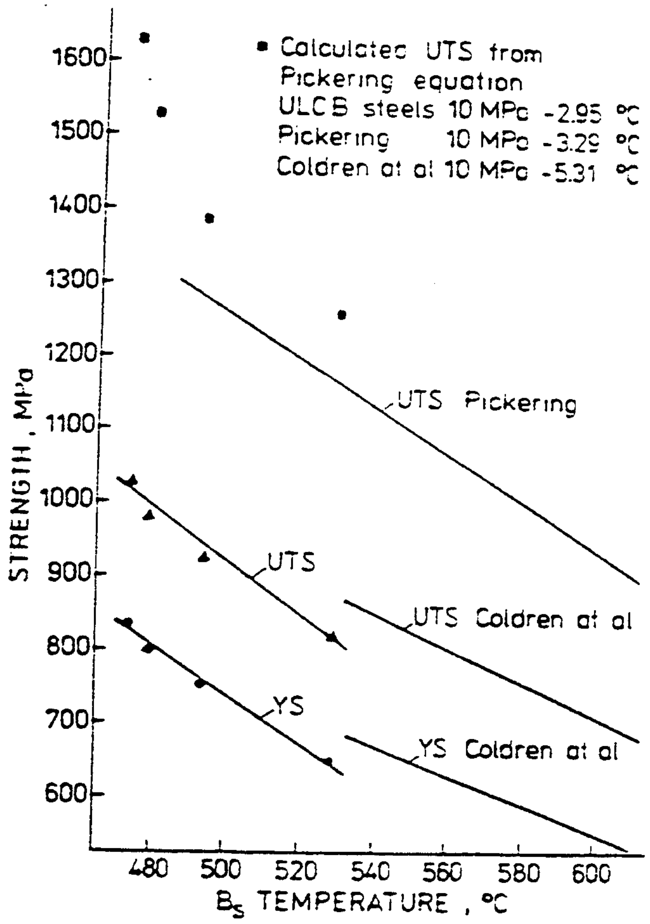

Figure 2.4 Comparison of Measured and Calculated Strength Versus B_s Temperature for Various Bainitic Steels

(Blicharski, 1988)

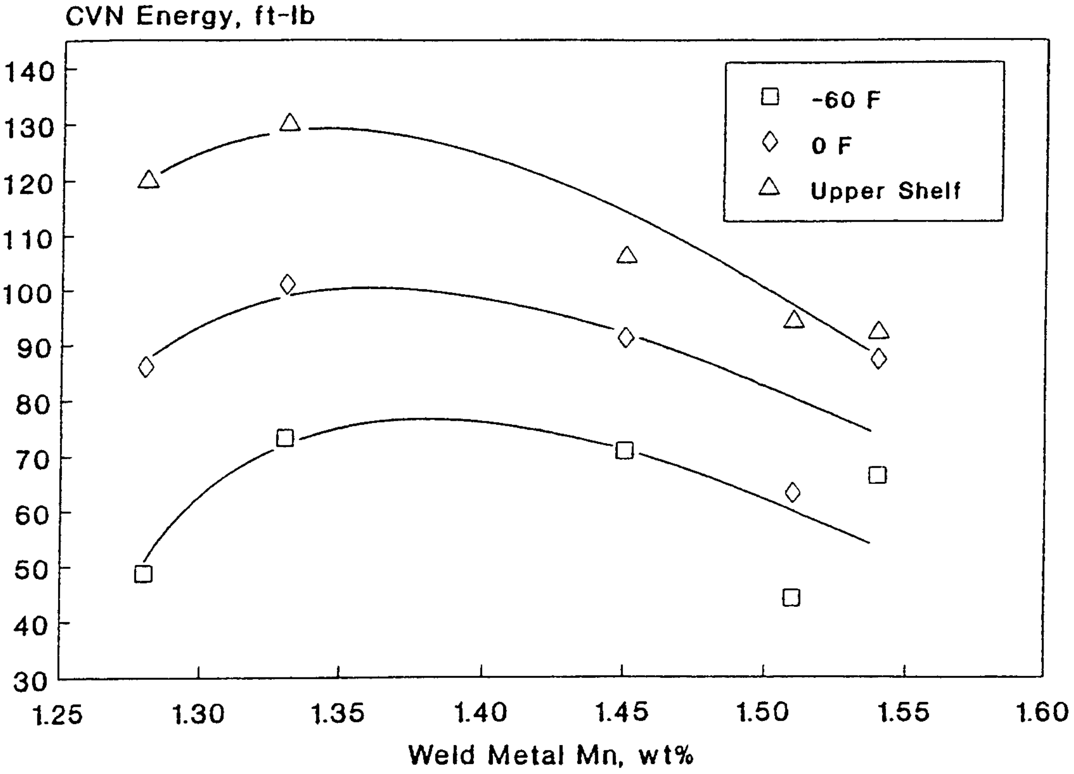

Figure 2.5 Effect of Manganese Content on CVN Performance on Submerged Arc Welds of HY-100 Steels

(DeLoach, 1993)

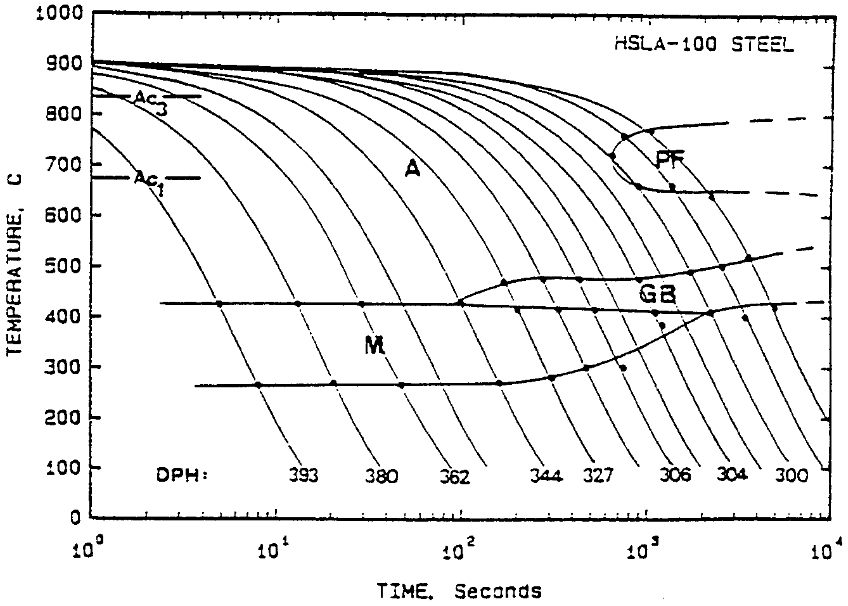

Figure 2.6 CCT Diagram for HSLA-100 Steel

(Wilson, 1988)

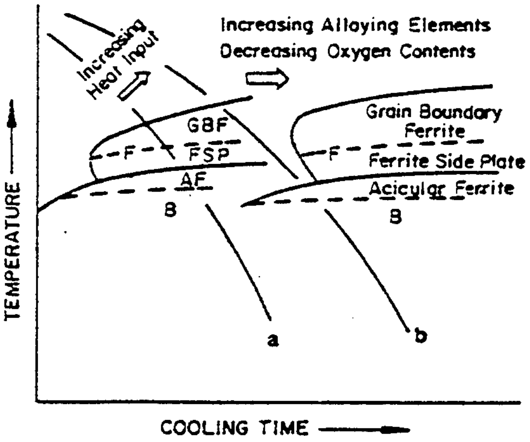
Increasing Heat Input
Increasing Alloying Elements
Decreasing Oxygen Contents
GBF
F
FSP
AF
B
Grain Boundary Ferrite
F
Ferrite Side Plate
Acicular Ferrite
B
a
b
TEMPERATURE
COOLING TIME

Figure 2.7 CCT Diagram for Low-Carbon, Low-Alloy Steel Weld Metal

(Kou, 1987)

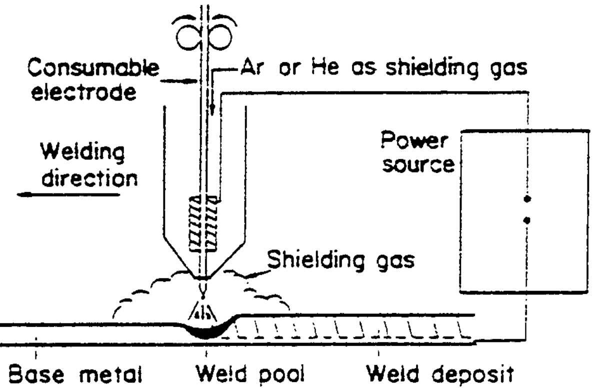
Consumable electrode
Ar or He as shielding gas
Welding direction
Power source
Shielding gas
Base metal
Weld pool
Weld deposit

Figure 2.8 Sketch of GMA Welding Process

(Kou, 1987)

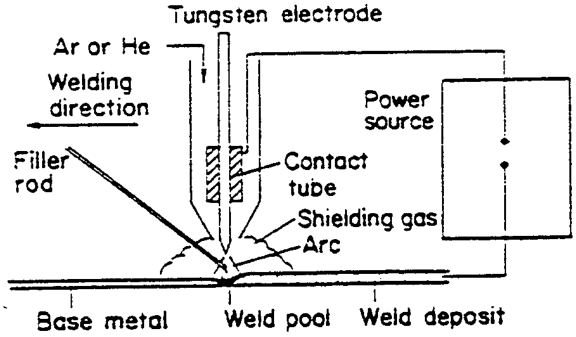
Tungsten electrode
Ar or He
Welding direction
Power source
Filler rod
Contact tube
Shielding gas
Arc
Base metal
Weld pool
Weld deposit

Figure 2.9 Sketch of GTA Welding Process

(Kou, 1987)

III. EXPERIMENTAL PROCEDURE

A. WELD SAMPLES

Seven samples of HSLA-100 steel plate welded with a ULCB (CS1B formulation) weld consumable were provided by the Naval Surface Warfare Center (NSWC), Annapolis. Four of the welds were multi pass GMA welds, while the other three were multi pass GTA welds. Additionally, cover gas and heat input parameters were varied. The types of cover gas used were pure argon (Ar) or a combination of 5% CO_2 and 95% argon (C5). Due to the extreme porosity encountered in the welding of sample MV3 using C5 gas, passes 7 and 8 (located in approximately the center of the fusion zone) of the MV20 sample were welded using C5 gas, while the rest were welded using pure argon. While the porosity of the MV3 weld rendered it useless, available data was used to verify the validity of the MV20 sample. Weld parameter information is included in Table 3.1. Fusion zone chemical analysis was provided by Luvak Inc. in Table 3.2. The methods used in analysis and respective confidence limits are listed in Table 3.3.

B. SAMPLE PREPARATION

Sectioned samples were grit sanded using a Struers Knuth-Rotor-3 and various grits of waterproof silicon carbide paper. Final polishing was conducted using one micron diamond compound on selvyt polishing cloth. The MV20 sample remained in the as polished condition for Scanning Electron Microscope (SEM) work, while all other samples were etched for 15 seconds in 5% nital for all additional work.

Sixteen transverse samples were cut from the fusion zone of the MV20 weld plate. The samples were polished and etched in the same manner as discussed previously, and weld passes 7 and 8 were marked longitudinally. The MV20 samples were then returned to NSWC for tensile and Charpy V Notch (CVN) impact testing.

Utilizing a carbon extraction method, inclusions were removed from the MV20 sample for Transmission Electron Microscope (TEM) Energy Dispersive X-ray (EDX) analysis. The polished MV20 sample was lightly etched for 5 seconds to allow for the location of weld passes 7 and 8, which were then outlined with a scribe. Then, the sample was deep etched for 60 seconds in 5% nital to loosen inclusions. Next, the sample was transferred to an Ernest Fullam EFFA MKII carbon coater where two carbon strands at a distance of 30 millimeters from the sample surface were used to impart a uniform 150-200 angstrom coating the sample surface. Weld passes 7 and 8 were then scribed into a grid pattern of 3 millimeter squares and placed into a bath of 5% nital, carbon side up. After three to five minutes, the 3 millimeter squares would float from the surface of the sample. These squares were carefully lifted from the 5% nital using a 400 mesh copper grid and placed into a solution of 20% acetone and 80% water, where the surface tension of the solution would straighten the sample. Finally, the sample was carefully lifted from the solution using a 400 mesh copper grid and air dried.

C. MECHANICAL TESTING

1. Microhardness Testing

Microhardness testing was conducted on all samples using Buehler Micromet 2003 and 2004 Microhardness Testers. Depending on the sample size, as many as 150 Vickers Hardness (HV) readings were obtained within the fusion zone of the weld. These HV readings were correlated to either columnar or grain refined microstructures using a Zeiss Stereomicroscope.

2. Tensile Testing

Tensile testing was performed by NSWC on samples of the MV weld series, machined from the weld fusion zones. Table 3.4 lists the tensile test results as provided by NSWC.

3. Fracture Toughness Testing

Charpy V- Notch (CVN) impact testing was also conducted by NSWC. CVN energy and total percent ductility were provided by NSWC, and those results are listed in Table 3.5

D. SCANNING ELECTRON MICROSCOPY

Inclusion number, size and volume fraction determination was conducted using a Cambridge Stereoscan 200 scanning electron microscope (SEM) with a LaB_6 filament energized to 20,000 volts. The SEM was operated in backscatter mode to enhance inclusion contrast and resolution. One hundred fields were randomly selected from pass 7 and 8 in the MV20 sample. Inclusion analysis was conducted at 4000 times magnification at a working distance of ten millimeters, resulting in a field of view of 557 square millimeters. Inclusions size and distribution data was then analyzed for average inclusion size and volume fraction. Inclusion statistics for samples MV1 through MV6 were determined in previous work (Beno, 1994).

Twelve Charpy bars were returned by NSWC for fractographic analysis in the SEM. The Charpy bars consist of one upper shelf and one lower shelf sample, or the most extreme high and low temperature sample if the appropriate shelf was not reached. Because of porosity problems, the MV3 sample was determined to be invalid, and was not returned for fractographic analysis. Samples were then studied and photographed in the SEM.

E. TRANSMISSION ELECTRON MICROSCOPY

A JEOL JEM-100 CX II transmission electron microscope (TEM) with a LaB_6 filament energized to 120,000 volts was used to perform EDX analysis of the carbon extracted inclusions of the MV20 sample. Carbon extraction of the inclusions allows for inclusion analysis without the interference of the surrounding steel matrix. When inclusion analysis was performed by SEM with EDX in previous studies, it was determined that inclusion compositional information was being affected by the surrounding matrix material. An erroneous result is obtained because the volume of interaction of the sample with which the SEM interacts extends approximately two microns below the surface of the sample. However, the average size of the inclusions being studied are only 0.5 microns in diameter. Hence, much of the information collected actually relates to the matrix, and not the inclusion.

Ten inclusions were analyzed for compositional data, with little change from one inclusion to the next. Inclusion composition for samples MV1 through MV6 were determined in previous work (Beno, 1994).

F. OPTICAL MICROSCOPY

The Zeiss Stereomicroscope was used to obtain Polaroid photographs of the MV20 sample which were then assembled into a mosaic of the weld cross section. This and previously obtained mosaics were used for qualitative comparison of the weld macrostructures. Specifically, the relative columnar grain size and percentage of grain refinement were of greatest importance to the conduct of this study.

A Zeiss Jenaphot 2000 optical photomicroscope with an attached Minolta 35 millimeter camera were used to obtain optical micrographs of all samples. These micrographs were used qualitative microstructural studies.

Table 3.1 Welding Parameters

Sample	**Weld Type/Passes**	**Cover Gas**	**Heat Input (KJ/in.)**
MV1	GMA/8	C5	60
MV2	GTA/23	Argon	60
MV3	GTA/7	C5	78-161
MV4	GMA/5	C5	97
MV5	GMA/14	C5	30
MV6	GMA/9	Argon	60
MV20	GTA/13(2)	Argon(C5)	63-127

Table 3.2 Weld Metal Compositions (wt%)

(MV - Luvak, Inc., CS1B - NSWC)

	HSLA - 100	ULCB (CS1B)	MV1	MV2	MV4	MV5	MV6	MV20
C	0.04	0.025	0.028	0.012	0.022	0.021	0.018	0.015
Mn	0.90	2.27	2.00	2.38	1.90	2.01	2.22	1.86
Si	0.25	0.21	0.17	0.21	0.15	0.13	0.22	0.11
P	0.01	0.006	<.004	<.004	0.007	<.004	<.004	0.005
S	0.005	0.005	0.006	0.003	0.004	0.006	0.003	0.010
Ni	3.50	1.99	1.90	1.92	1.92	1.89	1.91	1.92
Mo	0.60	0.97	0.94	0.98	0.94	1.02	0.96	0.88
Cr	0.60	0.24	0.35	0.31	0.33	0.26	0.32	0.30
Nb	0.03	0.053	0.046	0.050	0.043	0.044	0.049	0.054
Al	-----	0.007	0.006	0.006	0.005	0.004	0.009	0.0028
Ti	-----	0.011	0.004	0.006	0.008	0.006	0.007	0.0042
Cu	1.60	-----	0.29	0.18	0.34	0.078	0.23	0.17
O	-----	0.003	0.030	0.008	0.031	0.039	0.015	0.019
N	-----	0.007	0.008	0.008	0.009	0.008	0.010	0.0088

Table 3.3 Chemical Analysis Methods

(Provided by Luvak, Inc.)

Element	Analysis Method	Confidence Limit +/- (wt %)
Carbon	Combustion Infrared	0.001
Manganese	Plasma Emission	0.02
Silicon	Plasma Emission	0.01
Phosphorus	Plasma Emission	0.002
Sulfur	Combustion Automatic Titration	0.001
Nickel	Plasma Emission	0.05
Molybdenum	Plasma Emission	0.01
Chromium	Plasma Emission	0.02
Vanadium	Plasma Emission	0.001
Aluminum	Plasma Emission	0.002
Titanium	Plasma Emission	0.001
Zirconium	Plasma Emission	0.001
Copper	Plasma Emission	0.001
Oxygen	Inert Gas Fusion, TC 136	0.001
Nitrogen	Inert Gas Fusion, TC 136	0.001
Boron	Plasma Emission	0.001
Hydrogen	Vacuum Hot Extraction	0.00001
Niobium	Plasma Emission	0.001

Table 3.4 Weld Sample Ultimate Tensile Strength and Yield Stength (ksi.)

(Provided by NSWC)

	Yield (YS)	Ultimate (UTS)	YS/UTS
MV1	113.0	126.8	0.89
MV2	103.1	119.8	0.86
MV4	111.1	126.3	0.88
MV5	126.7	131.8	0.96
MV6	109.2	121.7	0.90
MV20	104.4	117.8	0.89

Table 3.5 Weld Sample CVN Energy (J) and (Total %Ductility)

(Provided by NSWC)

Temp (°C)	MV1	MV2	MV4	MV5	MV6	MV20
-84.4		21.0 (4.5)				
-51.1		164.1 (100)				
-18.6						32.5 (4.5)
-17.8	19.7 (15)	232.5 (99.5)	16.9 (12.5)	27.1 (40)	64.4 (55)	
-1.1						76.6 (38.5)
20	52.2 (20)	245.4 (100)	43.4 (12.5)	63 (52.5)	126.1 (77.5)	99 (72.5)
48.9	95.6 (71)		69.1 (72.5)	68.5 (65)	145.7 (90)	
55.8						160.7 (97)
82.2	103 (92.5)		105.8 (92.5)	79.3 (97.5)		
87.2						128.1 (95)
FATT(°C)	37.2	-68.3	38.3	12.2	-26.1	6.1

IV. RESULTS AND DISCUSSION

A. WELD METAL COMPOSITION

Results provided in Table 3.2 were used to investigate the deoxidizer depletion in the weld pool as oxygen content increased. As the amount of free oxygen increased in the weld pool, participation by the oxide formers (Al, Ti, Si, Mn and Cr) likewise increased, leading to a depletion of these elements in the weld pool. Deoxidization of the weld pool results in the formation of inclusions that are size and volume fraction dependent on the weld pool oxygen content. Furthermore, some of the deoxidizers that are removed from the weld pool are also important to the overall strength and toughness of the weld metal.

Al and Ti are the strongest deoxidizers, and would therefore be expected to drop rapidly as oxygen increases in the weld pool. Figure 4.1 is a plot of Al with respect to weld pool oxygen, showing a general downward trend in Al as oxygen increases. When GMA and GTA weld processes are considered separately, as is also shown in this figure, two trends can be observed. First, Al is clearly being depleted with increasing weld metal oxygen for both weld types. Secondly, it would appear that Al depletion occurs more readily during GTA welding. Ti would also be expected to decrease with increased oxygen. However, considerable data scatter made it difficult to spot a trend. Considering that the differences in weld pool concentrations of Ti, and even Al, are practically within experimental error of the analysis, as demonstrated by Table 3.3, this is, perhaps, not surprising.

As the weld pool oxygen content increases, Si and Mn participate more extensively in the deoxidation as shown in Figures 4.2 through 4.3. Similar to trends seen for Al depletion, Mn and Si appear to deplete more readily in GTA welds, and possibly at a higher rate than is observed in GMA welds.

Finally, consideration was given to the variation of carbon in the weld metal. Figure 4.4 shows that the carbon content generally increased in the weld metal with increased oxygen content. While the trend is an increasing carbon content with weld metal oxygen, the figure suggest that the GMA welds, specifically the GMA welds using C5 cover gas, have the highest carbon content. The increased amounts of carbon in the weld metal can be explained by Equations 4.1 and 4.2 below:

$$CO_2 = CO + \tfrac{1}{2}O_2 \tag{4.1}$$

$$CO = C + O \tag{4.2}$$

These two equations represent the probably dissociation of CO_2 which exists in the C5 cover gas, and explain why welds using C5 gas will have higher contents of both carbon and oxygen.

B. NON-METALLIC INCLUSIONS

Inclusion chemical and oxide composition data for MV20 are provided in Table 4.1 and 4.2 respectively. The inclusion chemical and composition data for all MV samples are summarized in Table 4.3. Table 4.4 contains inclusion number, size and volume fraction information while Table 4.5 is a presentation of inclusion size distribution data.

1. Composition

Inclusion compositional data, displayed in Table 4.3 provides a much clearer picture of the depletion of the most reactive deoxidizers, Al and Ti. Figures 4.5 and 4.6 show that with increased oxygen, both Al and Ti decrease rapidly in GMA welds. Likewise, a similar trend is suggested for GTA welds. At low weld metal oxygen contents, Al and Ti are capable of providing much of the weld pool deoxidation; hence, they are large contributors to the overall inclusion composition. As weld metal oxygen content approaches 200 ppm, the amount of oxygen in the weld pool is such that much of the Al and Ti are depleted, so much of the weld pool deoxidization is performed by the less reactive, but more abundant elements, Mn and Si.

With Al and Ti performing most of the weld metal deoxidation at low oxygen contents, and Mn and Si perform in the same manner at high oxygen contents, the inclusion compositional trends would be expected to be opposite of that seen for Al and Ti. Figures 4.7 and 4.8 verify that this is, indeed, the case. Also note that while Mn and Si depletion occurred more readily in the GTA welds, both appear to be more abundant in the GTA weld inclusions.

While Mn does not deoxidize as readily as Al, Ti and even Si, its overwhelming abundance in the consumable (2.27 wt.%) dominates inclusion composition, through the formation of MnO and MnS. Therefore, Mn is always the largest contributor to oxide/sulfide formation. Similarly, Si composition follows that of Al and Ti, resulting in small amount of SiO_2 oxide formation when a sufficient amount of Al and Ti exists for deoxidization. In the much higher oxygen content C5 welds, Si takes a larger role in the deoxidization process.

2. Size and Volume Fraction

Through the formation of non-metallic oxide inclusions, the amount of weld pool oxygen directly affects the average size (hereafter referred to only as "size"), and volume fractions (indicated by "V_f" in the associated plots) of these inclusions. Figure 4.9 shows a plot of both the size and volume fraction with respect to weld metal oxygen content. These two variable are shown together on one graph to illustrate that the variation of both size and volume fraction have a few similarities. Additionally, this figure suggests that both size and volume fraction experience two separate trends depending on oxygen content.

The two trends that size and volume fraction appear to follow are that both appear to increase until the weld metal oxygen content is in the vicinity of 200 to 300 ppm. Afterwards, both size and volume fraction appear to decline. Figure 4.10 illustrates the increasing trend while Figure 4.11 illustrates the decreasing trend. Note that the MV20 sample was included in both figures as a point of reference. Studies of HSLA steels welded by the Submerged Arc Welding (SAW) processes by Liu and Olson, concluded that inclusion size decreased at high oxygen concentration levels due to an increased occurrence in inclusions less than 0.1 microns in diameter. (Liu, 1986). While this study attributed these small inclusions to the reduction of inclusion size and volume fraction, the data presented here suggests the same results may also occur for GMA welding processes at high weld metal oxygen contents, despite the lack of any measured inclusion, 0.1 microns in size or less.

C. MECHANICAL PROPERTIES

Tensile test results, listing Ultimate Tensile Strength (UTS), Yield Strength (YS), and Charpy V-Notch (CVN) Toughness results are tabulated in Tables 3.4 and 3.5 respectively. Microhardness results are listed in Table 4.6.

1. Tensile Strength

The requirement for an acceptable weld consumable is that the YS of all samples must be in the range of 102-122 ksi. Because the strength requirements pertain specifically to YS, it will be the primary parameter of concern. Consideration will be given to UTS as is necessary for clarification or emphasis purposes.

Figure 4.12 shows an increase of both UTS and YS with increased oxygen content clearly demonstrating that strength is a function of the weld metal oxygen content. The effect of inclusion volume fraction on YS was unclear due to data scatter. The comparison of any data against power settings was generally difficult because of the limited amount of weld samples. Nevertheless, several affects on strength could be observed despite the limited data, and are shown in Figure 4.13. First, a general decrease in YS was observed as power increased. Second, GTA welds displayed lower strength then that of GMA welds that results, at least partially, from the grain refinement produced by reheat of the previous passes. The increase in the number of weld passes in the lower power GMA welds did not produce the same effect, since the low deposition GTA welds provide more frequent and extensive reheating of previous passes than did the GMA welds.

Although Mn and Si have a major Carbon Equivalent (CE) contribution, no strong relationship could be found between the contribution of either element to the overall weld composition and weld strength, including both UTS and YS. Carbon, on the other hand, was shown to have a major effect on the YS despite its extremely low content (0.012-0.028 wt%). Figure 4.14 shows the general increase of YS with increased carbon content. While the effect of carbon on increasing strength is a well documented and obvious conclusion, its effect upon strength at this low a content is worth noting.

2. Microhardness

Average fusion zone Vicker's Hardness (HV) listed in Table 4.6 were used for comparison against UTS. Figure 4.15 shows that HV increased linearly with UTS. Additional comparisons between HV and weld metal oxygen, volume fraction, size, and welding power verified the linearity that existed between HV and UTS.

3. Impact Testing

Recall that the specified Charpy V-notch (CVN) impact toughness requirement for the new weld consumable are 61 J (45 ft-lb) at -51°C (-60°F) and 81 J (60 ft-lb) at -18°C (0°F). The only sample that meets this requirement is MV2. NSWC did not conduct tests below -18°C (0°F) for the other samples when it was observed that they did not meet the higher temperature requirement. Tests conducted on these samples were used to determine upper shelf CVN energy values when variations of weld type, cover gas and power level were used. Using ductility information provided by NSWC, the Fracture Appearance Transition Temperature (FATT) was calculated. CVN curves will be compared to each other to determine the effect of each weld parameter, while the FATT will be used to relate the toughness of a given sample the other weld pool variables that have been discussed. Figures A.1 through A.6 are photographs of ductile and brittle CVN samples. Brittle samples are representative of minimum temperature samples. Ductile samples represent either upper shelf or maximum temperature samples, when the upper shelf was not well defined.

a. CVN Impact Curves

Figure 4.16 is a plot of the CVN impact toughness curves for all weld samples. Since the samples represented by these curves were welded with different welding processes (GMA and GTA), cover gases (argon and C5) and power levels (30-97 KJ/in.), comparisons were made by varying one of the parameters while holding the other two constant. These comparisons were then used to determine the effect that a given weld parameter on CVN toughness.

The difference in toughness between GMA and GTA weld sample toughness is shown in Figures 4.17 and 4.18. Both figures demonstrate that GTA welds have a superior toughness then GMA welds; although, the separation between the welds using C5 cover gas is less then those welds using argon. Increased grain refinement observed in multipass GTA welds is often credited with the improved weld toughness of GTA welds over GMA welds.

Figure 4.19 shows the difference in toughness when different cover gases are used. Apparent in this plot is that a weld conducted with argon gas (MV6) provides superior toughness than a weld conducted with C5 gas (MV1). Since the weld type and power settings are the same, the figure shows that the addition of CO_2 to the weld metal, by the C5 cover gas, has a significant effect on the weld toughness through either a contribution of carbon or oxygen. No GTA welds were conducted at the same power, with different cover gases. However, power did not appear to be a major factor in toughness, which will be discussed momentarily, so a CVN toughness comparison was made between the only two available GTA weld samples, MV2 and MV20, based on that assumption. Bearing in mind that these welds have different power levels, the sample with the lower toughness is, again, the one using C5 as a cover gas (MV20), as shown in Figure 4.20.

Figure 4.21 is a comparison of three GMA welds with C5 cover gas, conducted at different power levels. Despite the difference of at least 30 KJ/in. per weld, the CVN curves for these three samples plotted closely together. For the limited amount of samples in this study, it can only be concluded that power variations have a minimal effect on toughness.

A final comparison between a GMA weld conducted with argon (MV6), and a GTA weld conducted with C5 gas (MV20), plotted in Figure 4.22, shows that both welds have similar toughness characteristics. The level of toughness of these samples is intermediate with respect to all other samples. Figure 4.23 is an overlay of two previously compared samples, which reveals the following two trends. First, MV6 demonstrates an improvement in toughness over MV4 when the cover gas is changed from C5 to argon. Second, MV20 demonstrates improved toughness over MV4 when the weld process is switched from GMA to GTA.

These last two plots emphasize two specific trends that are repeated throughout the comparisons of the other CVN toughness curves. The first trend is that a change from GMA to GTA welding will improve weld toughness. This is a generally understood principle, which will be backed up by microstructural observations introduced later. The second trend is that samples welded by the argon cover gas have improved toughness over those welded by C5 cover gas. Through the cover gas introduction of CO_2 to the weld metal, either oxygen's contribution to inclusion volume fraction, carbon's contribution to the formation of harder bainitic or martensitic microstructures, or both are affecting weld toughness.

b. FATT Comparisons

Figure 4.24 shows that FATT generally increases as weld metal oxygen content increases. However, this figure also suggests that, above about 200 ppm, FATT levels off, followed by a decline as oxygen approaches 400 ppm. Recall that this trend was also observed when oxygen content was compared to the inclusion size and volume fraction. When FATT is compared to inclusion volume fraction, as shown in Figure 4.25, it is observed to increase in an approximately linearly fashion with volume fraction. The relationship between FATT and inclusion size is a bit more complicated. Figure 4.26 shows that FATT increased with increasing inclusion size, but then levels, and eventually drops as inclusion size exceeds 0.5 microns. While it would be expected that increased inclusion size would increase FATT, the reason why it decreases with continued size increase is unclear, and may be the result of data scatter.

Figures 4.27 and 4.28 clearly demonstrate that FATT also increases with increased carbon content and UTS. Both plots show that the variation of FATT with carbon content and UTS, is quite significant.

Again, due to the lack of weld samples conducted at different power settings, no trend was observable between FATT and power level. Nevertheless, some interesting points were observed, similar to the CVN comparisons when welds were analyzed for a given power setting. The use of argon as a cover gas, rather than C5, produced a significant reduction in FATT, while the switch from GMA to GTA produced reduction of FATT that was approximately one-half that seen by changing the cover gas. Also, there was a significant increase in FATT when power was increased from 30 KJ/in. (MV5) to 60 KJ/in. (MV1), but little additional change thereafter as power was increased to 97 KJ/in. (MV4). This phenomenon was not obvious in the comparison between CVN curves, and will be given further consideration in the next section.

D. FRACTOGRAPHY

Fractography of the ductile samples revealed failure that would typically be expected in such samples, as shown in Figure 4.29. The highlight of these samples is that the microvoids or dimples of all the fracture surfaces were nucleated by inclusions. In many cases, inclusions were observed in practically every dimple, as Figure 4.30 demonstrates. For the most part, fractographic studies of the weld samples focused on the brittle CVN samples, where mixed-mode failure was always observed. The brittle samples studied were taken from the lowest temperature fracture samples, and the analysis presented here is of a comparative nature. With the results of the CVN toughness curves and FATT in mind, an attempt was made to correlate features of the fractographs with weld parameters, weld pool chemistry and inclusion data.

Fractographs of two brittle samples welded at constant power and the same cover gas were analyzed first. Samples MV2 (GTA) and MV6 (GMA), welded at 60 KJ/in. with argon as a cover gas are shown in Figures 4.31 and 4.32. Both samples show mixed-mode failure that is almost entirely brittle cleavage. Other apparent features are a few small cracks in the matrix as well as small dimpled ridges. Both weld samples have a low carbon content and inclusion volume fraction as a result of the use of argon as a cover gas. Therefore, the amount of dimpling that can be seen in the fracture surface is small.

The next two brittle samples studied were also welded by different weld processes with constant power and the same cover gas. Samples MV4 (GMA) and MV20 (GTA), shown in Figures 4.33 and 4.34 differ in that they were welded using C5 cover gas, and higher power levels than the first two samples. These two samples have the highest volume fraction of inclusions of all samples. Evidence of the effect of a high volume fraction of inclusions is particularly obvious in the MV20 samples. Figure 4.35 shows inclusion in most of the visible dimples of MV20, again demonstrating that the increased volume fraction of inclusions is the most like cause of the formation of ductile ridges. A characteristic that is observed in all brittle samples. Furthermore, there does not appear to be a direct correlation between the inclusion volume fraction and the observable amount of intergranular cracking. Figure 4.36 suggests that intergranular cracking is extensive in the MV4 sample as compared to MV20. Although MV4 has a higher weld metal oxygen content than MV20, the average inclusion size of MV4 much less then that of MV20 while its inclusion volume fraction is about the same. This indicates two different trends: First, increased inclusion volume fraction has a partial effect of reducing toughness. Second, intergranular cracking further reduces toughness, but inclusion size or volume fraction do not appear to be directly related to this crack formation.

Samples MV4, MV5 and MV1 are all GMA welds with C5 cover gas. Figures 4.36 through 4.38 are SEM fractographs of all three samples. The MV5 weld, conducted at the lowest power setting, is mixed-mode failure, dominated by transgranular cleavage, with areas of ductile failure encircling the cleaved areas. Small cracks, similar to those observed in the MV6 sample, can also be seen throughout the fracture surface. MV1 and MV4, welded at higher power increments, exhibit a few additional features of note. First, the surfaces of both MV1 and MV4 exhibit more cleavage and intergranular failure than MV5. Unlike the general flat areas of ductile failure that is seen in MV5, the ductile failure observed in MV1 and MV4 appear more as an angled ridge of shear lip that extends from one area of cleavage to another. Second, the intergranular cracking that occurs in MV1 and MV4 is much more severe then that which is seen in MV5. Typical cracks in both samples are usually several times longer than those seen in MV 5 and tend to branch at granular triple points, suggesting the occurrence of extensive intergranular delamination in these samples.

Next, a comparison was made between MV1 and MV6 weld samples, comparing the effect of cover gas variation upon a GMA weld conducted at 60 KJ/in. Fractographs of these samples are shown in Figures 4.39 and 4.40. Refer also to Figures 4.32 and 4.38 for additional fractographs of these two samples. The MV1 sample, using C5 cover gas, exhibits extensive intergranular cracking, cleavage and a very uneven surface. The surface of MV6, using argon cover gas, is also generally cleaved, but different plains of cleavage are observable in this sample, connected by small ductile ridges. MV1 has a higher weld pool oxygen content, inclusion size and volume fraction than MV6. Thus, increased volume fraction in conjunction with extensive intergranular cracking observed in the fractographs, results in a lower toughness for the MV1 sample.

The final comparison conducted was between two GTA welds, MV2 and MV20, that were welded using different cover gases and power. Since the power difference between the higher power welds does not appear to be significant in determining toughness, it will be assumed that most of the differences in fractography can be related to cover gas. Figure 4.41 and 4.42 show these samples. Figures 4.31, 4.34 and 4.35 may also be used for reference. Both MV2 and MV20 samples have the least intergranular cracking of all weld samples. Also, a maximum inclusion size and volume fraction differences exist between these two samples, with MV20 having the larger of the two.

This comparison shows that inclusions, mainly inclusion volume fraction have a definite major effect on weld toughness.

E. MICROSTRUCTURAL ANALYSIS

1. Macroscopic

Figures B.1 through B.6 are photographic montages of the weld samples. Visual inspection of these photographs as compared to other weld parameters are summarized in the following paragraphs.

The two GTA welds, MV2 and MV20 (Figure B.1 and B.6), are easily discernible from the other samples, since both have the least amount of columnar grain structure. Both MV2 and MV20 have equally low strengths, while MV2 has the highest toughness of all samples by far. The lower strength, with respect of other samples can be attributed by a virtual absence of columnar grain structure, with exception of the final pass. While MV20 is slightly more columnar in nature, these photographs lend no additional information that explains why there exists such a large difference in toughness between the two.

Study of the three GMA welds with C5 cover gas and varying power, namely MV1 (Figure B.1), MV4 (Figure B.3) and MV5 (Figure B.4) yields the following information. With an increase in power, more heat is transferred to the weld pool since the consumable acts as the electrode in the GMA welding process. Hence, penetration of each weld pass is greater, and fewer weld passes are required, as expected. Another remarkable feature is the difference in appearance between MV5 and the other two welds. Because of the lower power of the MV5 weld, the columnar grains tend to grow in a roughly uniform vertical direction, and tend not to impinge upon one another at the centerline of each weld pass. While all three welds have similar impact toughness, MV5 has a significantly higher YS than the other welds two weld passes.

Although it was welded at the same power level as MV1, MV6 (Figure B.5) did not achieve the same amount of penetration. Furthermore, the use of argon with the

GMA welding, results in an unstable arc. This result can be seen near the magnification bar in the form of small amounts of porosity.

2. Microscopic

MV1, MV4 and MV5 are three GMA weld samples using C5 cover gas, and had the lowest toughness and highest strength. MV5 has the highest overall strength of all samples, followed by MV1 and MV4 which have similar UTS and YS. All have similar microstructures of lath bainite or martensite. Figures 4.43 and 4.44 are representative micrographs of this microstructure taken from the MV5 sample. It was also noted that the laths of the MV5 samples were a bit more continuous within a given grain and extended almost completely across the columnar grain. This may explain why the strength of MV5 is higher then that of MV1 and MV4. Figure 4.45 is a micrograph showing that this lath-like microstructure is arranged in "packets" in the grain refined region. The "packeted" laths are preferable from a toughness standpoint over the non-packeted laths because of their enhanced crack arresting ability. However, this region is relatively limited, so any increase in toughness provided by this region is obviously overridden by the columnar grain region.

Samples MV6 and MV20 demonstrated intermediate toughness, and strength that was in the low range for all samples. Both samples are similar in appearance in that their microstructures are lath-like in the columnar regions as shown in Figure 4.46. These two samples differ from the previous three that were discussed in that individual lath packets in these samples are smaller, and the individual lath lengths appear to be shorter. In the grain refined area that makes up about one half of MV6 and most of MV20, the lath packets have been refined, as shown in Figure 4.47 and 4.48. In addition to the smaller packets of lath bainite/martensite, evidence of equiaxed ferrite can also be seen.

Figures 4.49 is a typical micrographs of the highest toughness sample, MV2. This sample differs from all other samples in that its microstructure is primarily equiaxed ferrite throughout. The MV2 weld has the lowest carbon content of all welds. Hence, the microstructure that forms is equiaxed ferrite, explaining the high toughness and low strength of this sample.

One additional comparison was made between the MV20 and MV2 weld samples, both of which are GTA welds that were produced using C5 and argon cover gas respectively. While both samples have very similar UTS and YS values, a large difference exists in the CVN toughness between the two samples. Assuming, from previous arguments, that the weld power can be disregarded, then the toughness that results from microstructural differences between the weld types would be dependent on the cover gas. While the MV2 samples featured a microstructure of equiaxed ferrite, shown in Figure 4.49, the increase of carbon content in the MV20 of 0.007 wt% carbon may have been significant enough to begin the formation of lath microstructure of bainite, martensite, or a combination of the two. Recall, also that the higher oxygen content of the MV20 sample was responsible for removing alloying elements that were important to bainite start depression. The high cooling rate GTA welds, combined with a change in bainite start temperature may have resulted in the onset of martensite/bainite formation. In addition, the inclusion volume fraction in MV20 is much higher. Combined with the microstructural change in the weld, compared to that of MV2, would almost certainly mean that MV20 would have an inferior toughness to MV2. A similar effect would also be experienced in the GMA welds where the high weld metal oxygen content and higher carbon content are able to offset the reduced cooling rate in this weld type.

Table 4.1 MV20 Inclusion Chemical Composition (at%)

	Al	Si	S	Ti	Cr	Mn
1	0.21	12.23	19.14	1.82	0.66	65.95
2	0.98	14.71	10.81	2.74	0.44	70.32
3	0.13	17.62	12.03	1.52	0.76	67.94
4	0.39	18.22	9.08	2.66	0.63	69.02
5	0.06	17.48	11.83	1.82	0.59	68.22
6	0.29	12.63	17.49	1.99	0.45	67.16
7	0.40	14.68	17.33	1.69	0.94	64.95
8	0.27	12.89	21.25	1.88	1.05	62.66
9	0.38	13.12	21.44	1.79	0.57	62.70
10	0.18	13.73	22.77	2.83	0.35	60.14
Ave.	**0.33**	**14.73**	**16.32**	**2.07**	**0.64**	**65.91**

Table 4.2 MV20 Inclusion Oxides (wt%)

	Al_2O_3	SiO_2	TiO_2	Cr_2O_3	MnO	MnS
1	0.18	20.91	3.11	0.56	53.36	21.82
2	0.75	22.64	4.22	0.34	61.06	11.09
3	0.10	27.17	2.34	0.59	57.48	12.37
4	0.29	27.06	3.95	0.47	59.34	8.99
5	0.05	26.85	2.80	0.45	57.74	12.11
6	0.24	21.14	3.33	0.38	55.43	19.52
7	0.33	24.31	2.80	0.78	52.57	19.13
8	0.23	22.54	3.29	0.92	48.28	24.78
9	0.33	22.95	3.13	0.50	48.11	25.00
10	0.16	24.14	4.98	0.31	43.80	26.69
Ave	0.27	23.97	3.39	0.52	53.72	18.15

Table 4. 3 Inclusion Element and Oxide Compositions (wt%)

	MV1	MV2	MV3	MV4	MV5	MV6	MV20
Al	2.51	15.77	18.25	2.29	0.58	30.29	0.19
Si	12.85	2.88	7.86	13.88	13.65	1.88	8.49
S	3.82	5.37	2.83	4.58	4.98	3.86	11.17
Ti	5.92	24.47	7.66	4.45	2.37	22.30	2.12
Cr	0.00	0.00	1.53	0.00	0.00	0.00	0.71
Mn	74.90	51.52	61.88	74.79	78.42	41.66	77.32
Al_2O_3	4.63	23.93	28.72	4.05	1.05	42.66	0.27
SiO_2	16.25	3.01	8.47	17.02	17.06	1.79	23.97
TiO_2	7.19	25.22	8.22	5.37	2.92	21.02	3.39
Cr_2O_3	0.00	0.00	2.79	0.00	0.00	0.00	0.52
MnO	56.41	29.62	41.88	58.56	22.57	52.89	53.72
MnS	15.52	18.22	9.92	18.23	20.11	11.97	18.15

Table 4.4 Inclusion Statistics

(MV1 - MV6 Beno, 1994)

	Total Number of Inclusions	Average Size (microns)	Volume Fraction (%)
MV1	271	0.524	0.325
MV2	209	0.332	0.101
MV3	214	0.613	0.351
MV4	259	0.574	0.372
MV5	364	0.439	0.306
MV6	366	0.385	0.237
MV20	364	0.678	0.345

Table 4.5 Inclusion Size Distribution Data

(MV1 - MV6 Beno, 1994)

	MV1	MV2	MV3	MV4	MV5	MV6	MV20
0.1	0	0	0	0	0	0	0
0.2	19	57	10	2	31	62	0
0.3	52	88	41	48	112	124	1
0.4	59	28	37	50	87	71	22
0.5	42	20	31	40	51	59	75
0.6	35	10	23	33	41	32	101
0.7	17	5	14	35	22	10	40
0.8	16	1	13	23	7	5	77
0.9	15	0	10	11	8	2	15
1.0	9	0	15	7	2	0	17
1.1	2	0	4	3	0	0	5
1.2	1	0	3	1	0	0	6
1.3	0	0	5	0	0	1	1
1.4	2	0	1	1	0	0	1
1.5	1	0	1	1	1	0	1
1.6	0	0	1	0	1	0	0
1.7	0	0	1	3	0	0	0
1.8	0	0	1	1	1	0	1
1.9	0	0	1	0	0	0	0
2.0	0	0	1	0	0	0	0
2.1	0	0	1	0	0	0	0
2.2	1	0	0	0	0	0	0

Table 4.6 Weld Sample Vicker's Hardness Data

	Fusion Zone (FZ) Ave.	Columnar FZ	Grain Refined FZ	HAZ Ave.	Coarse Grained HAZ	Fine Grained HAZ	Base Metal
MV1	307.9	305.6	318.0	306.2	316.3	295.4	273.1
MV2	265.6	258.4	269.6	300.4	315.6	286.1	271.6
MV3	274.5	267.1	282.8	291.4	304.8	283.1	259.1
MV4	296.7	293.7	302.8	300.5	306.3	290.5	279.9
MV5	321.9	319	326.9	314.6	317.4	313.3	274.4
MV6	294.6	292.6	298.1	307.2	314.5	299.1	274.4
MV20	273.1	274.5	272.1	------	------	------	272.8

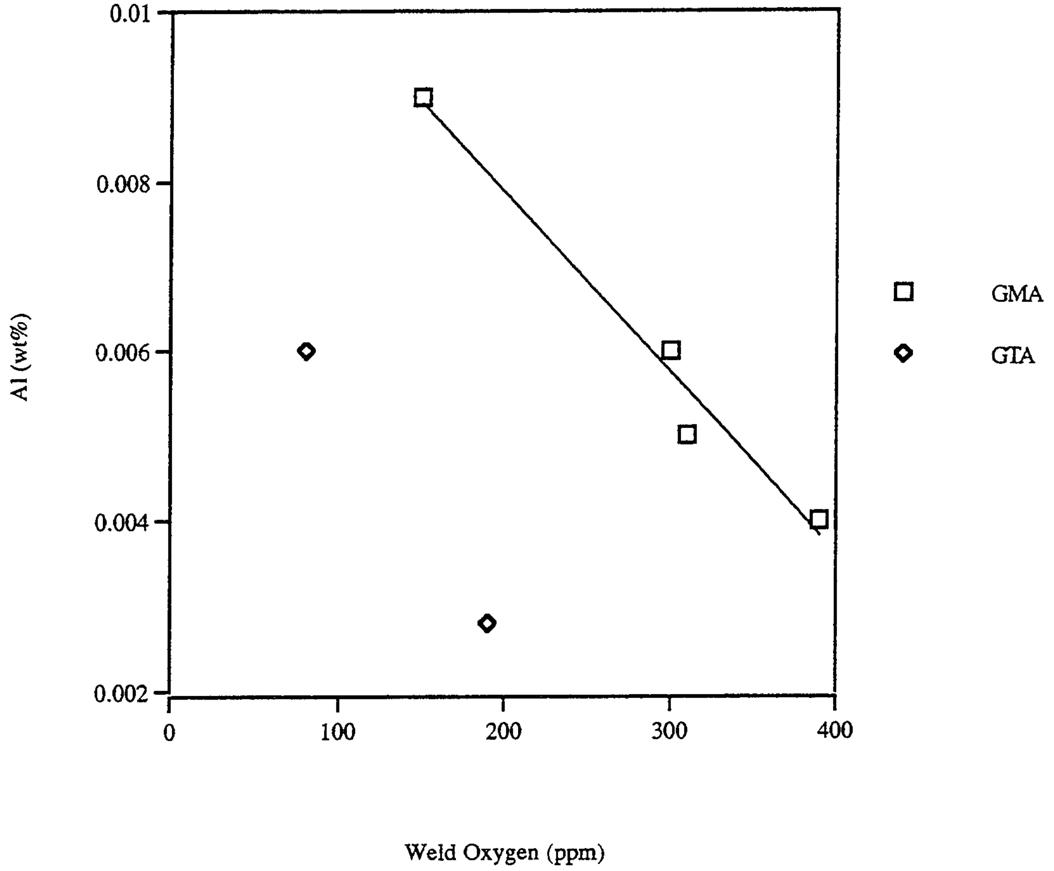

Figure 4.1 Weld Metal Aluminum vs. Oxygen

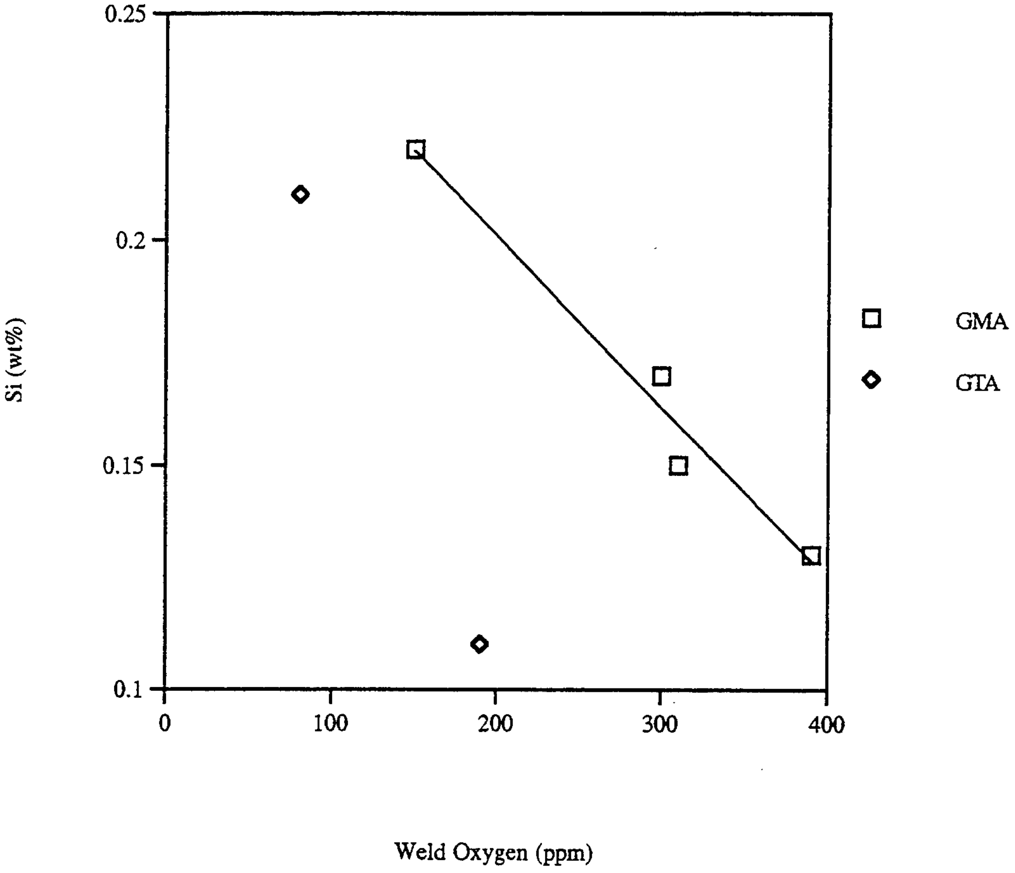

Figure 4.2 Weld Metal Silicon vs. Oxygen

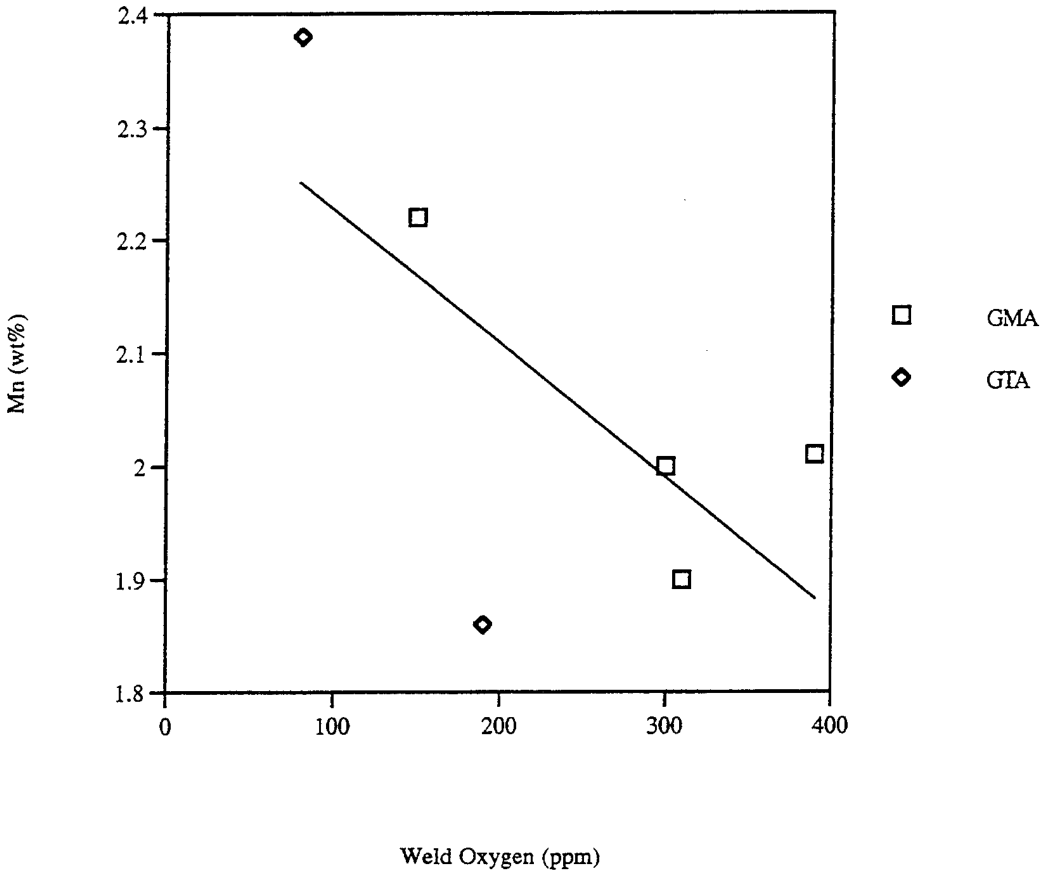

Figure 4.3 Weld Metal Manganese vs. Oxygen

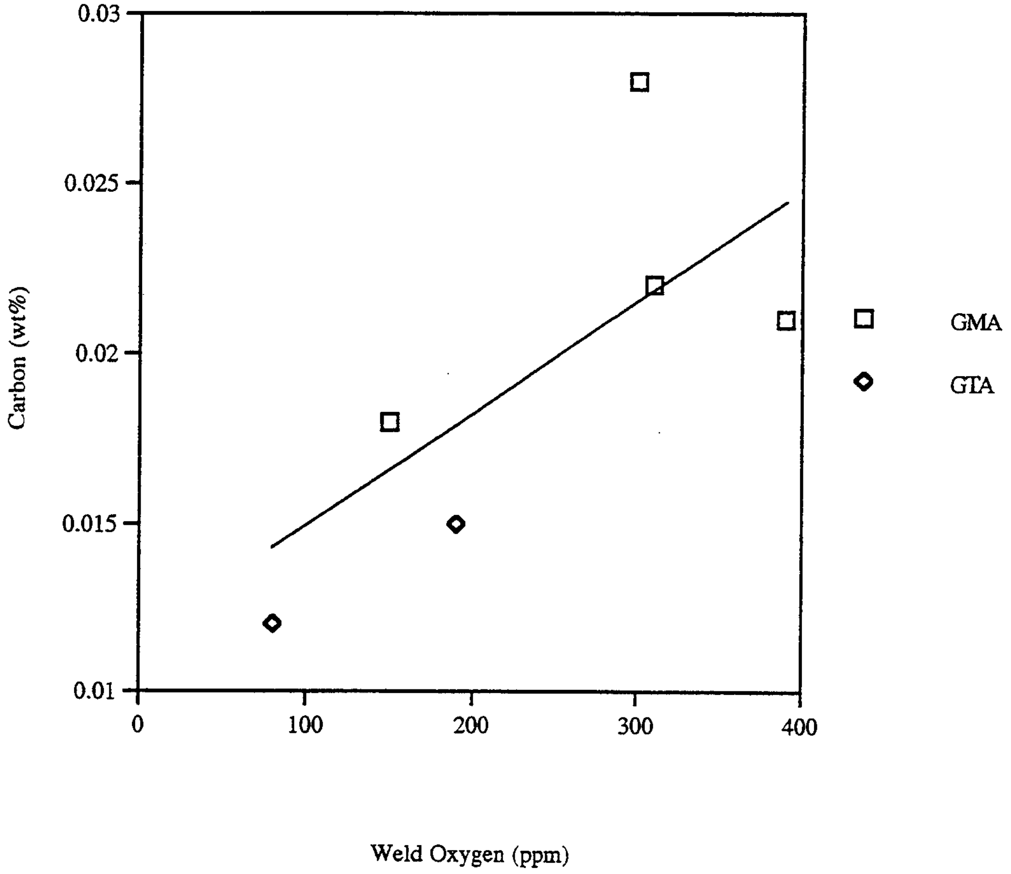

Figure 4.4 Weld Metal Carbon vs. Oxygen

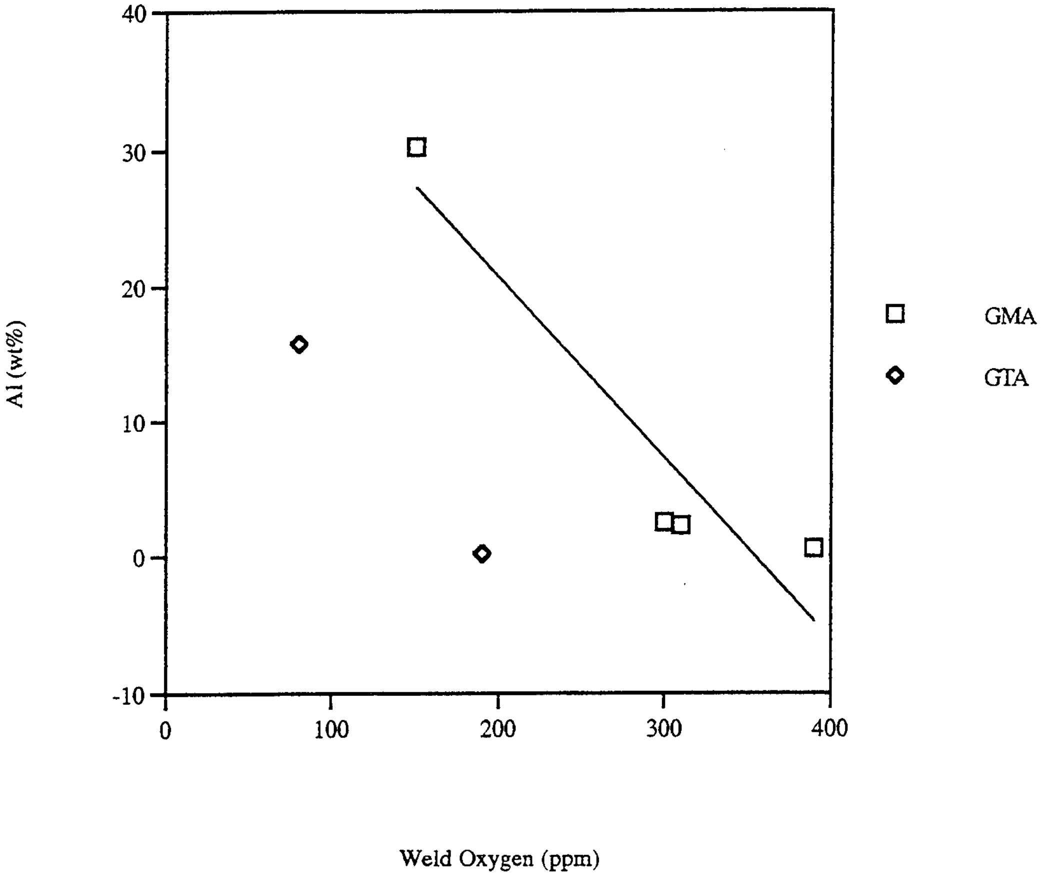

Figure 4.5 Inclusion Aluminum vs. Weld Metal Oxygen

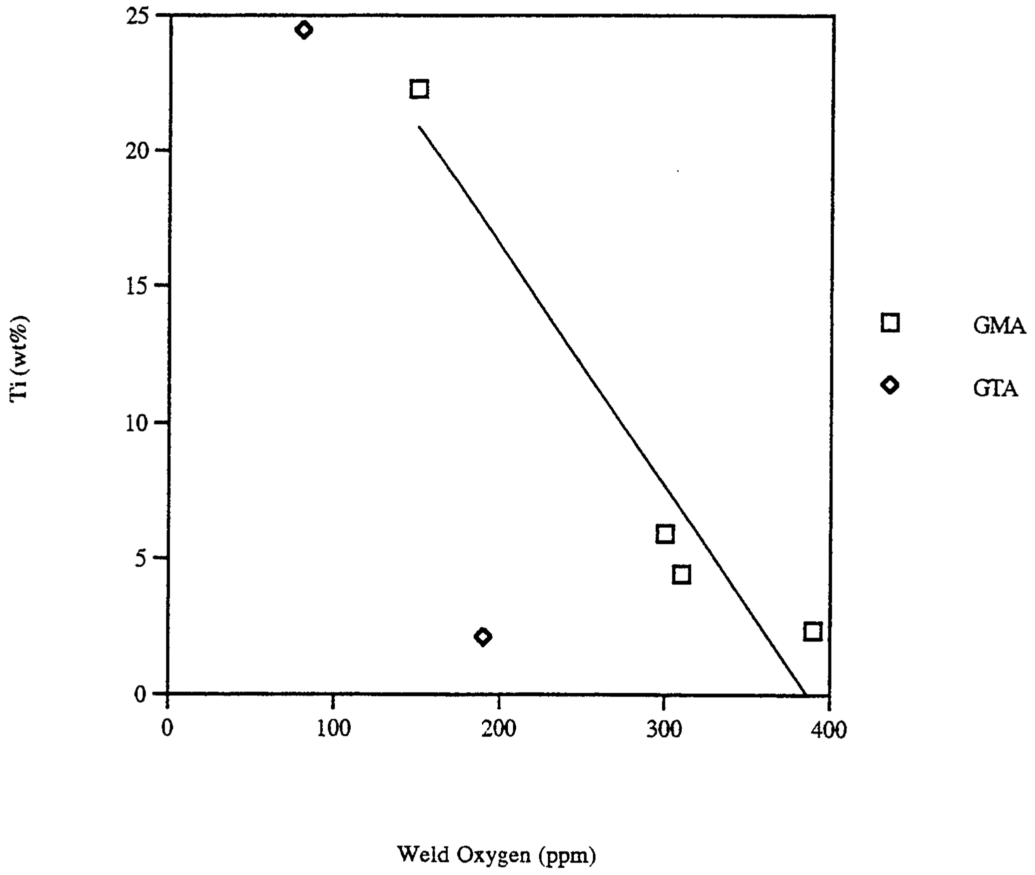

Figure 4.6 Inclusion Titanium vs. Weld Metal Oxygen

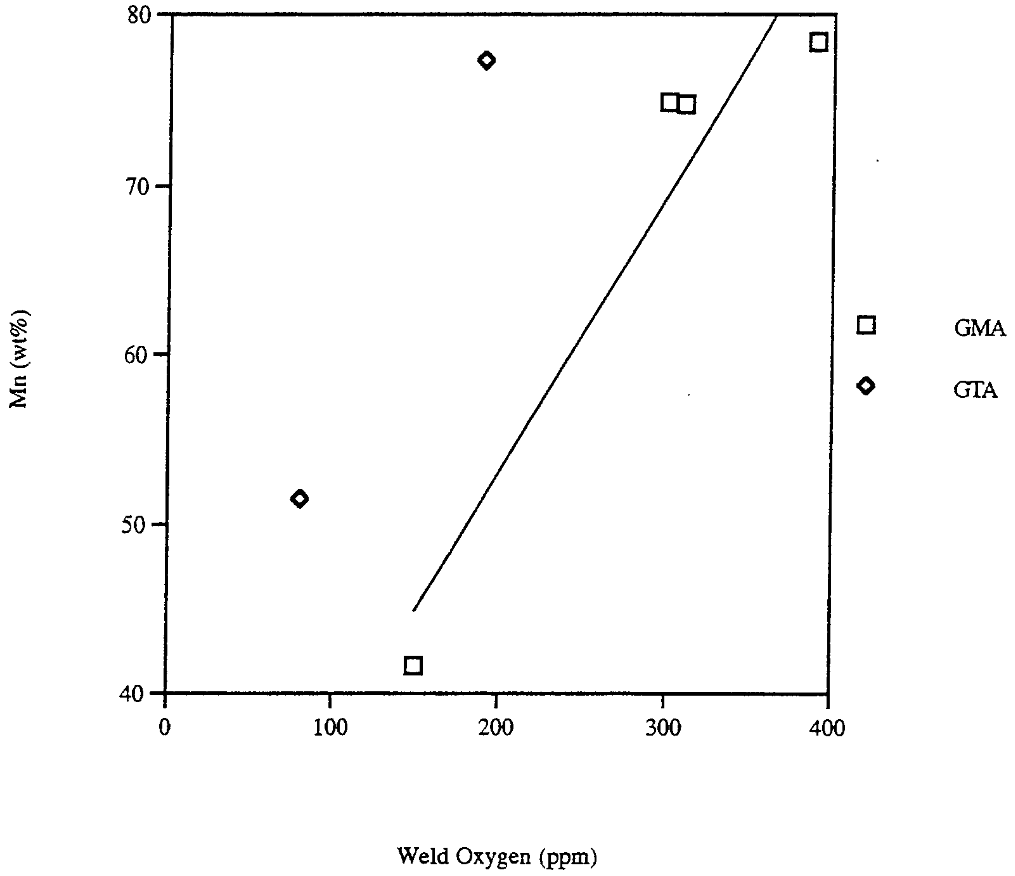

Figure 4.7 Inclusion Manganese vs. Weld Metal Oxygen

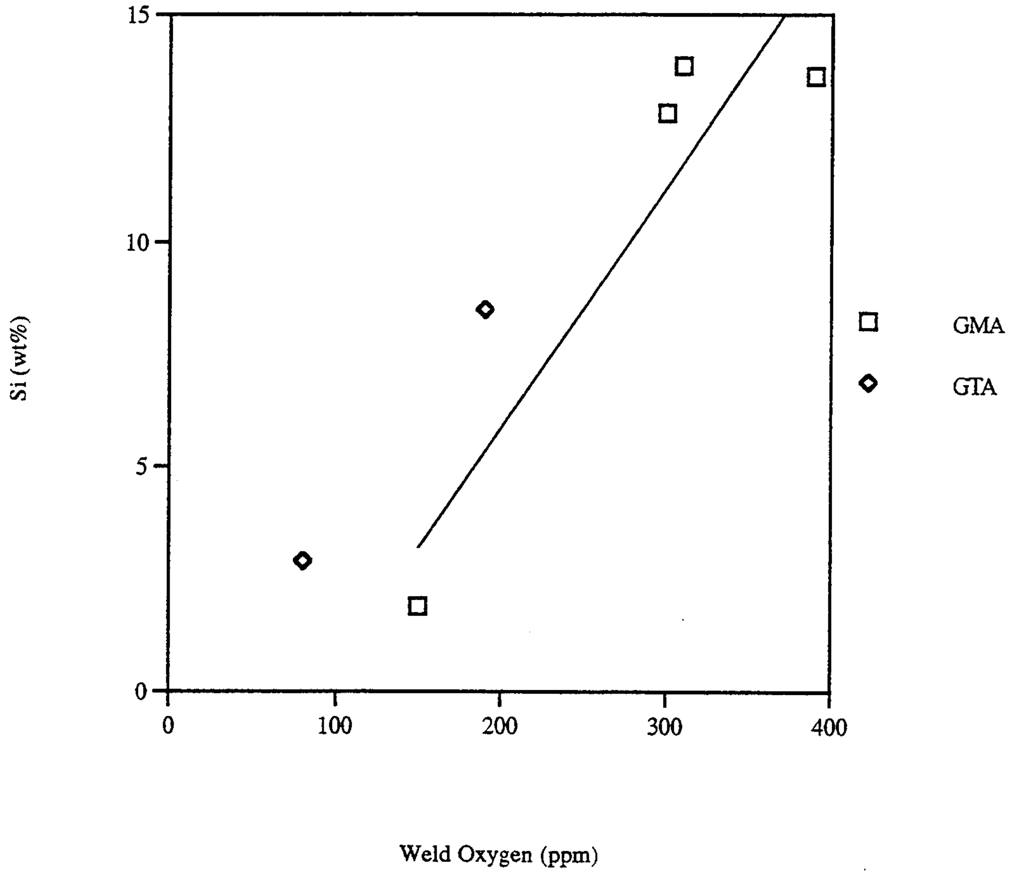

Figure 4.8 Inclusion Silicon vs. Weld Metal Oxygen

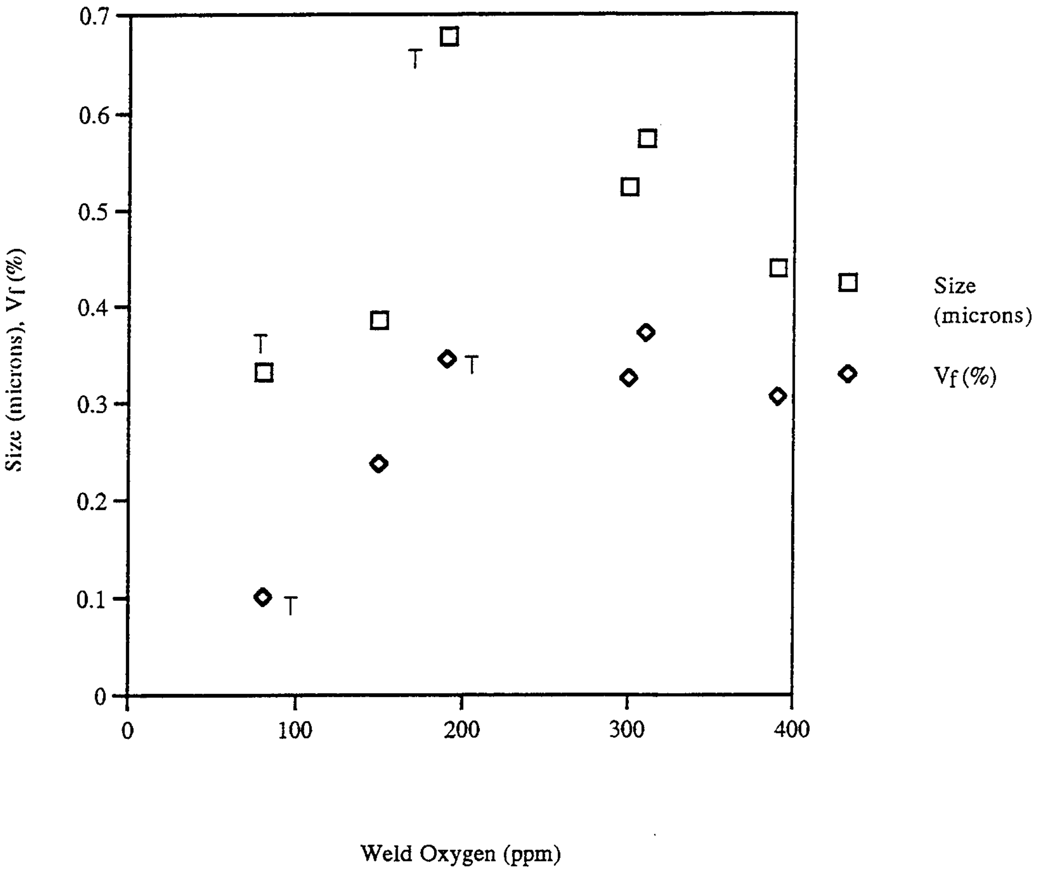

Figure 4.9 Inclusion Size and Volume Fraction (V_f) vs. Weld Metal Oxygen

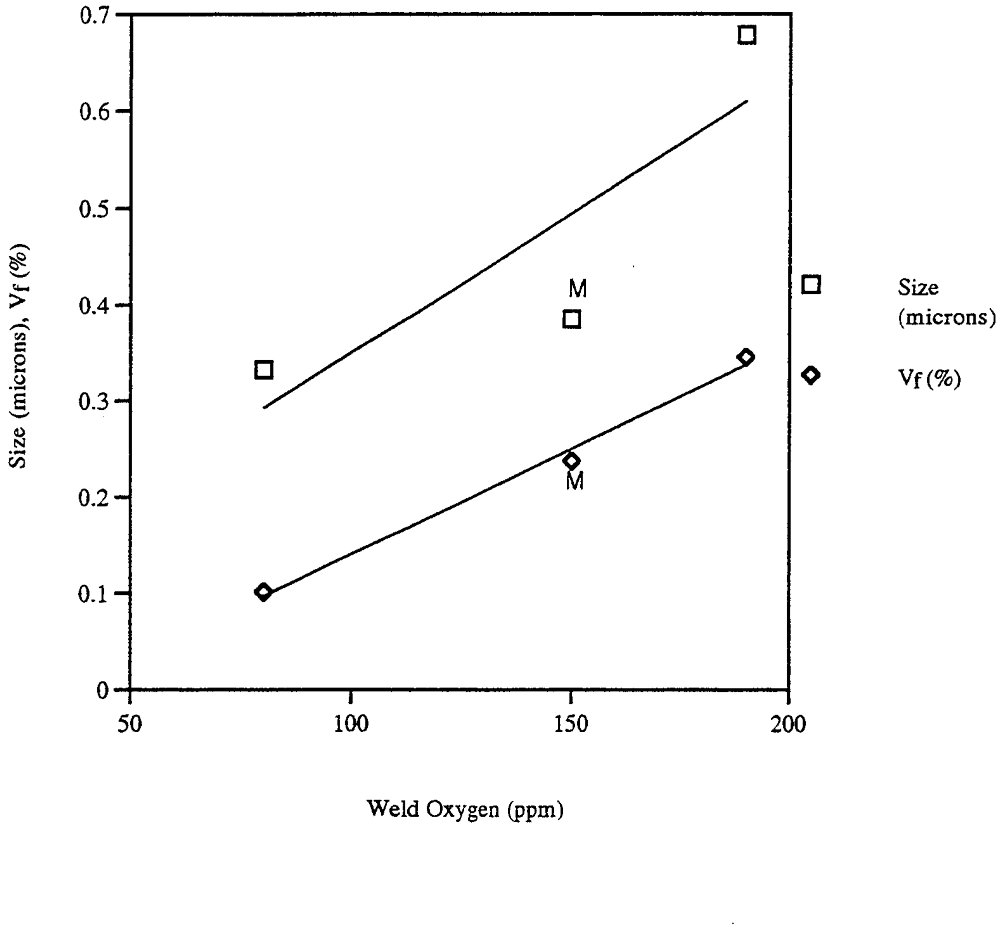

Figure 4.10 Inclusion Size and Volume Fraction (V_f) vs. Weld Metal Oxygen (Less than 200 ppm) (M - GMA)

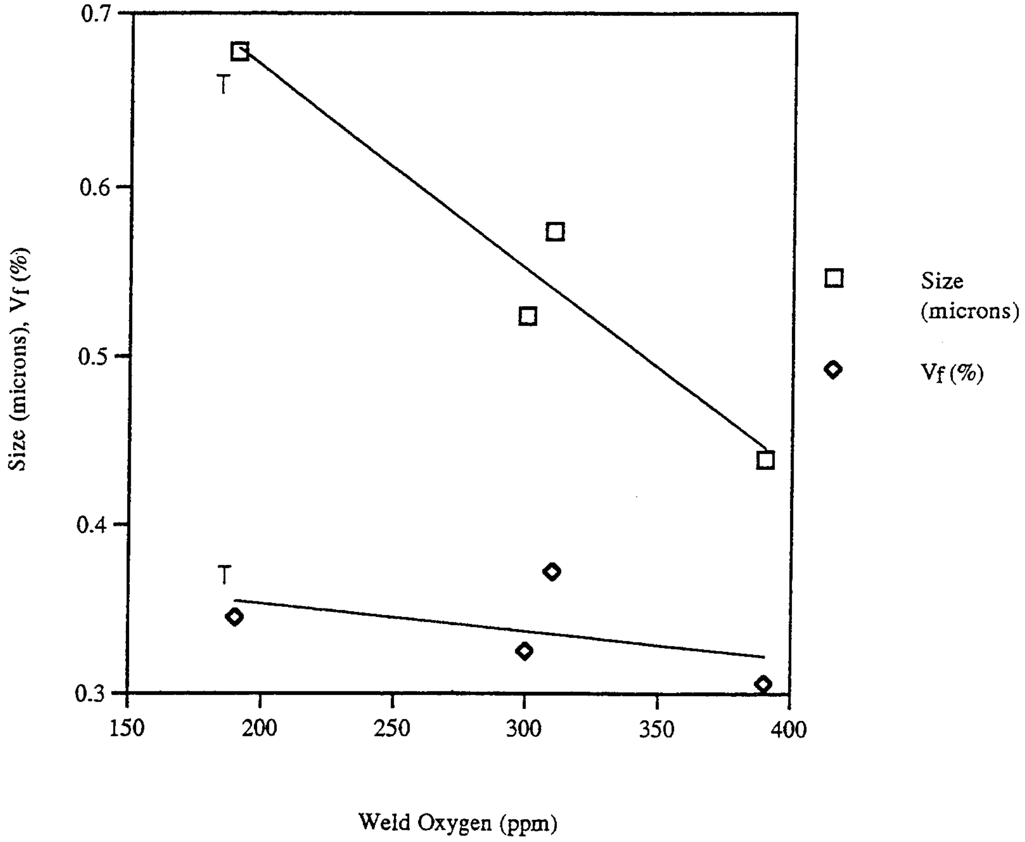

Figure 4.11 Inclusion Size and Volume Fraction (V_f) vs. Weld Metal Oxygen (Greater than 200 ppm) (T - GTA)

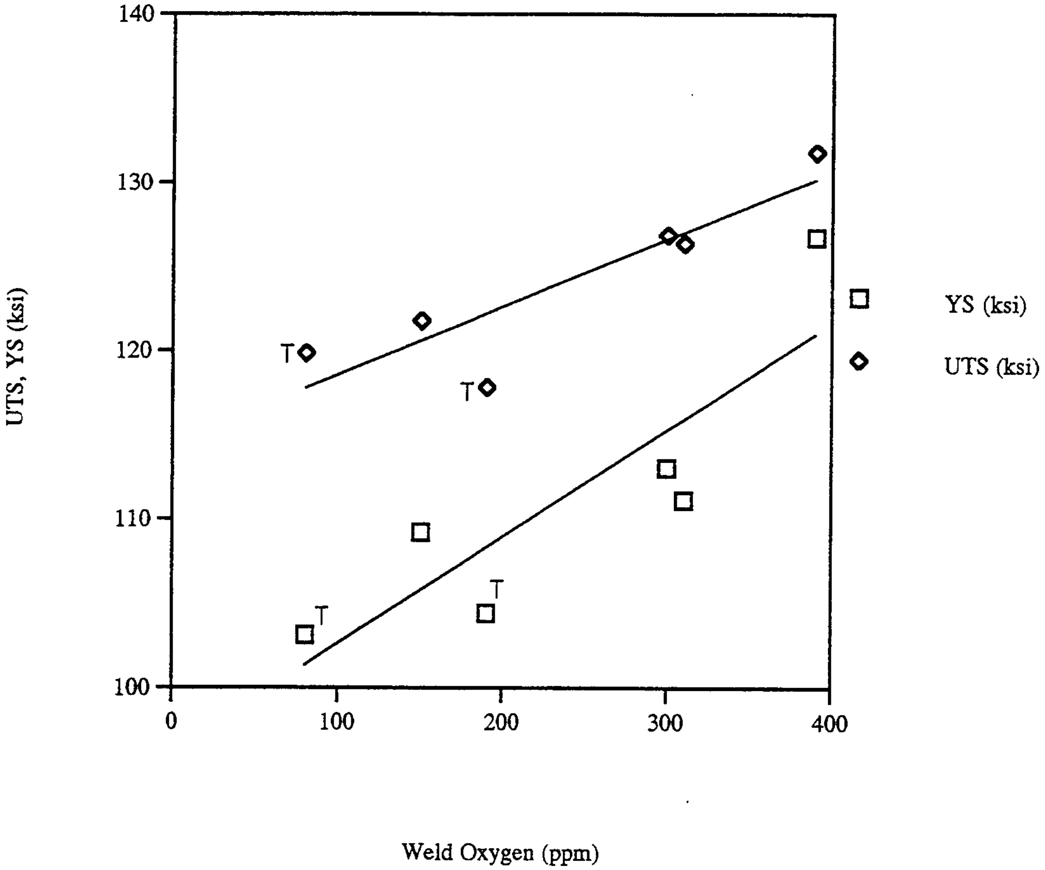

Figure 4.12 Ultimate Tensile Strength (UTS) and Yield Strength (YS) vs. Weld Metal Oxygen (T - GTA)

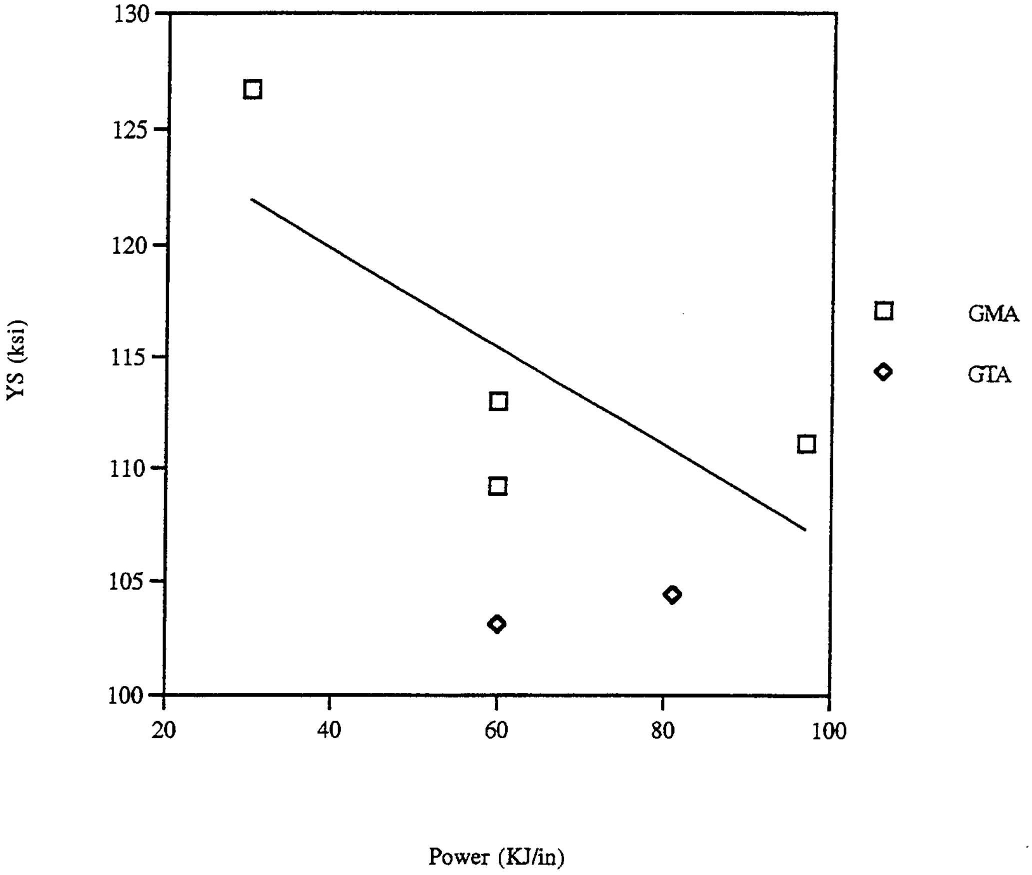

Figure 4.13 Yield Strength (YS) vs. Weld Power

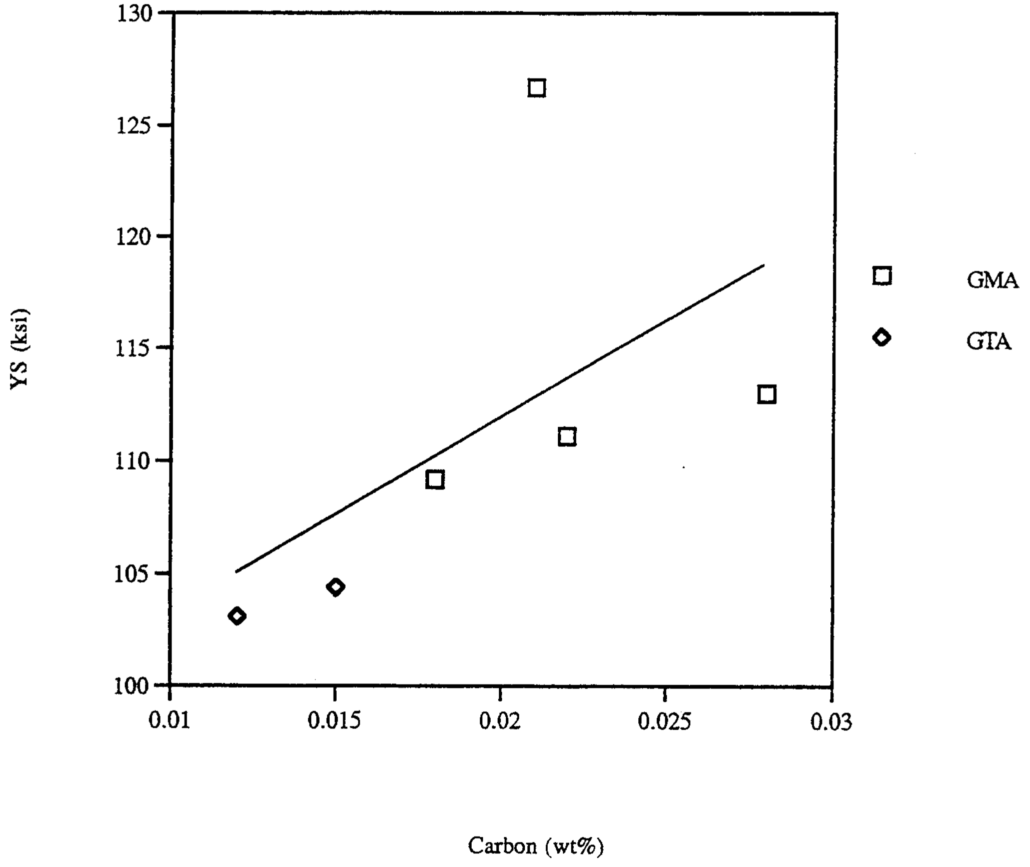

Figure 4.14 Yield Strength (YS) vs. Weld Metal Carbon

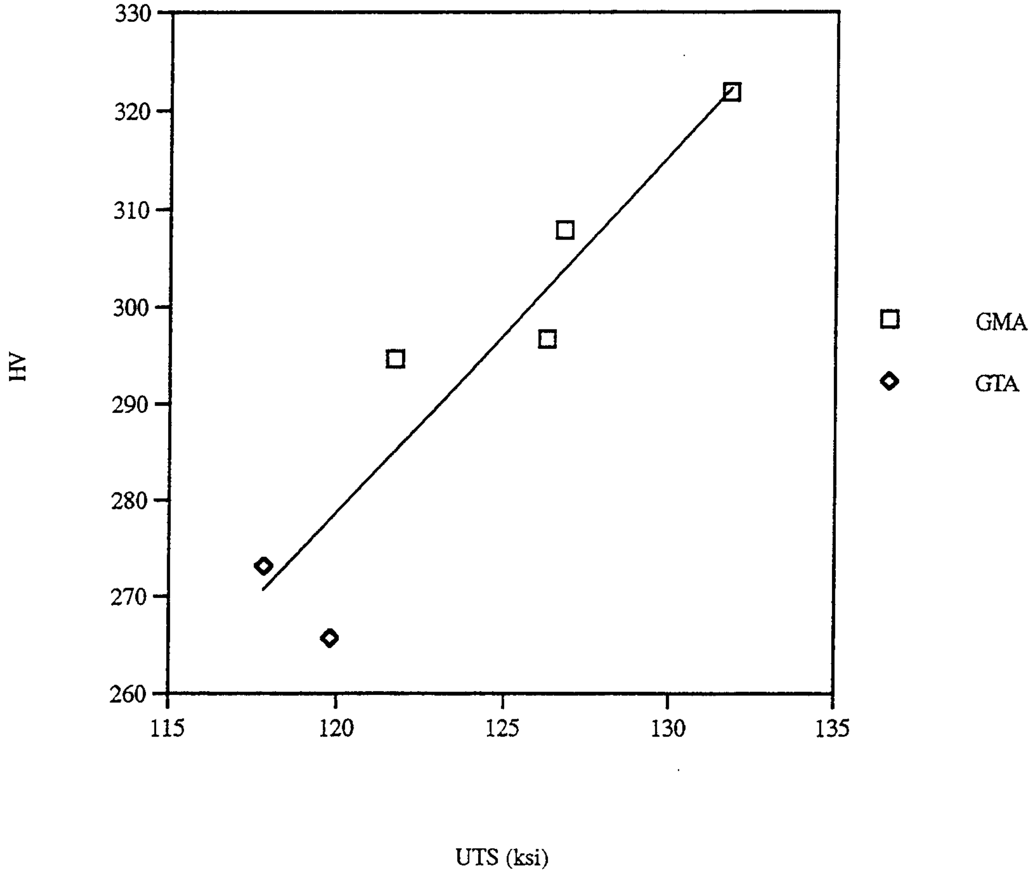

Figure 4.15 Vicker's Hardness (HV) vs. Ultimate Tensile Strength (UTS)

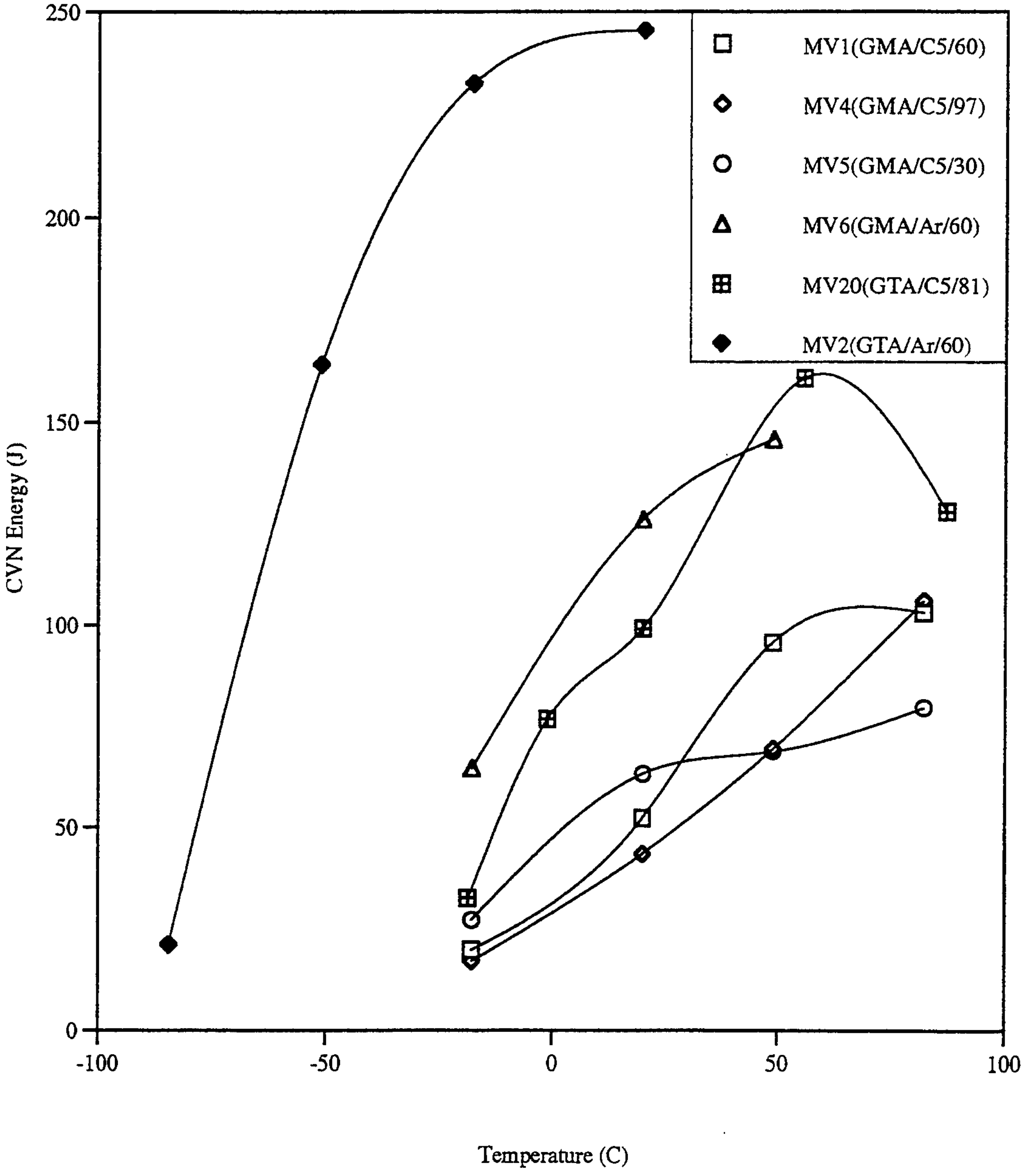

Figure 4.16 CVN Toughness Curves for All Weld Samples

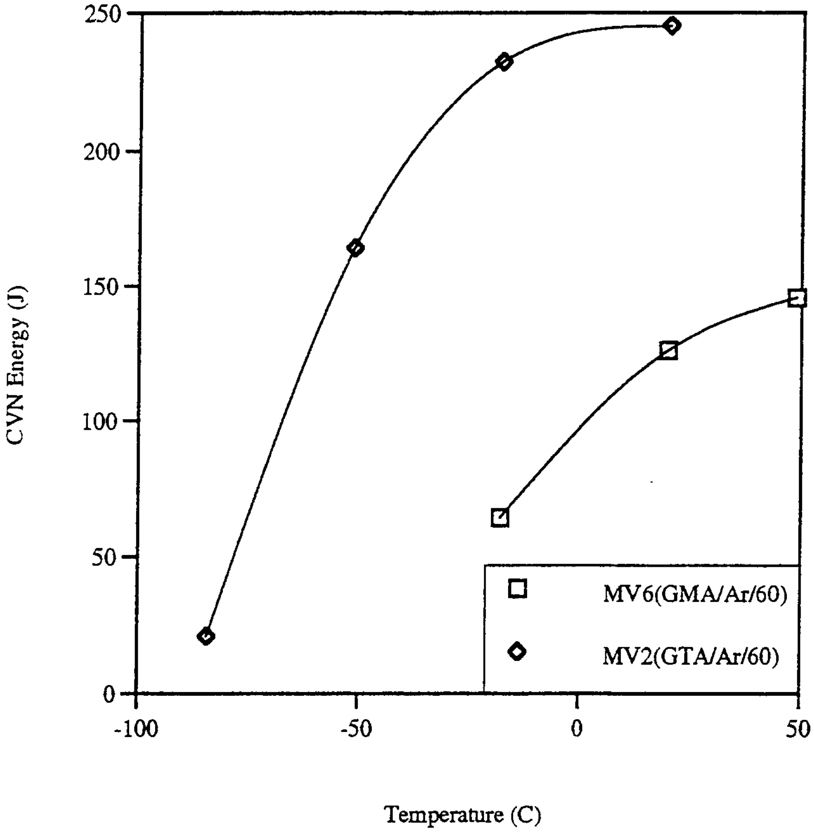

Figure 4.17 CVN Toughness Comparing GMA and GTA Welds Using Argon Cover Gas at 60 KJ/in. Power

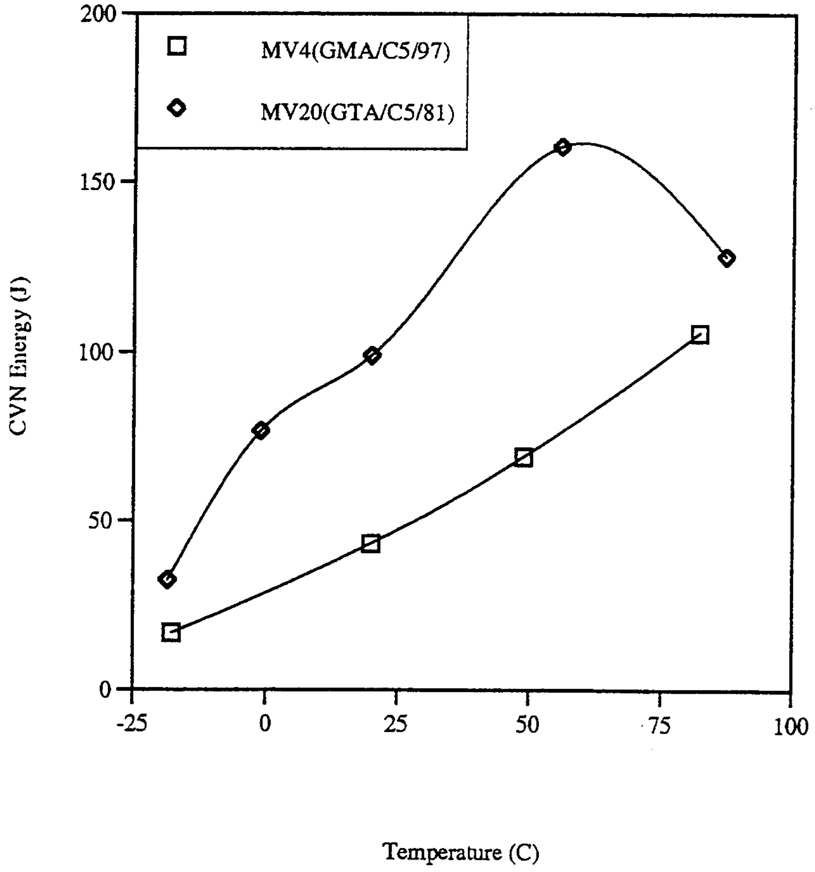

Figure 4.18 CVN Toughness Comparing GMA and GTA Welds Using C5 Cover Gas at 81 and 97 KJ/in. Power

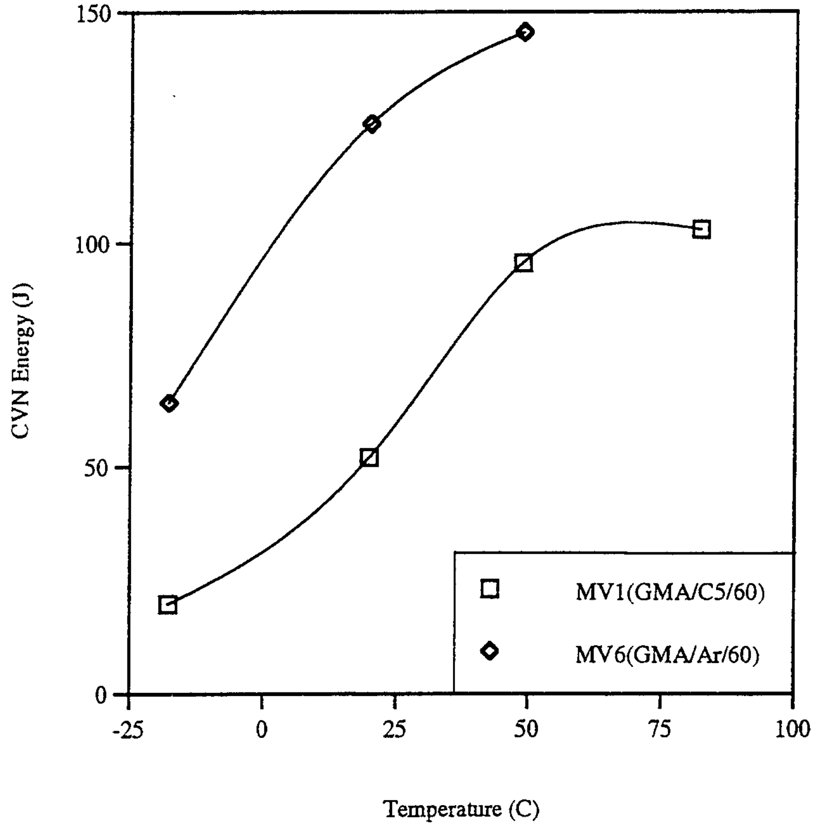

Figure 4.19 CVN Toughness Comparing Argon and C5 Cover Gas GMA Welds at 60 KJ/in. Power

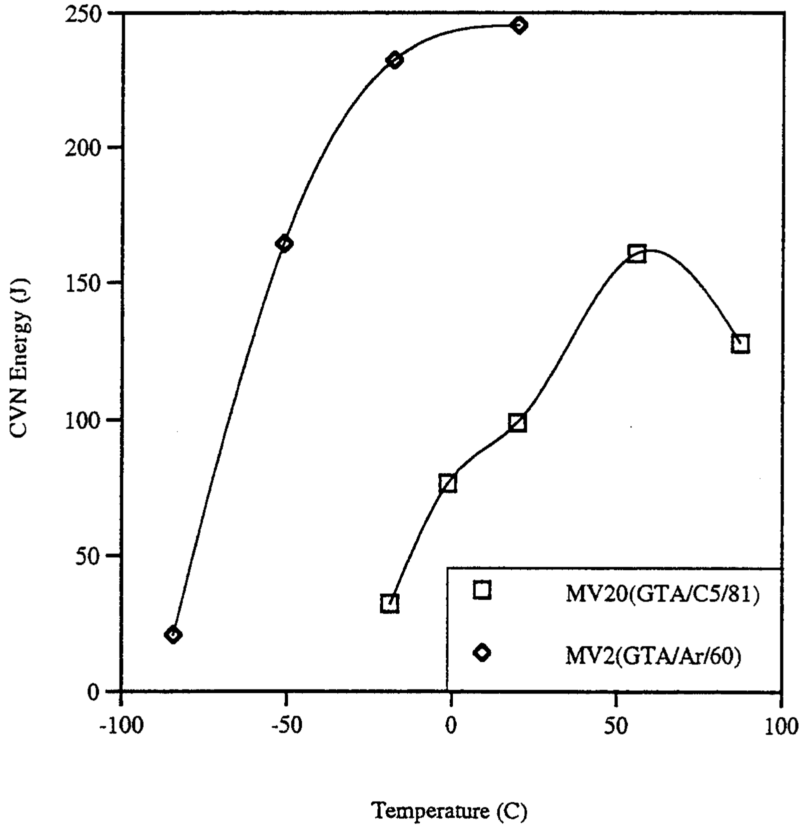

Figure 4.20 CVN Toughness Comparing GTA Argon - 60 KJ/in. Power and C5 - 81 KJ/in. Power Welds

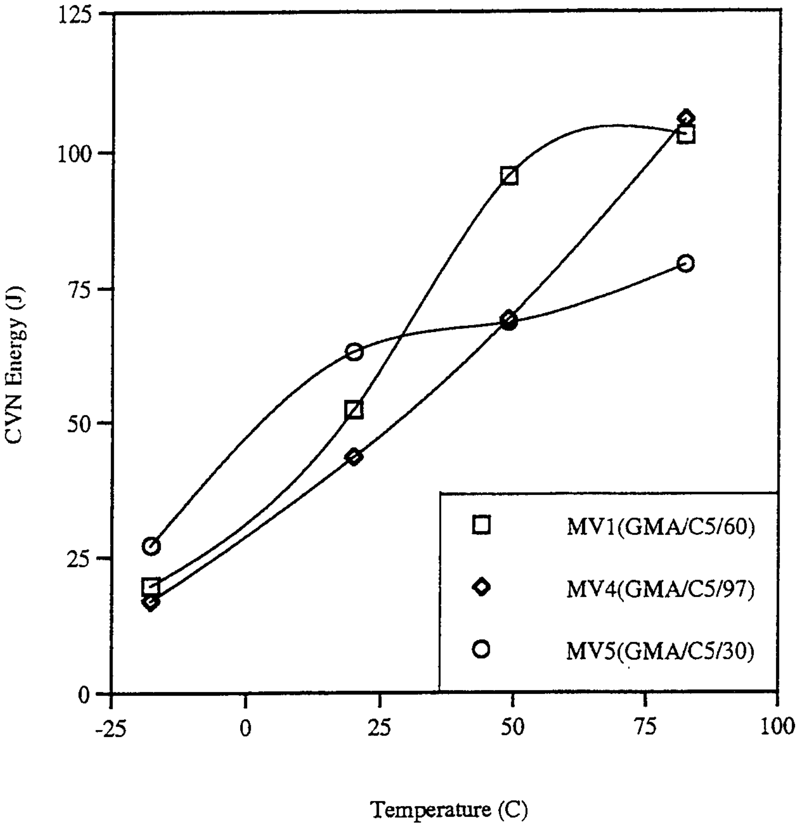

Figure 4.21 CVN Toughness Comparing GMA - C5 Cover Gas Welds at Various Power Levels

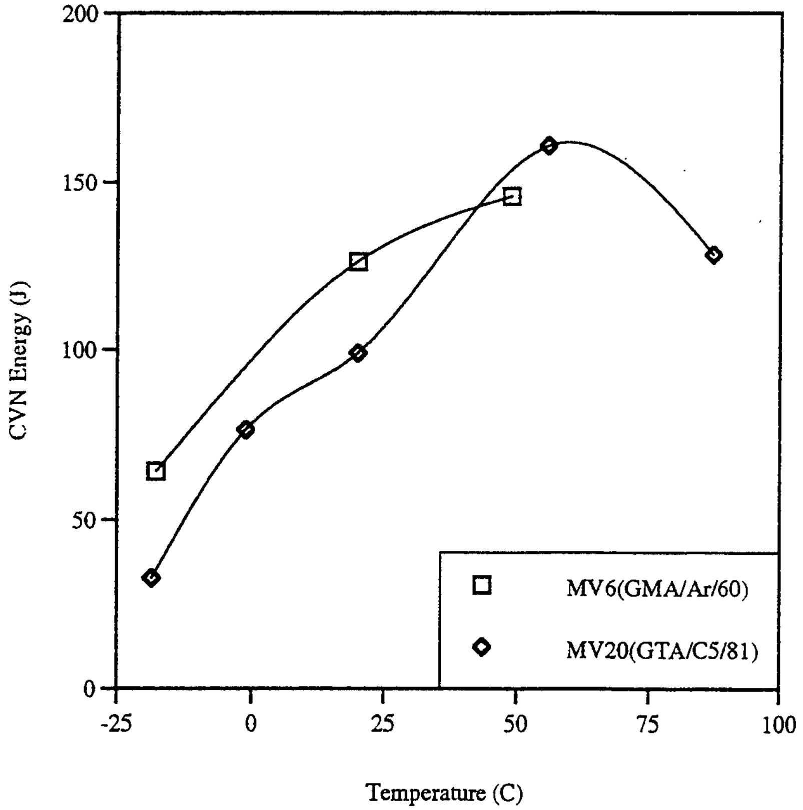

Figure 4.22 CVN Toughness Comparing Weld Sample MV6 (GMA/Argon/60) to MV20 (GTA/C5/81)

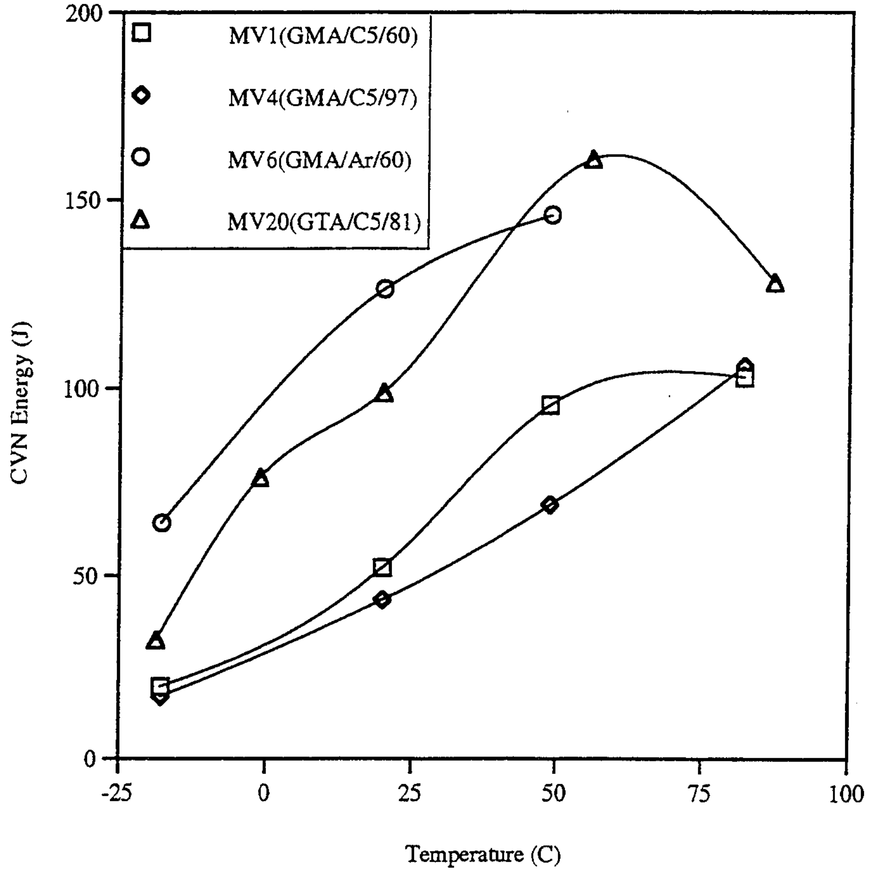

Figure 4.23 CVN Toughness Showing the Improvement of Toughness Achieved by Using Argon Cover Gas and GTA Welds

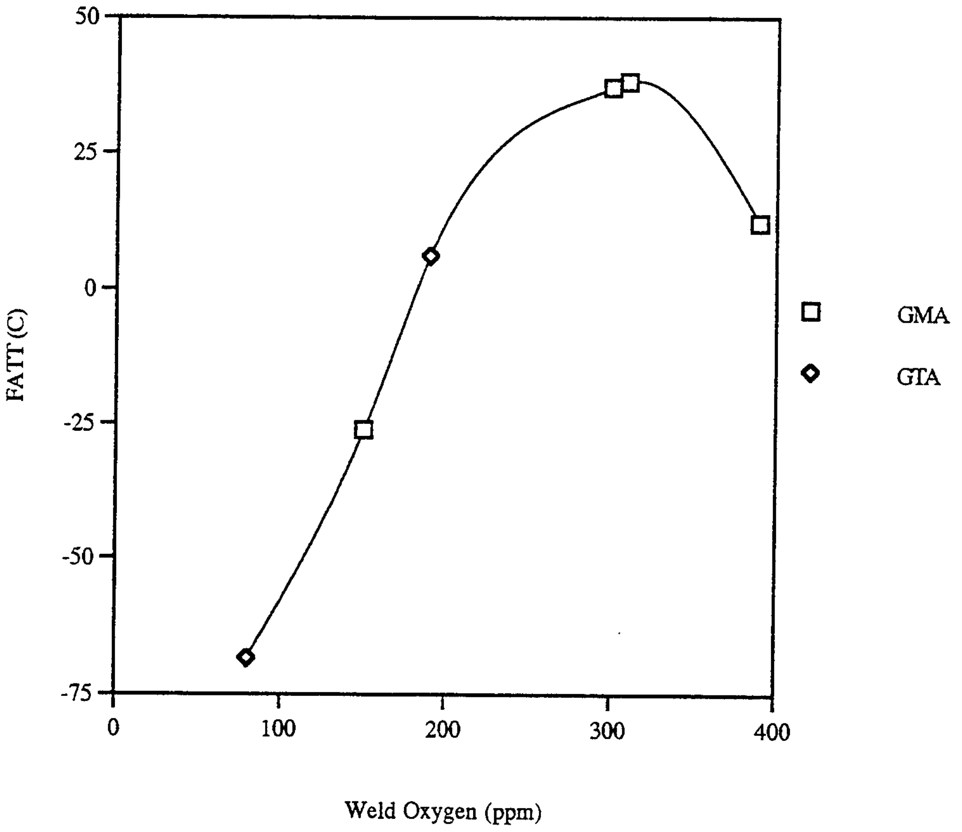

Figure 4.24 Fracture Appearance Transition Temperature (FATT) vs. Weld Metal Oxygen

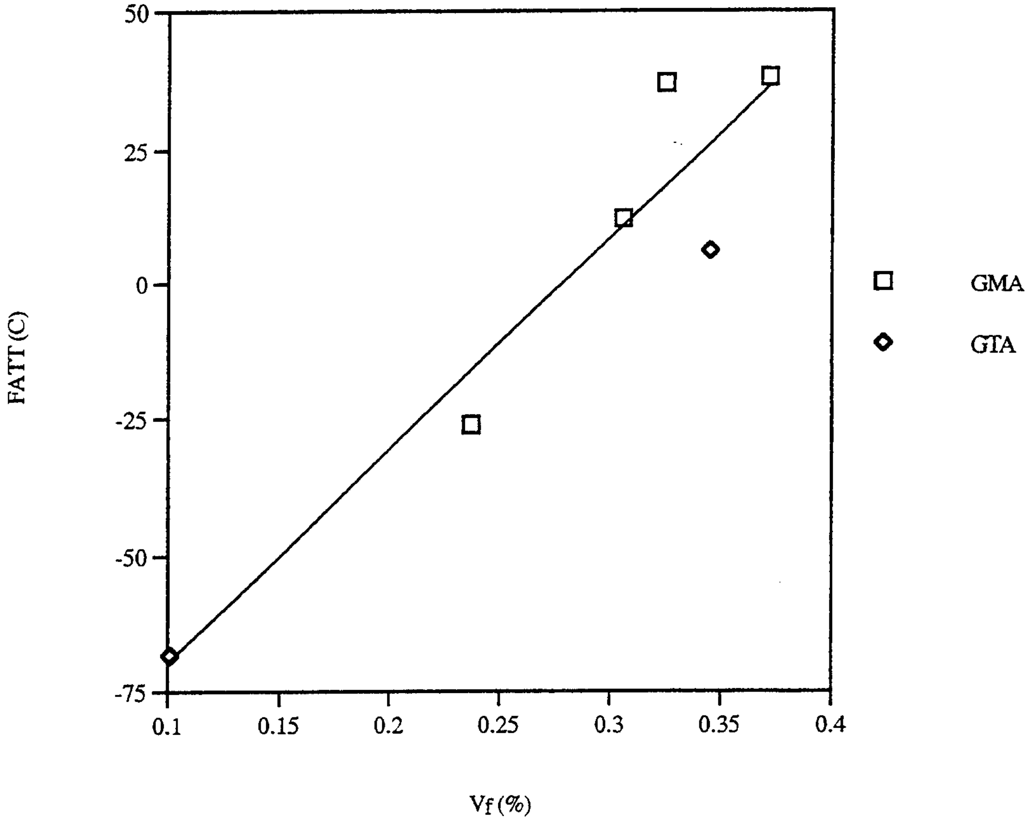

Figure 4.25 Fracture Appearance Transition Temperature (FATT) vs. Inclusion Volume Fraction (V_f)

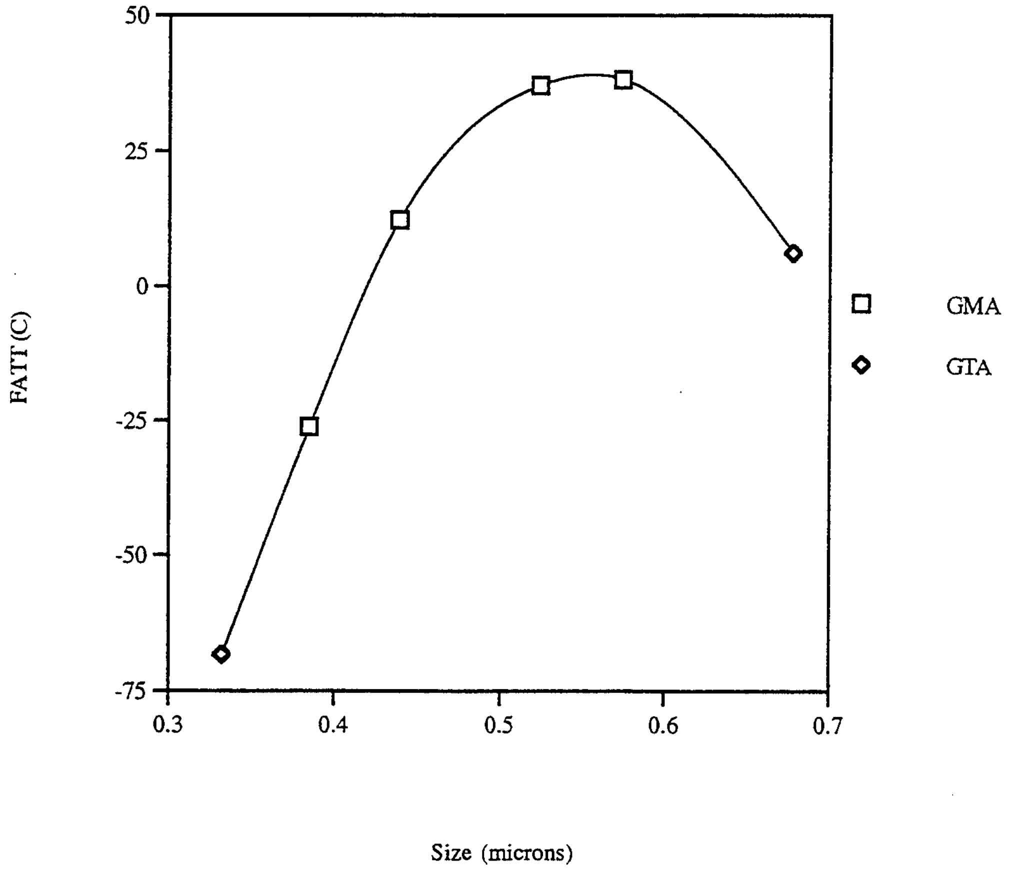

Figure 4.26 Fracture Appearance Transition Temperature (FATT) vs. Average Inclusion Size

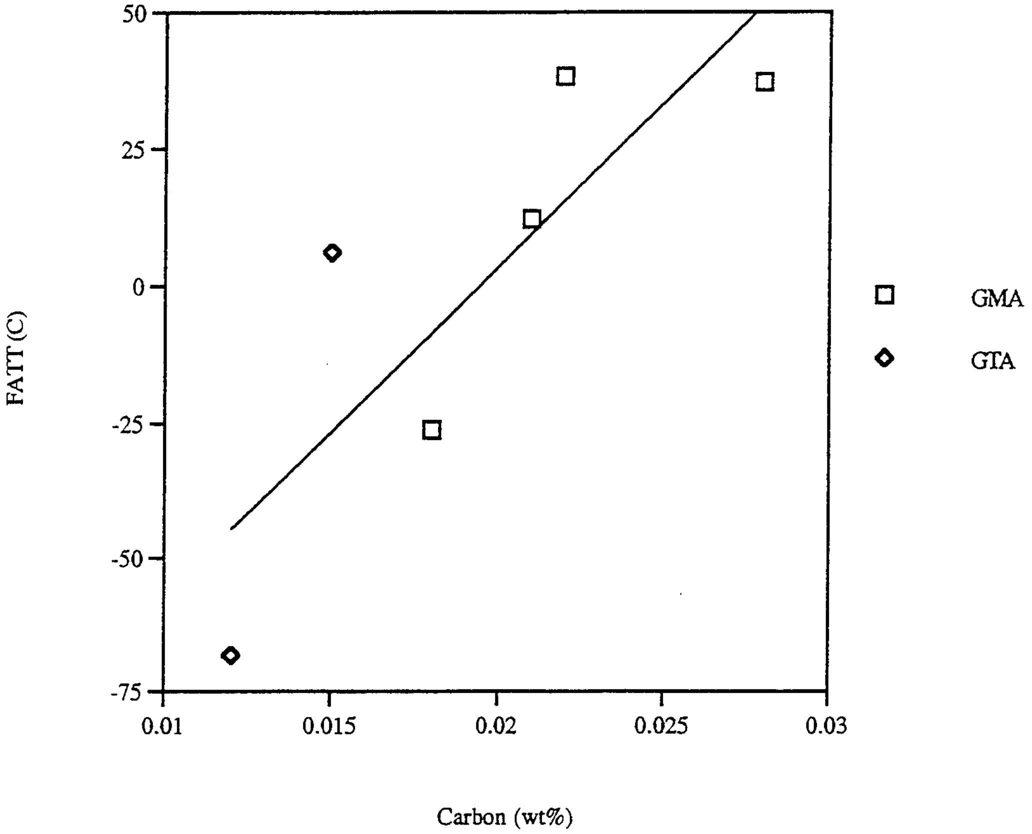

Figure 4.27 Fracture Appearance Transition Temperature (FATT) vs. Weld Metal Carbon

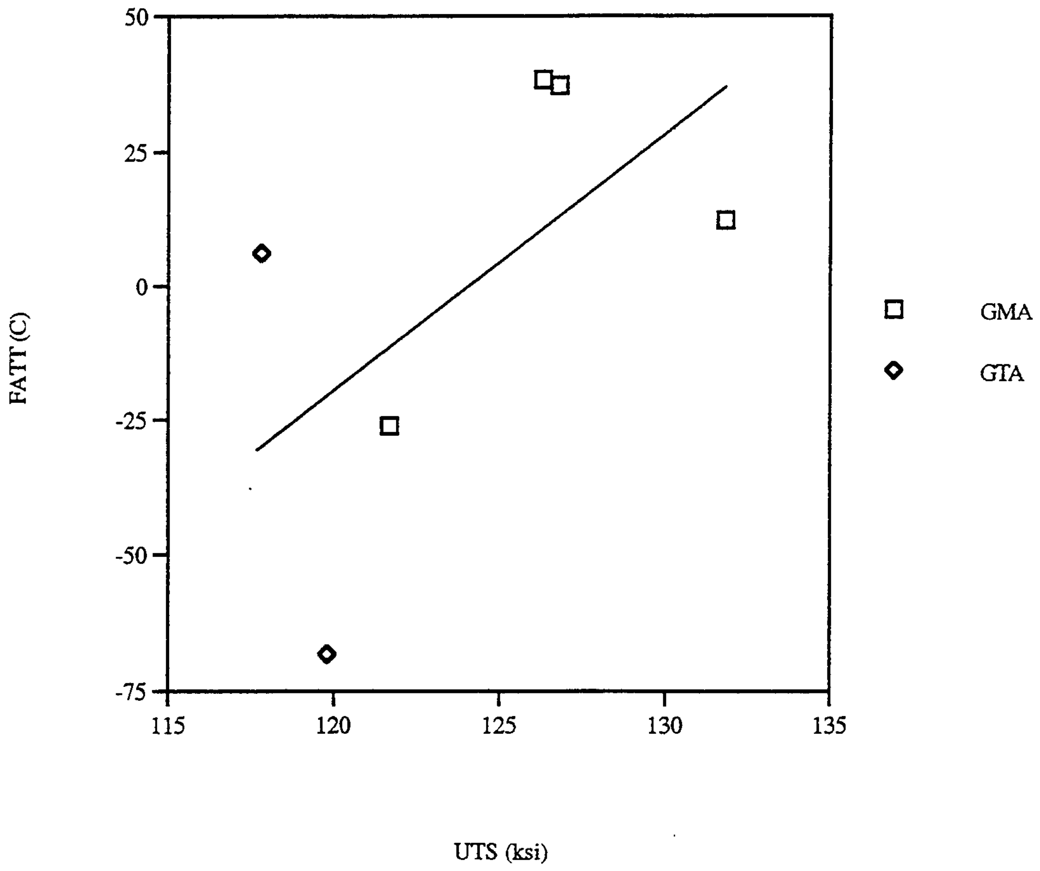

Figure 4.28 Fracture Appearance Transition Temperature (FATT) vs. Ultimate Tensile Strength (UTS)

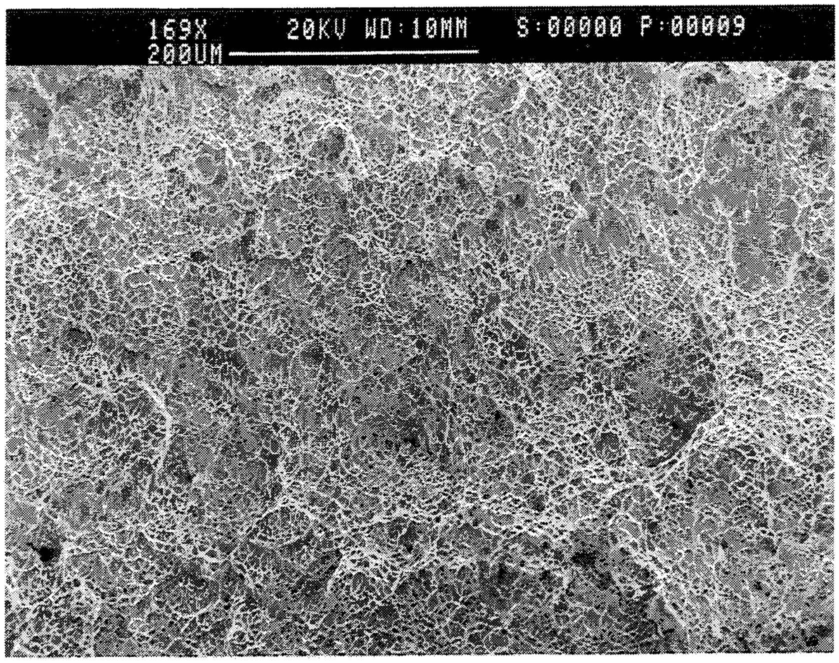
169X 20KV WD:10MM S:00000 P:00009
200UM

Figure 4.29 MV4 - Showing the Fracture Surface of a Typical Ductile Sample

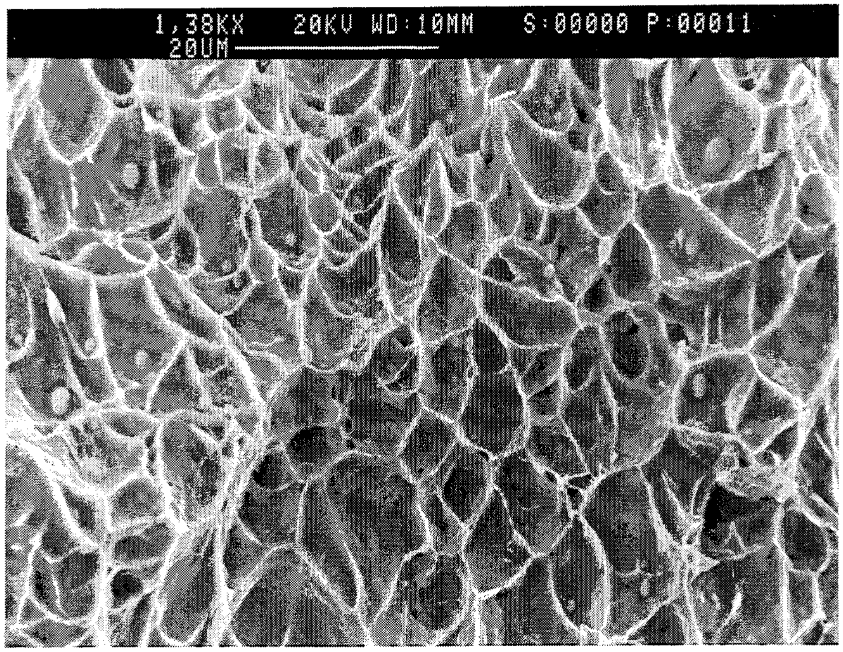
1,38KX 20KV WD:10MM S:00000 P:00011
20UM

Figure 4.30 MV4 - Showing Void Formation by Inclusions in Ductile Samples

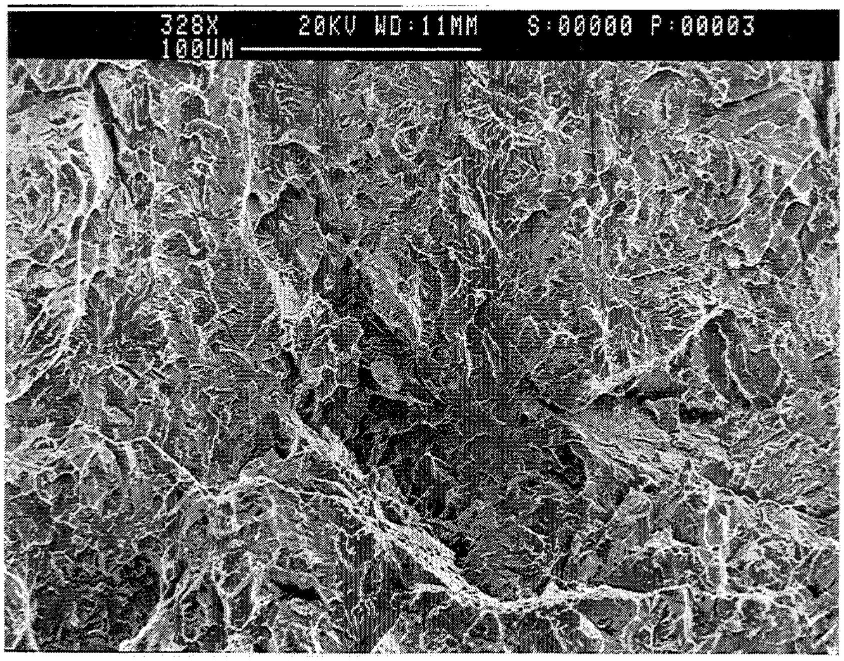
328X 20KV WD:11MM S:00000 P:00003
100UM

Figure 4.31 MV2 - GTA Weld using Argon Cover Gas

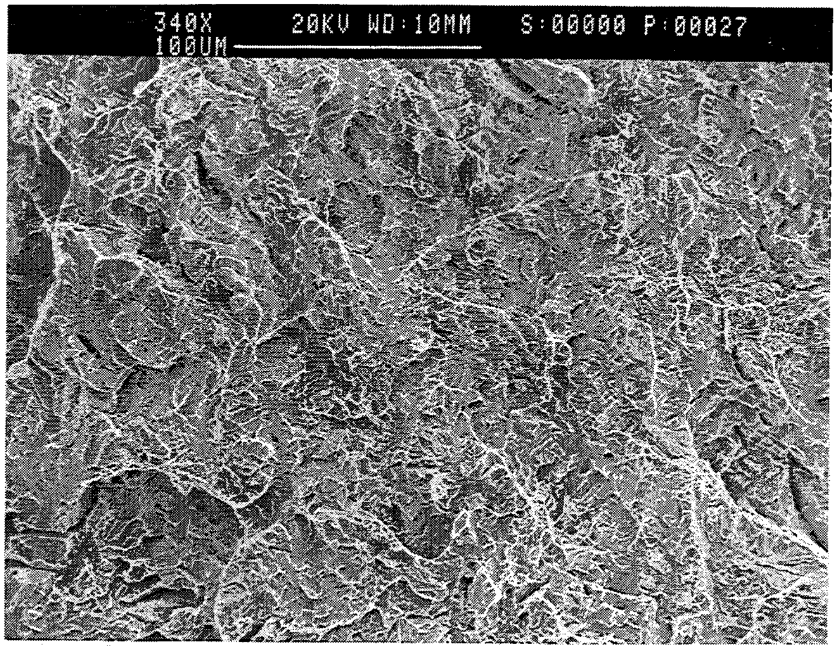
340X 20KV WD:10MM S:00000 P:00027
100UM

Figure 4.32 MV6 - GMA Weld Using Argon Cover Gas

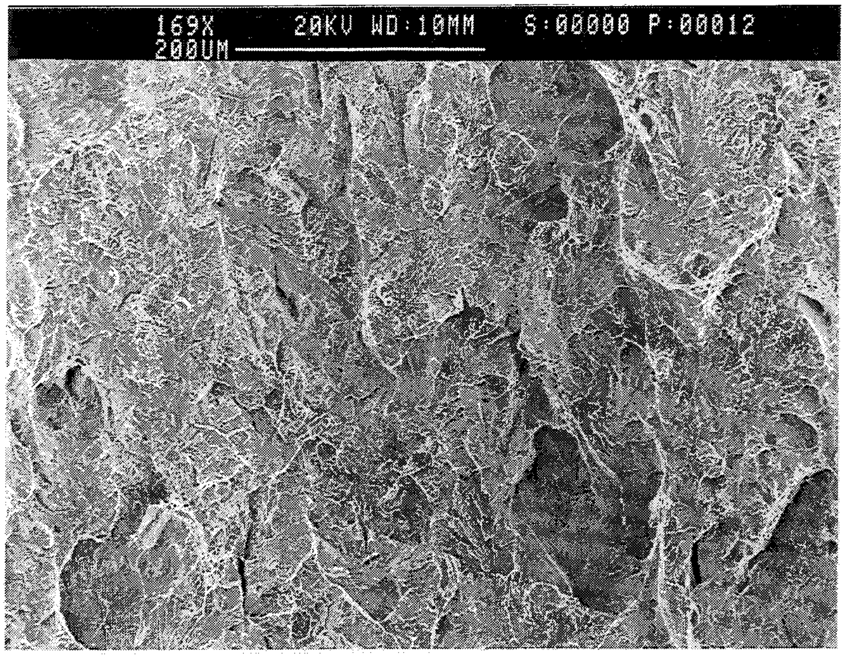
169X 20KV WD:10MM S:00000 P:00012
200UM

Figure 4.33 MV4 - GMA Weld Using C5 Cover Gas

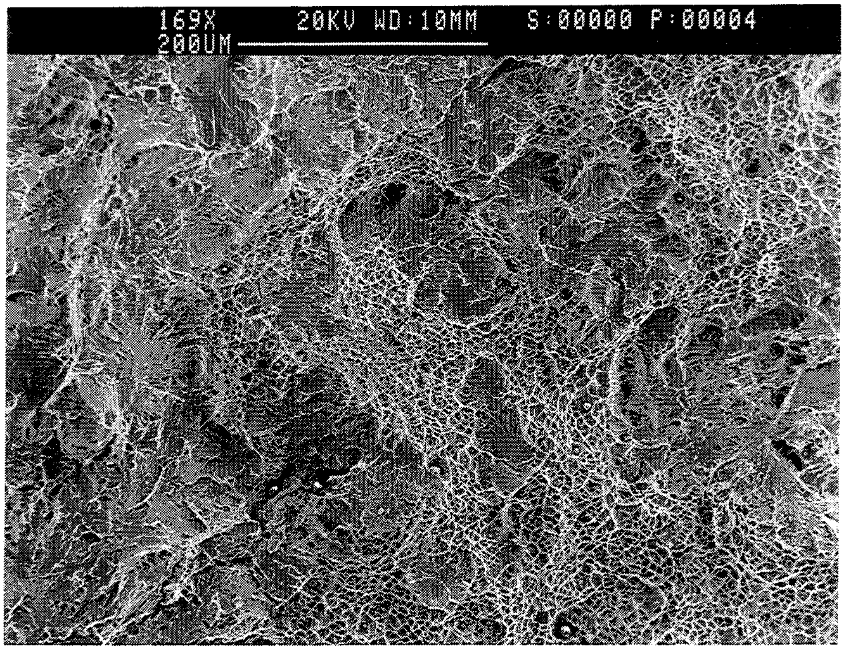
169X 20KV WD:10MM S:00000 P:00004
200UM

Figure 4.34 MV20 - GTA Weld Using C5 Cover Gas Showing Extensive Areas of Ductility and Crack Formation by Large Inclusions

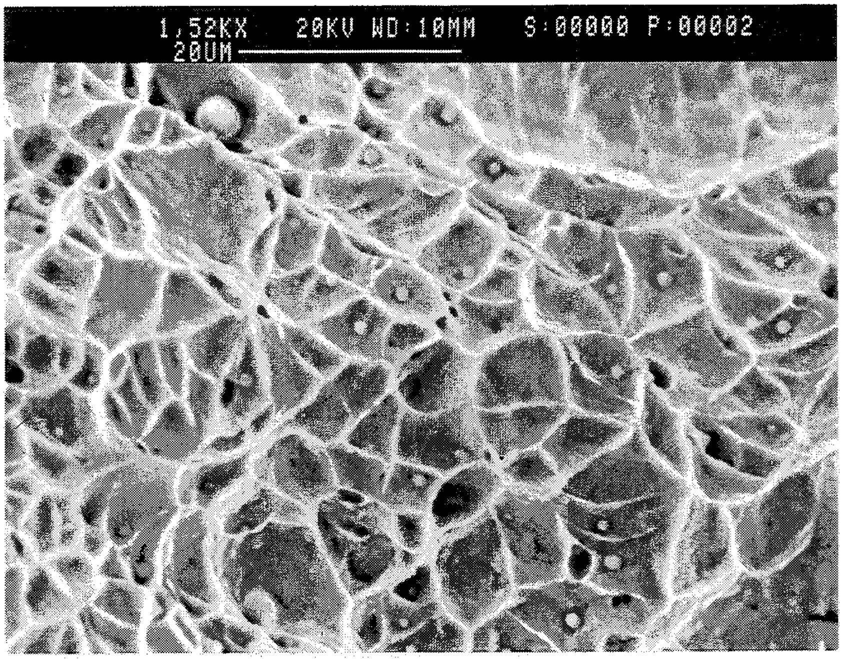
1,52KX 20KV WD:10MM S:00000 P:00002
20UM

Figure 4.35 MV20 - Showing Void Formation by Inclusions in Ductile Regions of Lower Shelf Samples

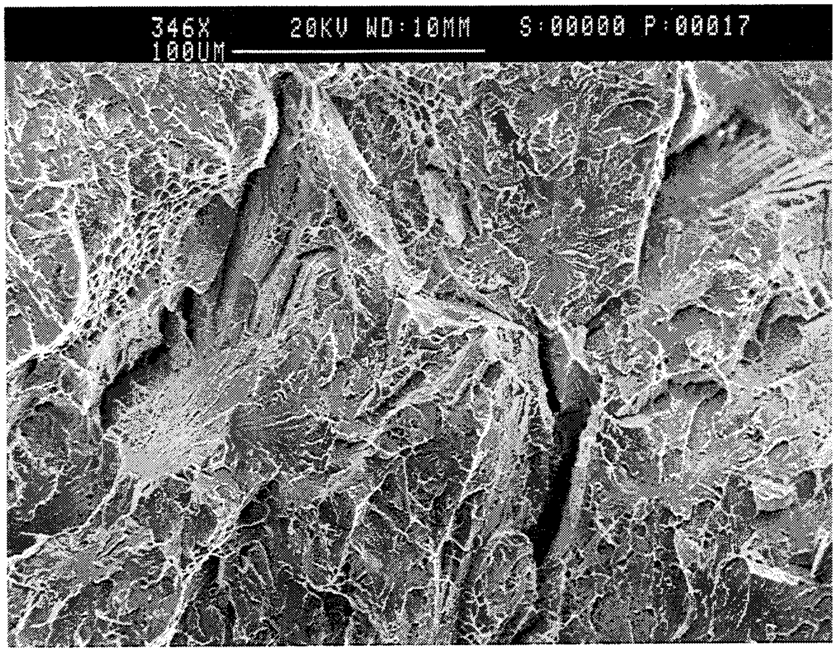
346X 20KV WD:10MM S:00000 P:00017
100UM

Figure 4.36 MV4 - GMA Weld Using C5 Cover Gas Showing Extensive Intergranular Cracking

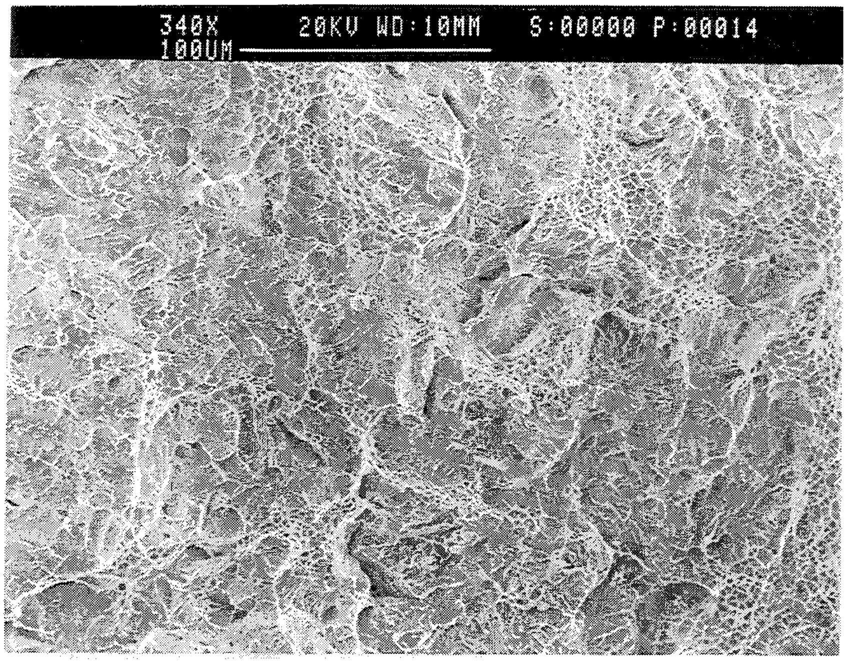
340X 20KV WD:10MM S:00000 P:00014
100UM

Figure 4.37 MV5 - GMA Weld Using C5 Cover Gas Showing Intergranular Cracking and Ductile Areas

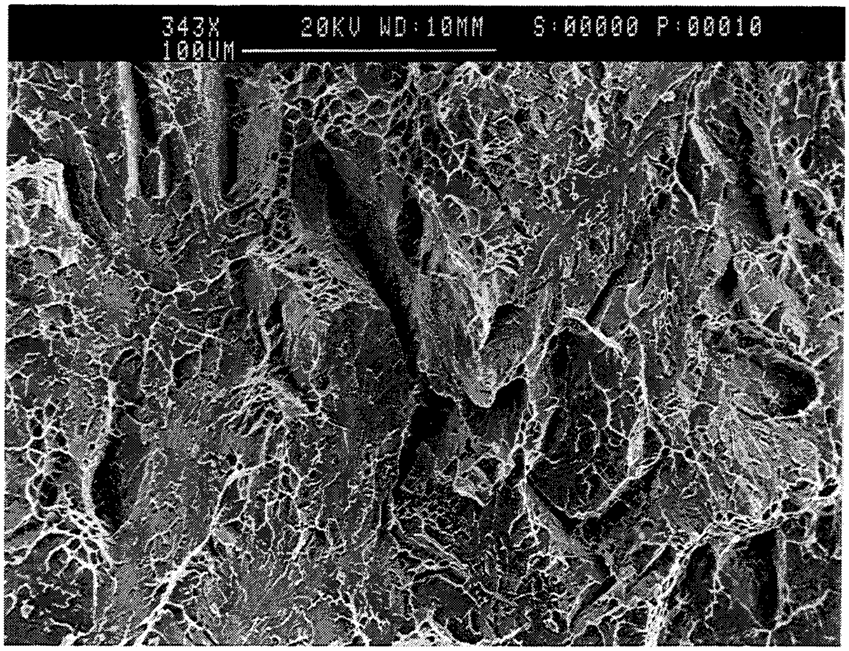
343X 20KV WD:10MM S:00000 P:00010
100UM

Figure 4.38 MV1 - GMA Weld Using C5 Cover Gas Showing Intergranular Cracking

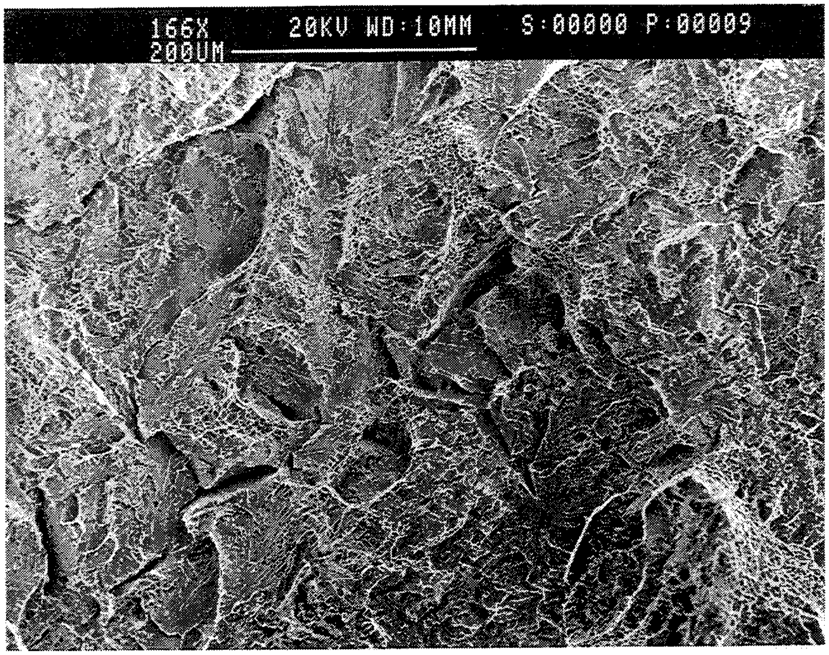
166X 20KV WD:10MM S:00000 P:00009
200UM

Figure 4.39 MV 1 - GMA Weld Using C5 Cover Gas Showing Intergranular Cracking and Uneven Cleavage

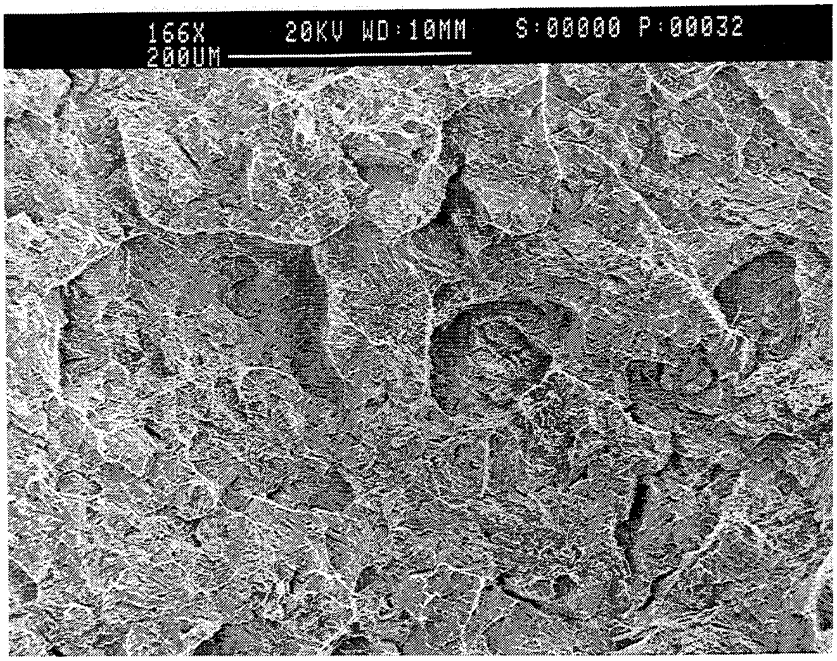
166X 20KV WD:10MM S:00000 P:00032
200UM

Figure 4.40 MV6 - GMA Weld Using Argon Cover Gas Showing Uneven Cleavage Connected by Ductile Ridges

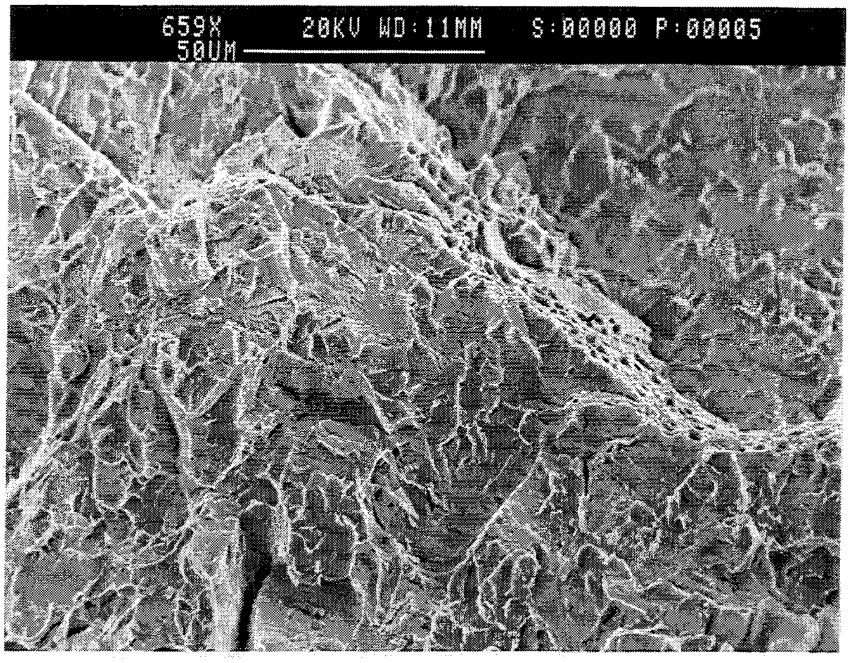
659X 20KV WD:11MM S:00000 P:00005
50UM

Figure 4.41 MV2 - GTA Weld Using Argon Cover Gas

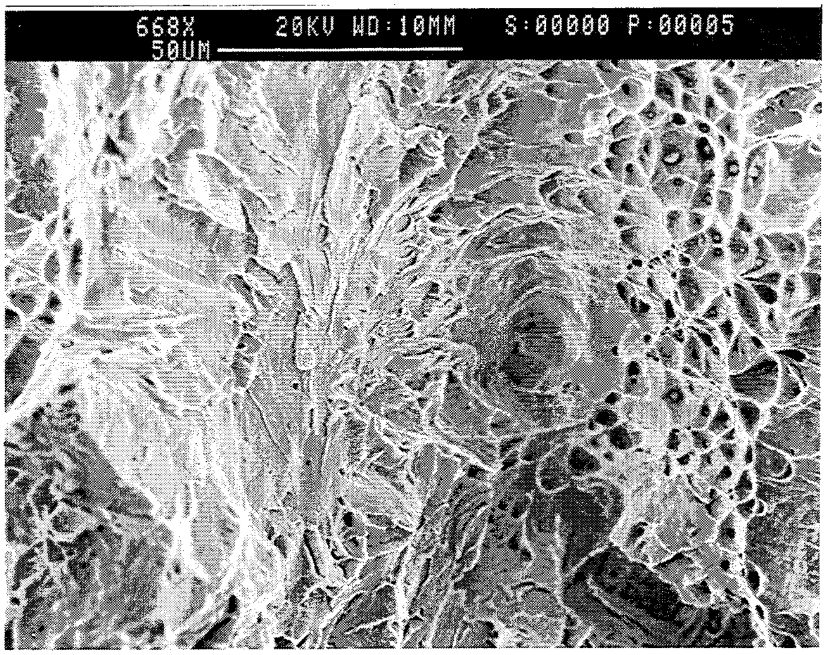
668X 20KV WD:10MM S:00000 P:00005
50UM

Figure 4.42 MV20 - GTA Weld Using C5 Cover Gas Showing Cleavage and Ductile Areas Nucleated by Inclusions

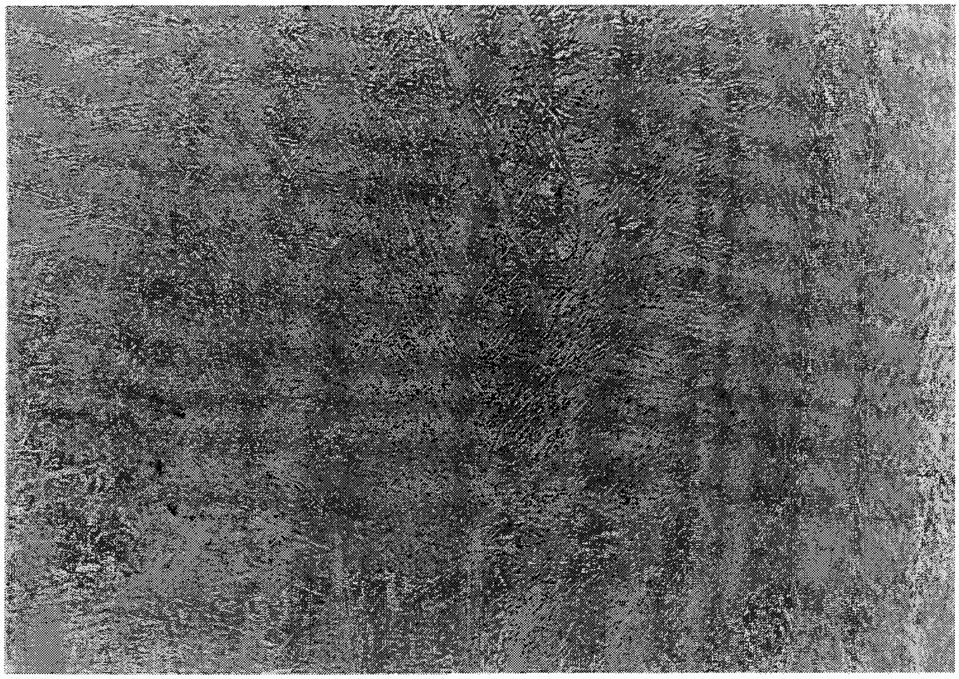

Figure 4.43 MV5 - Showing Lathlike Microstructure Typical to Columnar Grains of GMA Welds Using C5 Cover Gas (400 x)

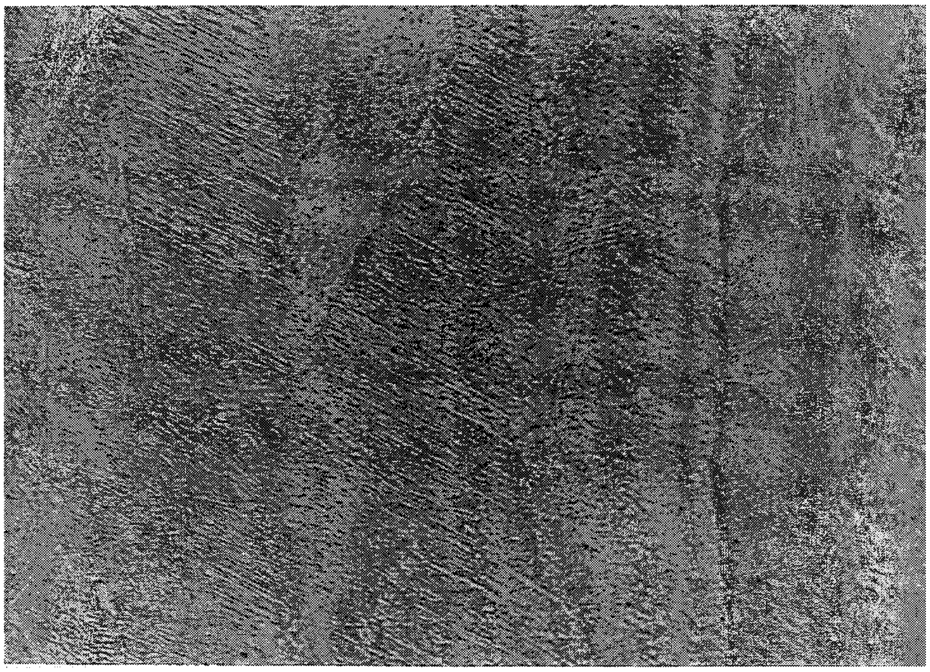

Figure 4.44 MV5 - Showing the Extension and Continuity of Laths in Columnar Grains (400 x)

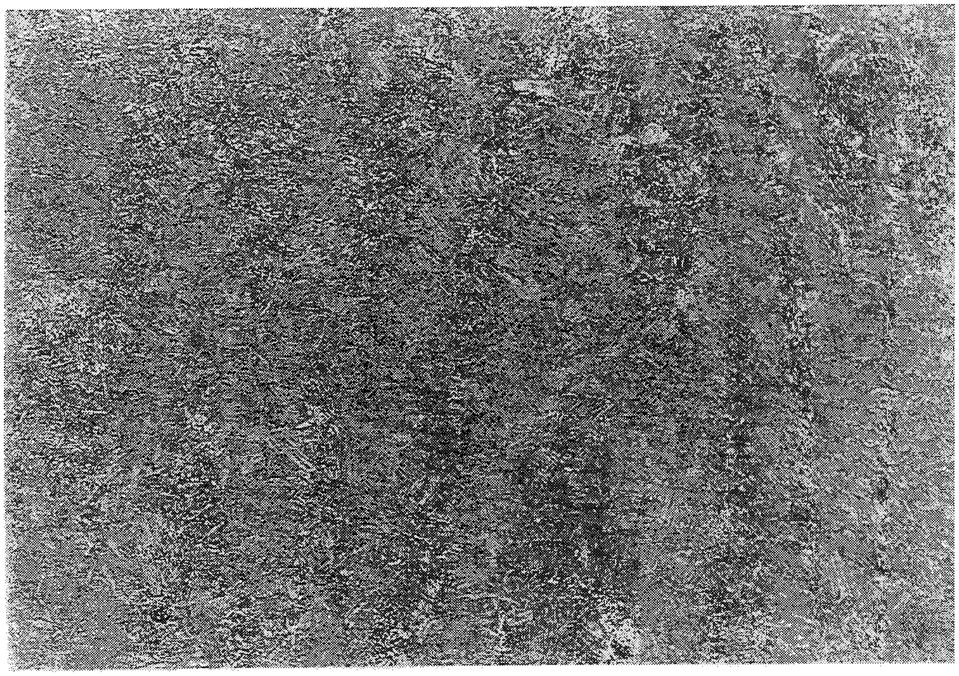

Figure 4.45 MV1 - Showing Lathlike Packets of Bainite/Martensite in Grain Refined Regions of Typical GMA Welds Using C5 Cover Gas (200 x)

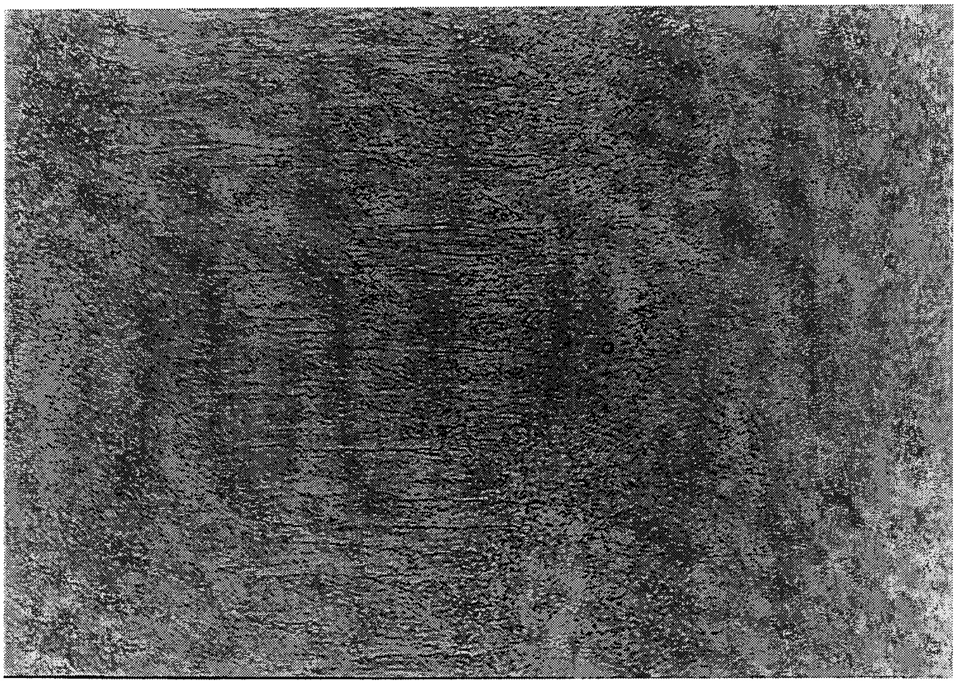

Figure 4.46 MV6 - Showing Lathlike Microstructure in the Columnar Region of a GMA Weld Sample Using Argon Cover Gas (400 x)

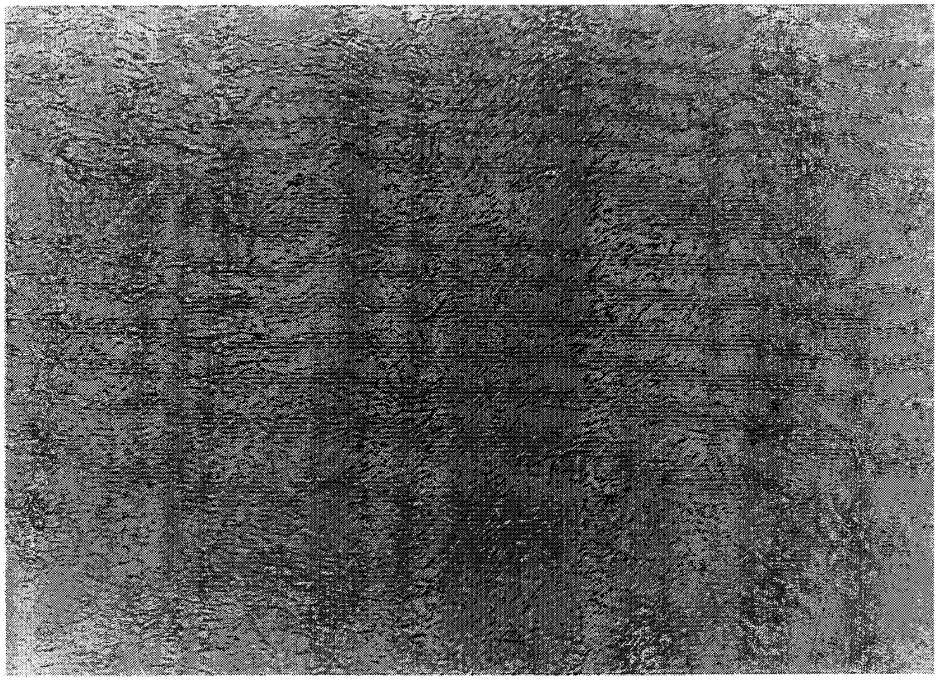

Figure 4.47 MV6 - Showing Lathlike and Equiaxed Microstructures in Grain Refined Regions of a GMA Weld Using Argon Cover Gas (400 x)

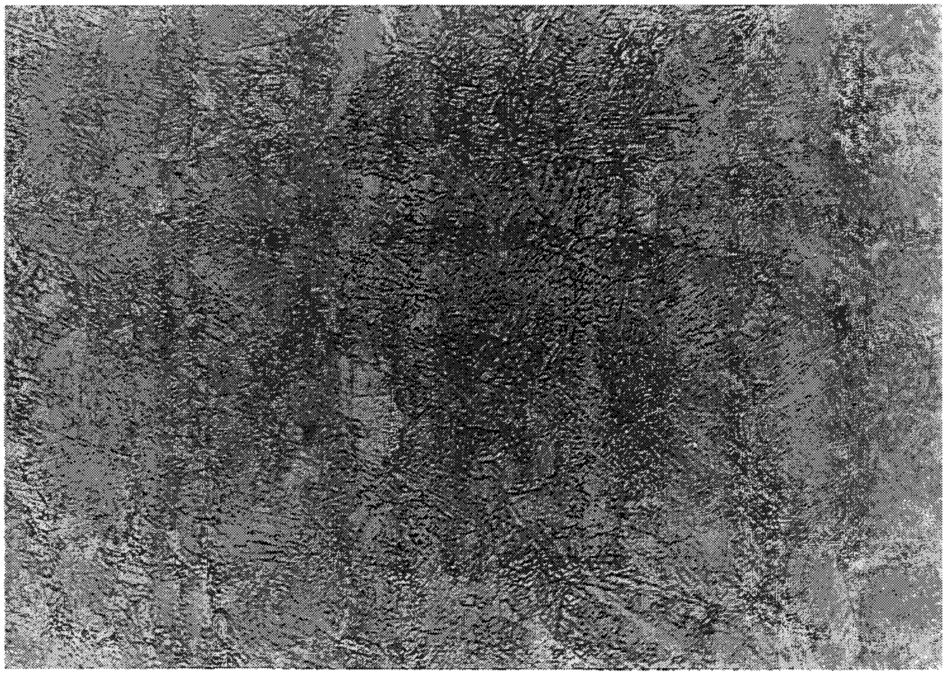

Figure 4.48 MV20 - Showing Lathlike Bainite/Martensite in Grain Refined Regions of a GTA Weld Using C5 Cover Gas (400 x)

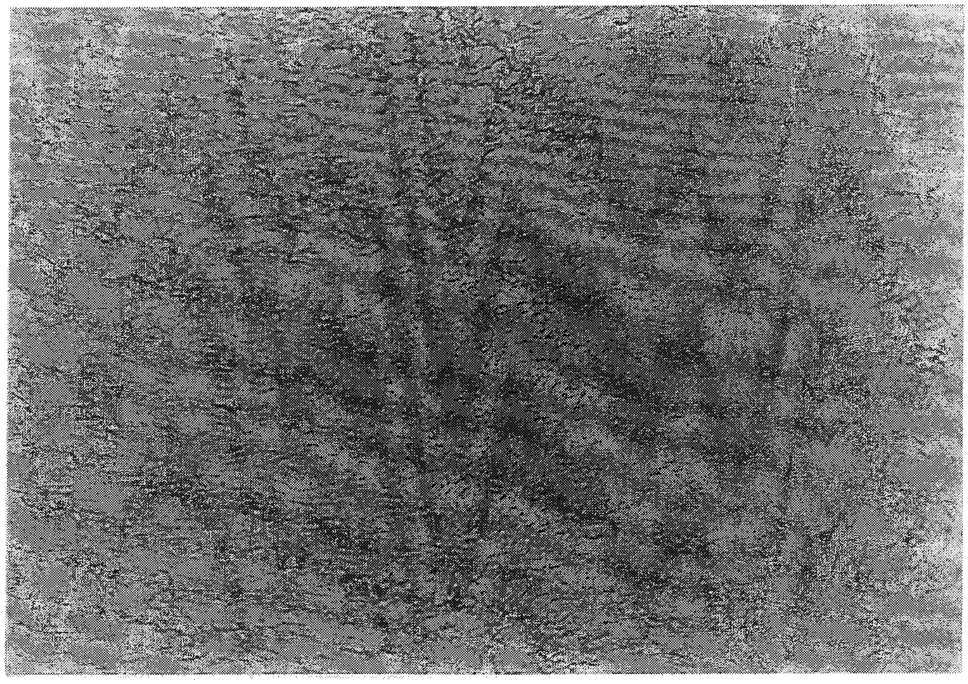

Figure 4.49 MV2 - Showing Equiaxed Ferrite Microstructure in a GTA Weld Using Argon Cover Gas (400 x)

V. SUMMARY

A. CONCLUSIONS

The use of C5 cover gas, particularly in GMA welds was observed to have a major effect on the weld strength and toughness. The dissociation of CO_2 in the weld pool resulted in increased levels of both oxygen and carbon. Strength was observed to increase with the addition of both oxygen and carbon. However, it was believed that only carbon significantly affected the strength through increased hardenability, while oxygen had very little strengthening effect. On the other hand, the addition of oxygen and carbon resulted in a detrimental affect upon the CVN toughness. The increased oxygen content resulted in an increase in the inclusion volume fraction through the formation of oxides of Al, Ti, Si and Mn. Although inclusion size was observed to have a similar effect, the trend was not as clearly defined. Increased carbon resulted in reduced toughness, apparently through the increase of weld strength and formation of brittle microstructures.

Microscopy revealed that the microstructure of the higher strength GMA weld samples were dominated by columnar grains containing a lathlike microstructure of bainite or martensite. The formation of these microstructures correlated well with the increase of carbon, suggesting that the minor changes in the carbon content caused a shift in the microstructure from equiaxed ferrite to either bainite or martensite. The increase of strength with carbon content resulted in an opposite effect on the toughness such that the highest strength samples had the lowest toughness. The correlation could be tied to the formation of lath bainite or martensite that existed as a result of carbon addition to the weld pool from the C5 cover gas.

In the case of the GTA weld microstructures, it was observed that toughness improved with a decrease in both strength and carbon content. When C5 cover gas was used, the lath bainite or martensite microstructure still existed, but the low deposition, high weld pass nature of the GTA weld process had effectively broken the existing bainite/martensite microstructure into smaller packets of laths, as well as forming some equiaxed grains which are possibly ferrite. The maximum toughness, lowest strength GTA welds produced using argon as a cover gas were characterized by an equiaxed ferrite microstructure, and a total absence of any lath-like microstructures. The maximum toughness produced by the equiaxed ferrite microstructure results from its crack arresting capabilities of the relatively soft ferrite, and a low volume fraction of inclusions, but its low carbon content severely reduces strength.

SEM fractography suggests that cracks which exist along the columnar welds of GMA welds using C5 cover gas may result from the delamination of these grain boundaries during the formation of the lath bainite or martensite. Likewise, extensive intergranular cracking was also observed in the fracture surfaces of these same samples. These samples were also observed to contain a high inclusion size and volume fraction. While inclusions larger than the average inclusion size were observed to nucleate small cracks, the extensive intergranular cracking that was observed could not be correlated to the inclusion size or volume fraction in the GMA weld metals.

B. RECOMMENDATIONS

Transmission Electron Microscopy (TEM) should be conducted on all samples to determine if the lath microstructure is bainite, martensite, or a mixture of both. If martensite formation is occurring, additional consideration will be necessary to determine how to suppress the formation of this microstructure.

GMA weld samples should be generated using C5 cover gas and a consumable that is carbon free. Carbon would be supplied to the weld metal through the dissociation of the CO_2 contained in the cover gas, as well as from the dilution of the base plate. This would effectively lower the carbon content of the weld pool, minimizing the formation of hard bainite/martensite microstructures and limiting amount of intergranular cracking, both of which appear to be the result of higher carbon contents. These combined effects would, therefore, have the effect of increasing toughness. A sufficient amount of carbon should remain in the weld pool so that strength would meet specifications without toughness being compromised.

APPENDIX A. CVN FRACTURE SURFACES

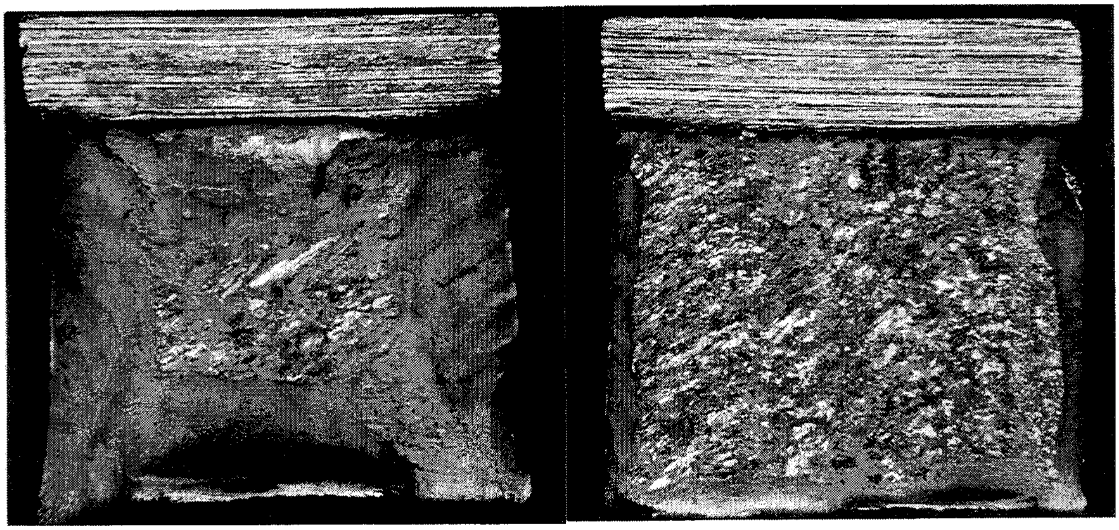

Figure A.1 MV1 Ductile and Brittle Fracture Surfaces (6.4 x)

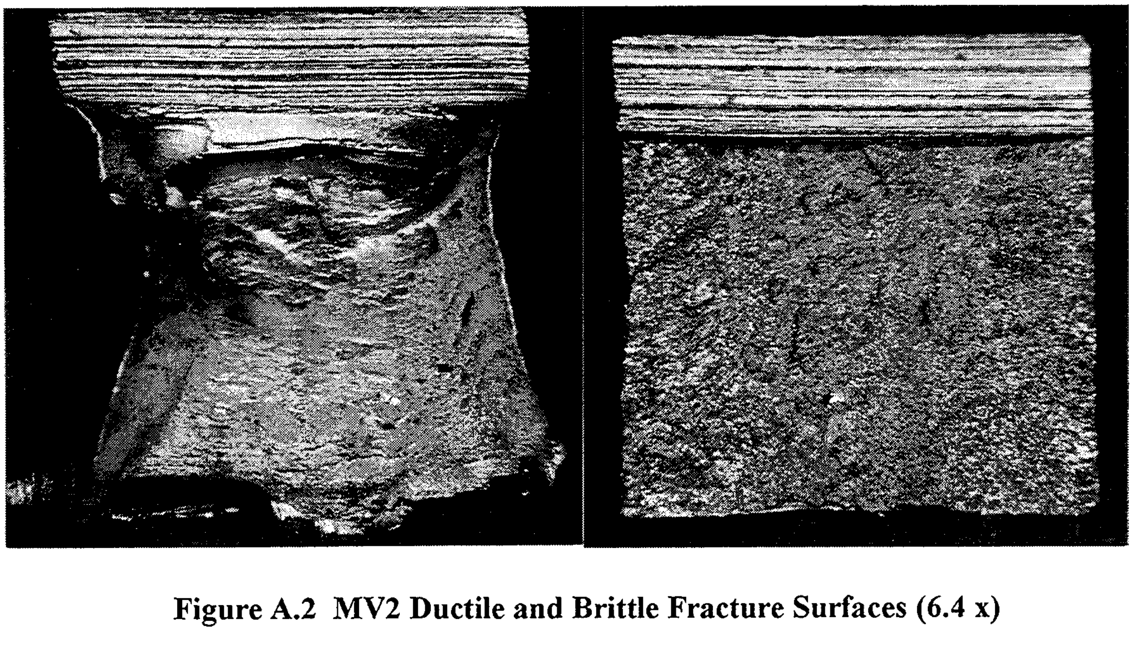

Figure A.2 MV2 Ductile and Brittle Fracture Surfaces (6.4 x)

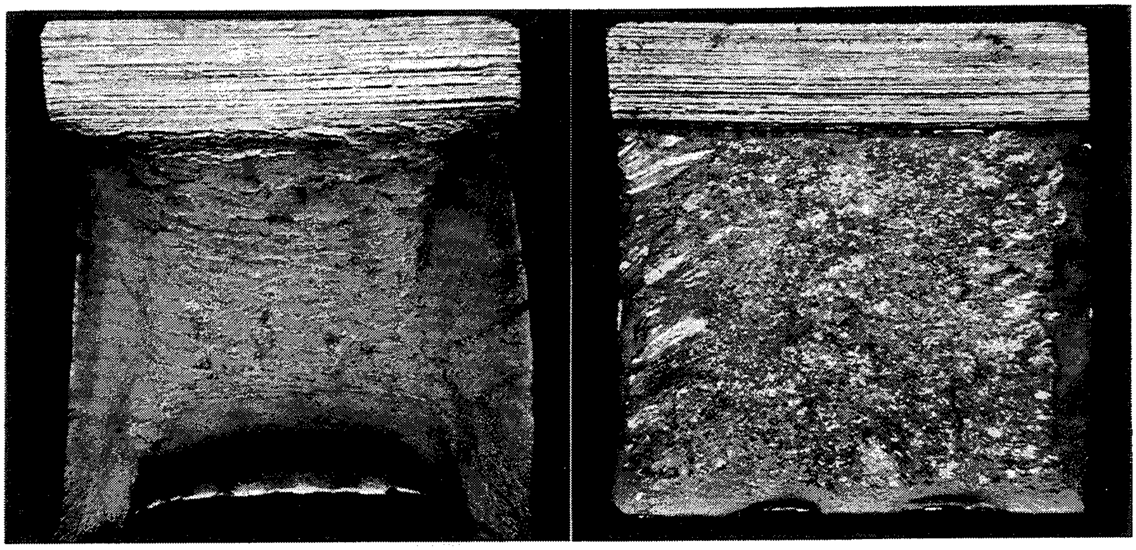

Figure A.3 MV4 Ductile and Brittle Fracture Surfaces (6.4 x)

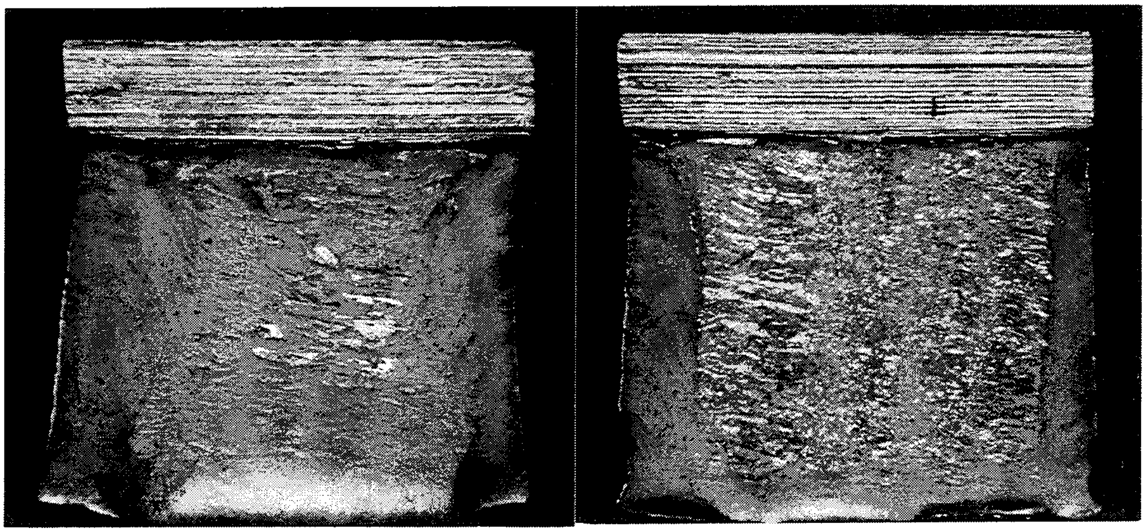

Figure A.4 MV5 Ductile and Brittle Fracture Surfaces (6.4 x)

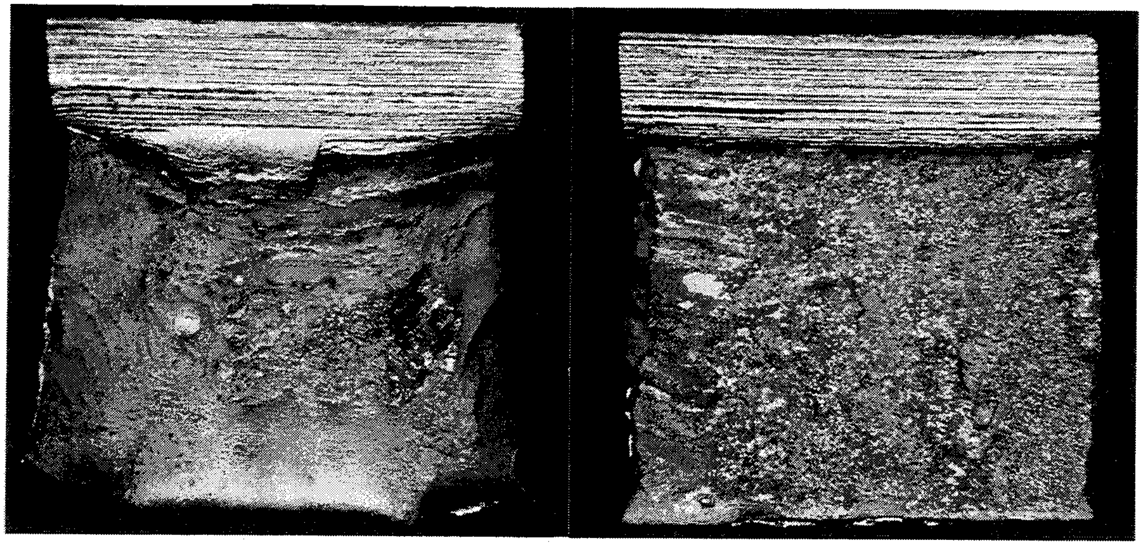

Figure A.5 MV6 Ductile and Brittle Fracture Surfaces (6.4 x)

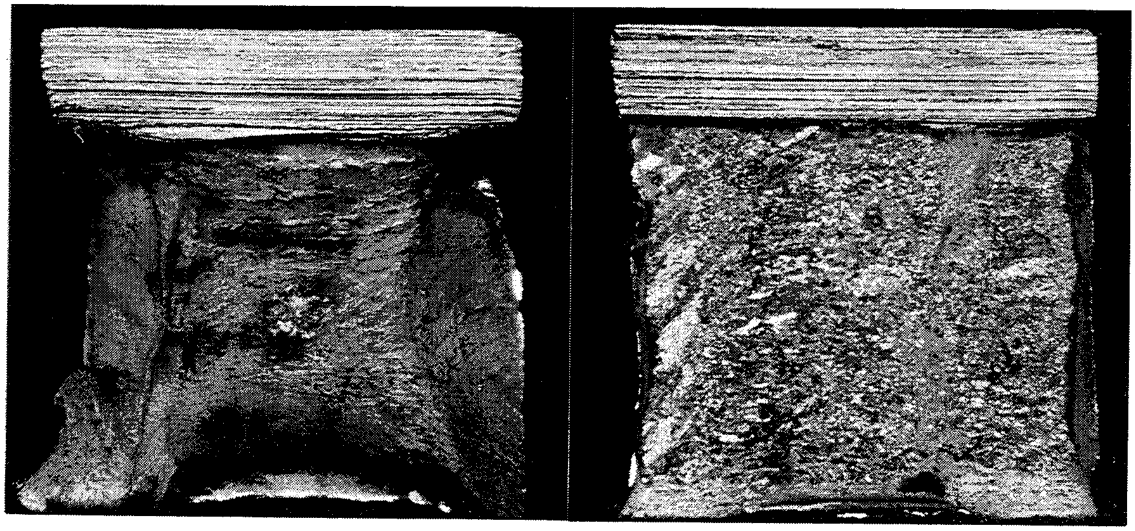

Figure A.6 MV20 Ductile and Brittle Fracture Surfaces (6.4 x)

APPENDIX B. OPTICAL MACROSCOPIC PHOTOGRAPHS

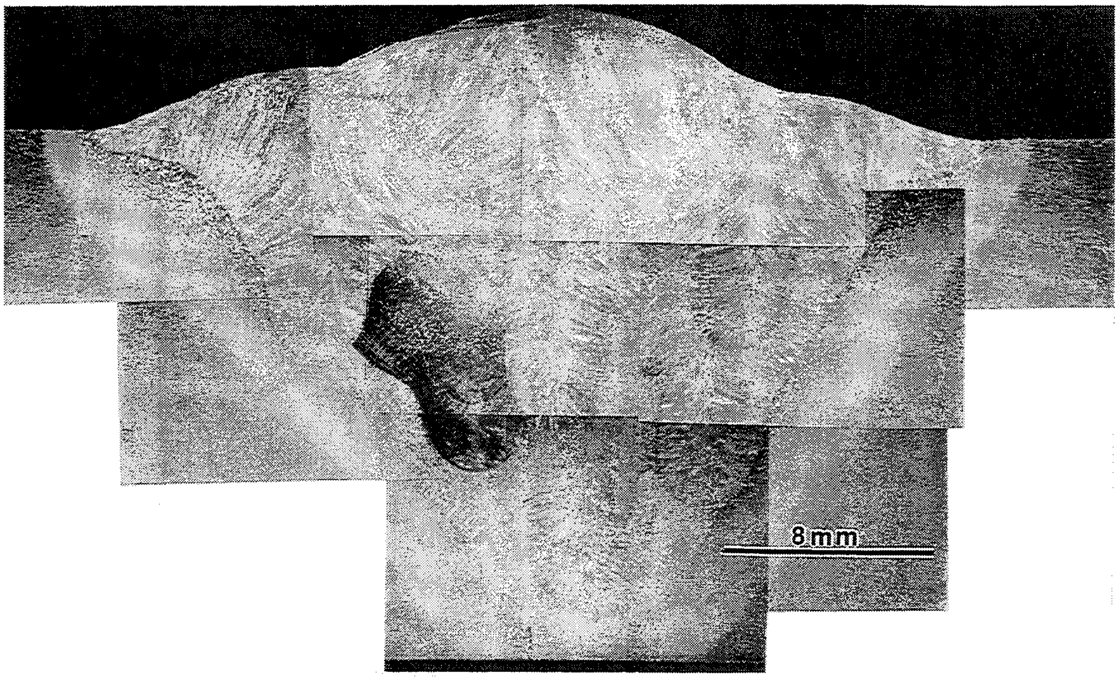

Figure B.1 MV1 (GMA/C5/60 KJ/in.)
(Beno, 1994)

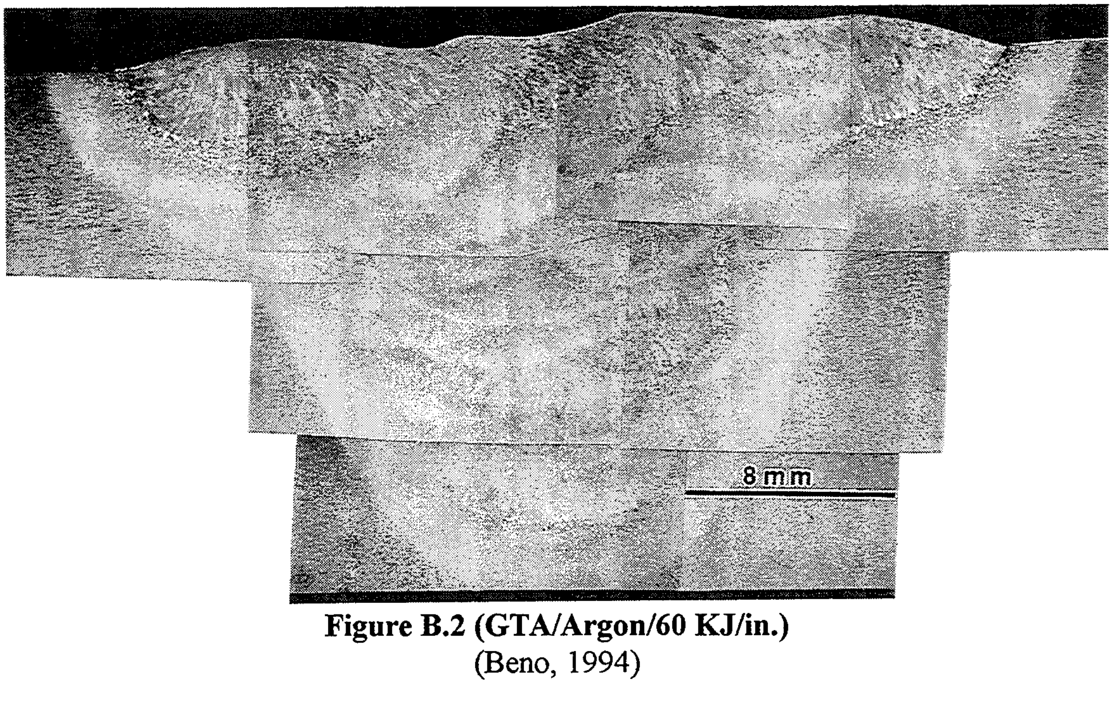

Figure B.2 (GTA/Argon/60 KJ/in.)
(Beno, 1994)

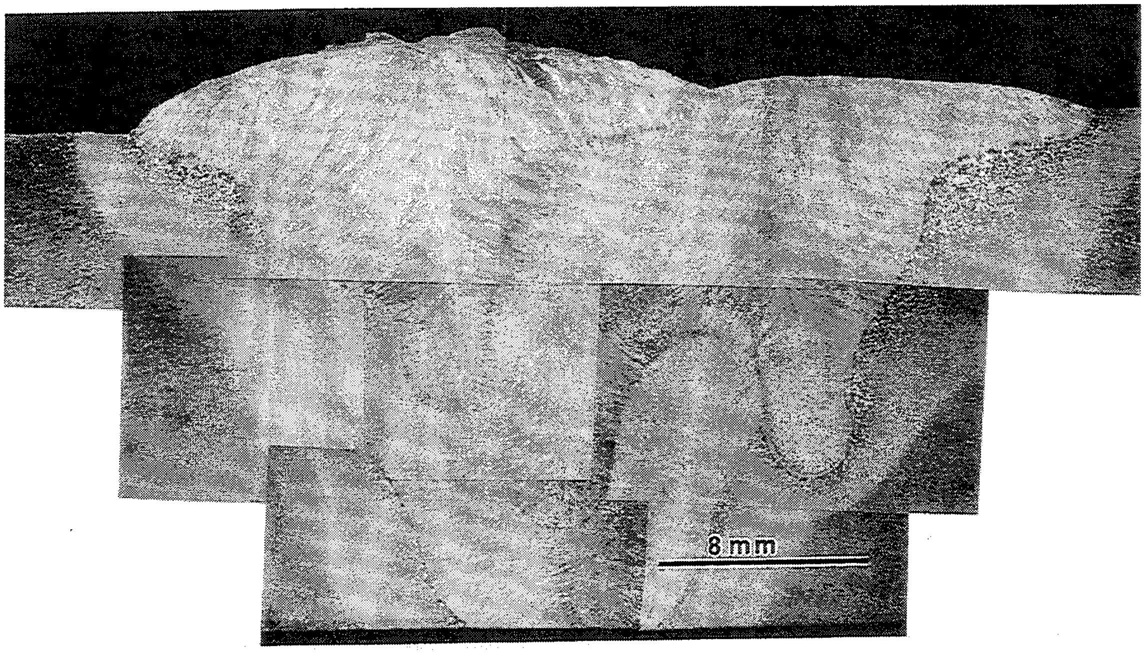

Figure B.3 MV4 (GMA/C5/97 KJ/in.)
(Beno, 1994)

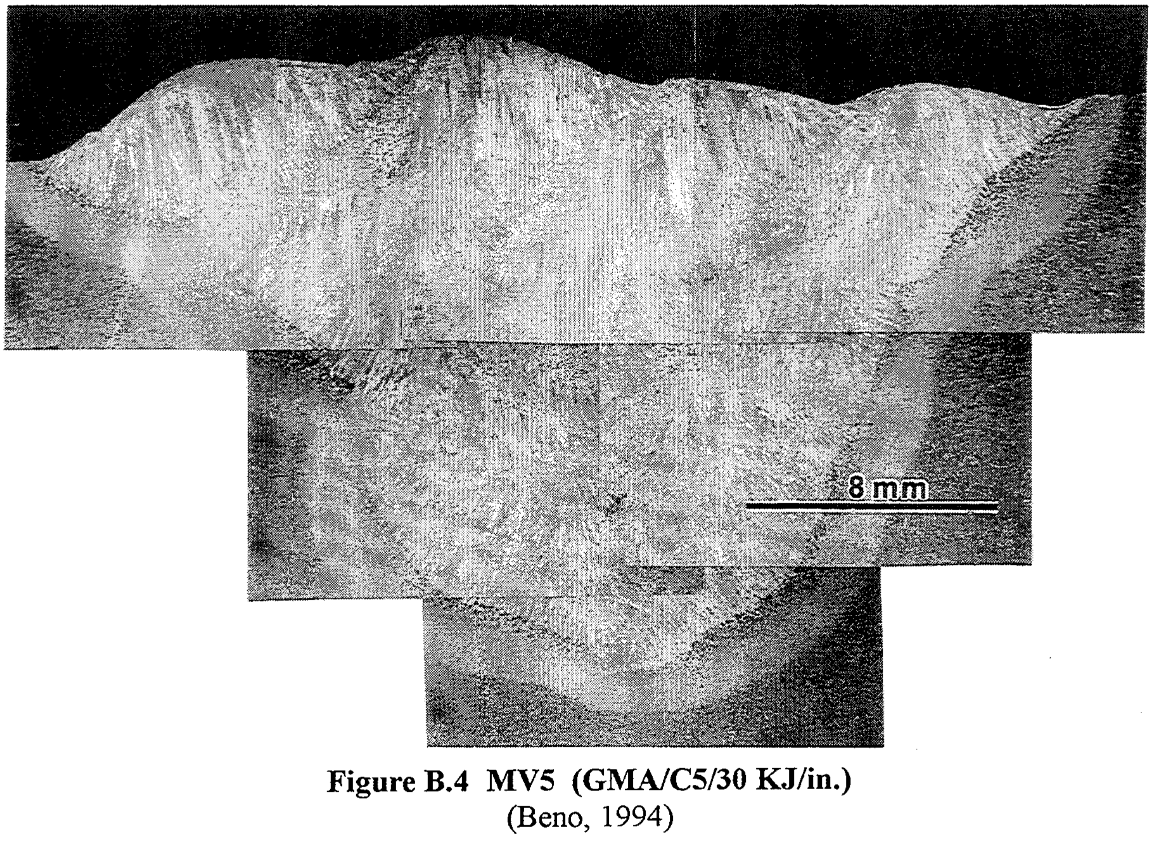

Figure B.4 MV5 (GMA/C5/30 KJ/in.)
(Beno, 1994)

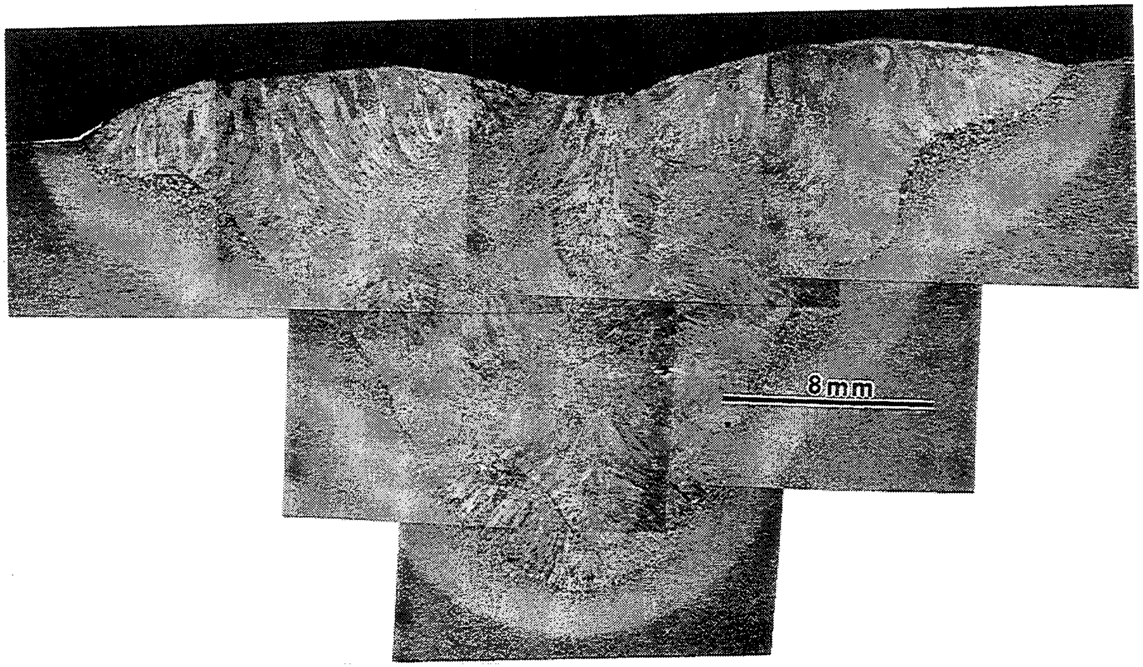

Figure B.5 MV6 (GMA/Argon/60 KJ/in.)
(Beno, 1994)

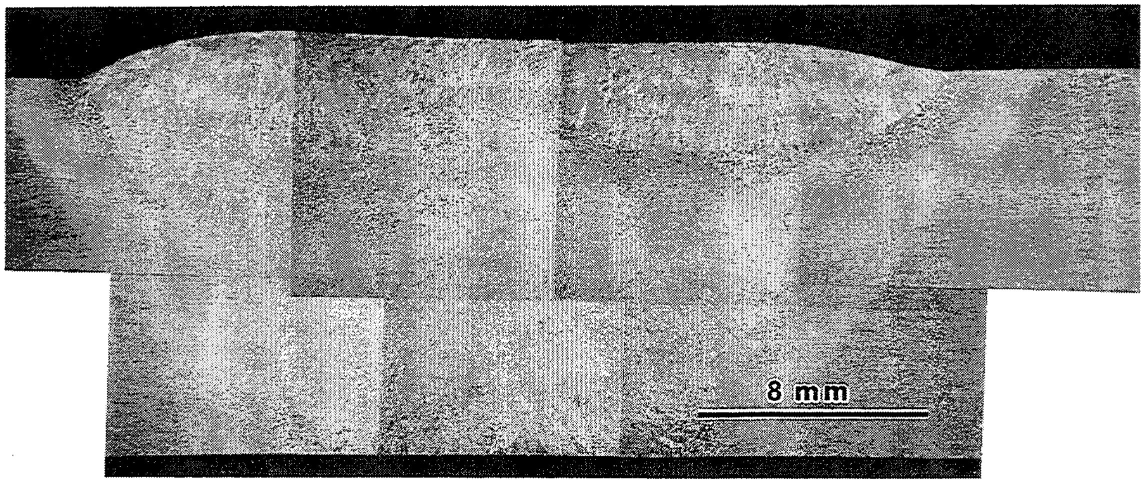

Figure B.6 MV20 (GTA/Argon & C5/81 KJ/in.)

LIST OF REFERENCES

Abson, D.J., Dolby, R.E., and Hart, P.H.M., "The Role of Nonmetallic Inclusions in Ferrite Nucleation in Carbon Steel Weld Metals." *International Conference on Trends in Steel and Consumables for Welding*, The Welding Institute, London, 13-16 November 1978, pp. 75-101.

Abson, D.J., and Pargeter, R.J., "Factors Influencing As-Deposited Strength, Microstructure, and Toughness of Manual Metal Arc Welds Suitable for C-Mn Steel Fabrications," *International Metals Review*, Vol. 31, No. 4, 1986.

Beno, M.L., *Characterization of Ultra-Low Carbon Bainitic Steels for Use as Weld Wire Consumables*, Master's Thesis, Naval Postgraduate School, Monterey, California, September, 1994.

Bhadeshia, H.K.D.H. and Christian, J.W., "Bainite in Steels," *Metallurgical Transactions A*, Vol. 21A, April 1990, pp. 767-797.

Bhatti, A.R., Saggese, M.E. Hawkins, D.N., Whiteman, J.A. and Golding, M.S., "Analysis of Inclusions in Submerged Arc Welds in Microalloyed Steels," Welding Research Supplement, July, 1984, pp.224s-230s.

Blicharski, M.R., Garcia, C.I., Pytel, S., and DeArdo, A.J., "Structural and Properties of ULCB Plate Steels for Heavy Section Application," *Processing, Microstructure and Properties of HSLA Steels*, The Minerals, Metals & Materials Society, pp. 317-329, 1988.

Brothers, D.G., *The Origin of Acicular Ferrite in Gas Metal Arc and Submerged Arc Welds*, Master's Thesis, Naval Postgraduate School, Monterey, California, March, 1994.

Butler, D.E., *The Quantitative Microstructural Characterization of Multipass TIG Ultra Low Carbon Bainitic Steel Weldments and Correlation with Mechanical Properties*, Masters's Thesis, Naval Postgraduate School, Monterey, California, September, 1993.

Callister, W.D., *Materials Science and Engineering: An Introduction*, John Wiley & Sons, Inc., New York, 1991.

Cullison, A. "Two Paths, One Goal: A consumable to Weld HSLA 100," Welding Journal, Vol. 73, No. 1, January, 1994, pp. 51-53.

Czyryca, E.J., Link, R.E., Wong, R.J., Aylor, D.A., Montemarano, T.W. and Gudas, J.P., "Development and Certification of HSLA-100 Steel for Naval Ship Construction," *Naval Engineers Journal*, May, 1990, pp.63-82.

DeLoach, Jr., J.J., Franke, G.L., Vassilaros, M.G., Wong, R.J. and DeNale, R., "Current Welding Consumables Research in the U.S. Navy," , Carderock Division, Naval Surface Warfare Center, CARDIVNSWC-SSM-61-93/09, March, 1993.

Dowling, J.M., Corbett, J.M. and Kerr, H.W., "Inclusion Phases and the Nucleation of Acicular Ferrite in Submerged Arc Welds in High Strength Low Alloy Steels," *Metallurgical Transactions A*, Vol. 17A, September 1986, pp. 1611-1623.

Eakes, M.W., *Correlation of Inclusion Size and Chemistry with Weld Metal Composition and Microstructure in Arc Weldments of High Strength Steels*, Master's Thesis, Naval Postgraduate School, Monterey, California, December, 1994.

Edwards, G.R. and Liu, S., "Recent Developments in HSLA Steel Welding," *Proceedings from the First United States - Japan Symposium on Advances in Welding Metallurgy*, American Welding Society, June, 1990, pp. 213-292.

Francis, R.E., Jones, J.E. and Olson, D.L., "Effect of Shielding Gas Oxygen Activity on Weld Metal Microstructure of GMA Welded Microalloyed HSLA Steel.", *Welding Research Supplement*, November, 1990, pp. 408s-415s.

Garcia, C.I., Lis, A.K. and DeArdo, A.J., "The Physical Metallurgy of Ultra-Low Carbon Bainitic Steels," *Metallurgy of Vacuum Degassed Steel Products*, The Minerals, Metals & Materials Society, pp. 461-467, 1990.

Green, R.S., Sampath, K., Devletian, J.H., Singh, D., Howden, D.G. and Zhang, L., "Filler Wire Development for GMA Welding of HSLA-100 Steel", *Proceedings, International Conference on Trends in Welding Research*, 3rd 1992, pp. 359-64, ASM, 1993.

Grong, O., and Matlock, D.K., "Microstructural Development in Mild and Low-Alloy Steel Weld Metals," *International Metals Reviews,* Vol. 31, No. 1, 1986.

Kiessling, R., *Nonmetallic Inclusions in Steel: Part I-IV*, The Metals Society, London, 1978.

Kiessling, R., *Non-Metallic Inclusions in Steel: Part V*, The Institute of Metals, London,1989.

Komizo, Y and Fukada, Y., "Toughness Improvement in Weld Metal of Carbon and HSLA Steels in Japan," Sumitomo Metal Industries, Ltd., 1988.

Kou, S., *Welding Metallurgy*, John Wiley & Sons, Inc., New York, 1987.

Liu, S., "Metallography of HSLA Steel Weldments," *Key Engineering Materials*, Vols. 69 & 70 (1992) pp. 1-20.

McDonald, E.P., *Factors Influencing the Microstructure and Mechanical Properties of Ultra Low Carbon Bainite 100 Tungsten Inert Gas Multipass Weldments,* Master's Thesis, Naval Postgraduate School, Monterey, California, September, 1992.

Ohkita, S., Homma, H., Matsuda, S., Wakabayashi, M, and Yamamoto, K., "Improvement of HAZ Toughness of HSLA Steel by Finely Dispersed Titanium Oxide." *Nippon Steel Technical Report*, No. 37, April, 1988, pp. 10-16.

Pickering, F.B., *Physical Metallurgy and the Design of Steels*, Applied Science Publishers Ltd., London, 1978.

Wang, S-C and Kao, P-W, "The Effect of Alloying Elements on the Structure and Mechanical Properties of Ultra Low Carbon Bainitic Steels," *Journal of Materials Science*, 28(1993), pp. 5169-5175.

Wilson, A.D., Hamburg, E.G., Colvin, D.J., Thompson, S.W. and Krauss, G., "Properties and Microstructures of Copper Precipitation Aged Plate Steels," *Proceedings of Microalloying '88, ASM International*, 1988, pp-. 259-274.

Widgery, D.J., "Deoxidization Practice for Mild Steel Weld Metal," *Welding Research Supplement*, March, 1976, pp. 57s-61s.

INITIAL DISTRIBUTION LIST

		Number of Copies
1.	Defense Technical Information Center Cameron Station Alexandria, VA 22304-6145	2
2.	Library, Code 52 Naval Postgraduate School Monterey, CA 93943-5101	2
3.	Naval Engineering Curricular Office, Code 34 Naval Postgraduate School Monterey, CA 93943-5100	1
4.	Department Chairman, Code ME Department of Mechanical Engineering Naval Postgraduate School Monterey, CA 93943-5100	1
5.	Dr. Alan G. Fox, Code ME/FX Department of Mechanical Engineering Naval Postgraduate School Monterey, CA 93943-5100	2
6.	Dr. Joseph Blackburn Naval Surface Warfare Center Carderock Division, Annapolis Detachment Code 615, 3A Leggett Circle Annapolis, MD 21402-5067	1
7.	Dr. Ivan Kaplan Naval Surface Warfare Center Carderock Division, Annapolis Detachment Code 0115, 3A Leggett Circle Annapolis, MD 21402-5067	1
8.	Lt. Victor Reck Jr. 1013 Parkview Avenue New Kensington, PA 15068	2